Development and application of novel analytical method to determine thermal denaturation process of soil organic matter

Division of Science for Bioproduction and the Environment
Graduate School of Bioresources and Environmental Sciences
Ishikawa Prefectural University

Naoya Katsumi

September 2015

博士論文

土壌有機物の熱変性プロセス解明のための新規分析手法の開発と適用

石川県立大学大学院

生物資源環境学研究科自然人間共生科学専攻

勝見　尚也

2015 年 9 月

To the late "big-boned" soil scientist,

(今は亡き恩師へ)

Acknowledgments

This work for my Ph. D. thesis was carried out at the Division of Science for Bioproduction and the Environment Graduate School of Bioresources and Environmental Sciences Ishikawa Prefectural University under the guidance of Professor Dr. Masanori Okazaki from April 2013 to September 2015.

First of all, I wish to express my sincere appreciation to Professor Dr. Masanori Okazaki and emeritus Professor the late Dr. Koyo Yonebayashi of Ishikawa Prefectural University for their constant guidance during the course of this research. They always gave me helpful suggestions and warm words of encouragement throughout the present study.

I also wish to express my sincere appreciation to associate Professor Dr. Yukiya Minami and associate Professor Dr. Shumpei Kitamura of Ishikawa Prefectural University. They gave me many advisements to write up this Ph.D thesis.

I'd like to express my appreciation to Dr. Chuichi Watanabe and Dr. Akihiko Hosaka of Frontier Laboratories Ltd. for measurement of Py-GC/MS and EGA-MS.

I appreciate to express my appreciation to Professor Dr. Nobuaki Ishida and associate Professor Dr. Yuji Honda of Ishikawa Prefectural University for advice on optimization of the ^{13}C NMR conditions.

I'd also like to express my appreciation to thank Professor Dr. Nobuhide Fujitake of Kobe University for measurement of ^{13}C NMR.

I'd like to express my appreciation to thank Professor Dr. Satoshi Oke of Ishikawa Prefectural University for advice on the life as a researcher and warm words of encouragement.

I wish to thank associate Professor Dr. Toshihiko Momose, associate Professor Dr. Ryohei Yamashita and Mr. Shun Nishiyama of Ishikawa Prefectural University for valuable discussion.

I also wish to thank Tech. Tomoe Nishi of Ishikawa Prefectural University for technical assistances. She gave me much guidance how to use analytical equipment.

In the last but not least, my parents, Masaru and Atsuko Katsumi, and my brother, Taichi and Yusuke Katsumi deserve special acknowledgement for their constant support and encouragement through my life.

September 2015

Naoya Katsumi

Contents

Figure lists

Chapter 1

Chapter 2

Chapter 3

present study. These nanostructure models used theoretical values for La and approximate value for Nc.

Chapter 4

Chapter5

Table list

Chapter 1

Chapter 2

Chapter 3

Chapter 4

Chapter 5

Chapter 1. General introduction

1.1. Carbon cycle in soil ecosystem

In terrestrial ecosystems, soils represent the major reservoir of carbon (C). The soil organic C (SOC) means the C content of soil organic matter (SOM), which mostly around 50 to 60%. At the global level, the SOM and soil inorganic C pool (estimated up to 1 m depth) contains about 1,580 Pg (Pg = petagram = 10^{15} g = 1 billion ton) and 945 Pg of C, about 610 Pg are stored in the vegetation and about 750 Pg are present in the atmosphere (Schimel 1995). Estimation values of soil organic and inorganic C stocks and C densities of world soils are listed in Table 1-1 (data taken from Lal, 2004). The SOC density ranges from low in soils of the arid regions to high in soils of the temperate regions, and extremely high in Histisols (Lal 2004).

Simplified diagram of the soil C cycle are shown in Fig. 1.1. The total amount of organic C stored in a soil is the net balance of all C fluxes entering and leaving the soil over time. In soil ecosystem, the source of SOM is from net primary production. In net primary production, most SOM entering the soil originates from plants. Above-ground litter, mainly derives from woody tissues, leaves, flowers, fruits, mosses, lichens and fungi; below-ground inputs include dead roots and their associated mycorrhizal hyphae, root exudates (mainly sugars and organic acids) and sloughing of root surface tissues (Rodeghiero et al. 2009). In soil ecosystem, losses of C from the soil derive mainly decomposition and mineralization processes of SOM, which lead to the release of CO_2 and some other trace gases (CH_4 and CO). Leaching can also cause C losses from soil via disserved organic C (DOC) and dissolved inorganic C (DIC). Erosion can lead to considerable C losses at the plot scale, but net effects are harder to predict when up-scaling since it depends on the fate of the C in the deposition area (Rodeghiero et al., 2009). It is estimated that about 1.14 Pg of C may be annually emitted into the atmosphere through erosion-induced processes (Lal 2001).

1.2. Soil organic matter

SOM generally refers to the non-living organic material within the soil matrix. SOM originated from plant, animal or microbe and consists of a continuum of materials in various stages of alteration due to both biotic and abiotic processes (Baldock and Skjemstad 2000). SOM is the major component of soil and plays important roles in providing nutrients to plants, pH buffering, interactions with heavy metals and persistent organic pollutants, and the supply of water and release of gas with formation of aggregate structure (Hillel 2007). Furthermore, SOM

Table 1.1. Estimation of soil organic and inorganic C stocks (to 1 m depth) and C densities of world soils (data taken from Lal, 2004).

Soil order	Area	Soil organic carbon		Soil inorganic carbon	
	(Mha)	Density (Mg C ha^{-1})	Pool (Pg C)	Density (Mg C ha^{-1})	Pool (Pg C)
Alfisols	1262	125	158	34	43
Andisols	91	220	20	0	0
Aridisols	1570	38	59	290	456
Entisols	2114	42	90	124	263
Gelysols	1126	281	316	6	7
Histosols	153	1170	179	0	0
Inceptisols	1286	148	190	26	34
Mollisols	901	134	121	96	116
Oxisols	981	128	126	0	0
Rocky land	1308	17	22	0	0
Shiftinf sand	532	4	2	9	5
Spodsols	335	191	64	0	0
Ultisols	1105	124	137	0	0
Vertisols	316	133	42	50	21
Total	13083		1526		945

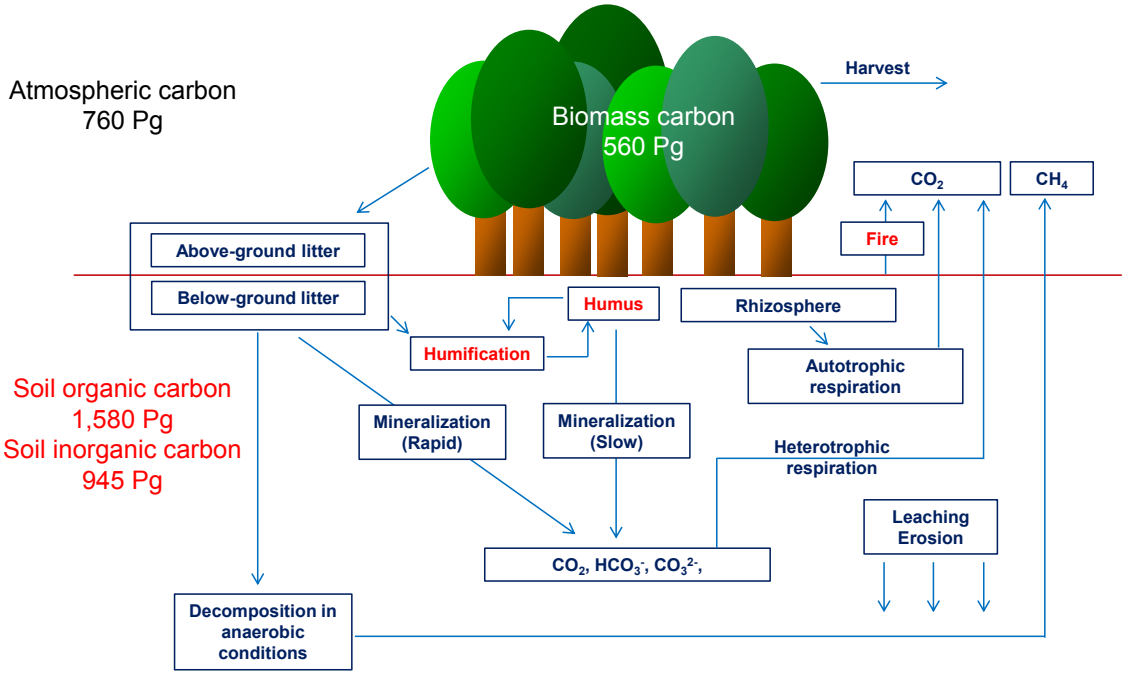

Fig. 1.1. Simplified diagram of the soil C cycle

is the largest C pool in terrestrial ecosystems and has the potential to be a sink or source of atmospheric CO_2 (Lal 2004). Accordingly, the identification of the factors controlling accumulation of SOM is an important subject. However, the prediction of organic matter dynamics in soil is hampered by the complexity of SOM distribution and chemical composition (Foereid et al. 2012). Accumulation of SOM in soil may be controlled by following 3 theories; (1) physical protection in soil aggregate (Gregorich et al., 1989), (2) chemical binding to the soil matrix (Sollins et al. 1996) and (3) biological degradability depending on their chemical structure (Wagai et al. 2013). To balance the global C budget and sustain biological production, the relationship between chemical structure and residence time of SOM should be understood.
Some SOM components can be assigned to bimoleculars (i.e., amino acids, carbohydrates and lipids), while others have lost their initial structure through biotic and abiotic (catalytic) reaction. Those materials characterized by brown or dark color are called humic substances (Kumada 1987). Humic substances are dark heterogeneous mixtures of structurally complex, high molecular weight aromatic and aliphatic components bearing many acidic functional groups with various pK_a values and having a wide molecular weight distribution (Yonebayashi 1997). Humic substances, which are the major constituents of organic matter in soil, sediment, and water, are believed to be biochemically and chemically synthesized in the environment from biomass constituents and their metabolites (Stevenson 1994). The development of models for their chemical structure can be expected to improve our understanding of their genesis and environmental behavior (Schnitzer and Khan 1972). Figure 1.2. (Schlten and Leinweber, 2000) is one of the concept models for the humic substances of their chemical structure.

Humic substances have traditionally been isolated using alkali solution. Furthermore, humic substances can be operationally divided into three main fractions according to their solubility in acid and alkali (Fig. 1.3): fulvic acids (FAs, alkali- and acid-soluble fraction), humic acids (HAs, alkali-soluble and acid-insoluble fraction), and humin (alkali- and acid-insoluble fraction). In Japan, HAs are further divided into Type A, Type B, Type P, and Type Rp according to relative color intensity (A_{600}/C) and color coefficient (Δlog K), and degree of darkness increase in the order Type A, Type B, Type P, Type Rp (Ikeya et al., 2004). A_{600}/C and Δlog K are defined as follows:

A_{600}/C: where A_{600} is absorbance at 600 nm and C is the organic C concentration.

Δlog K: log A_{400} − log A_{600}, where A is absorbance at 400 and 600 nm of the same HAs solution used for A_{600}/C determination.

Thus, A_{600}/C is regarded as color density of HAs and Δlog K, as the slope of the absorption spectra of HAs.

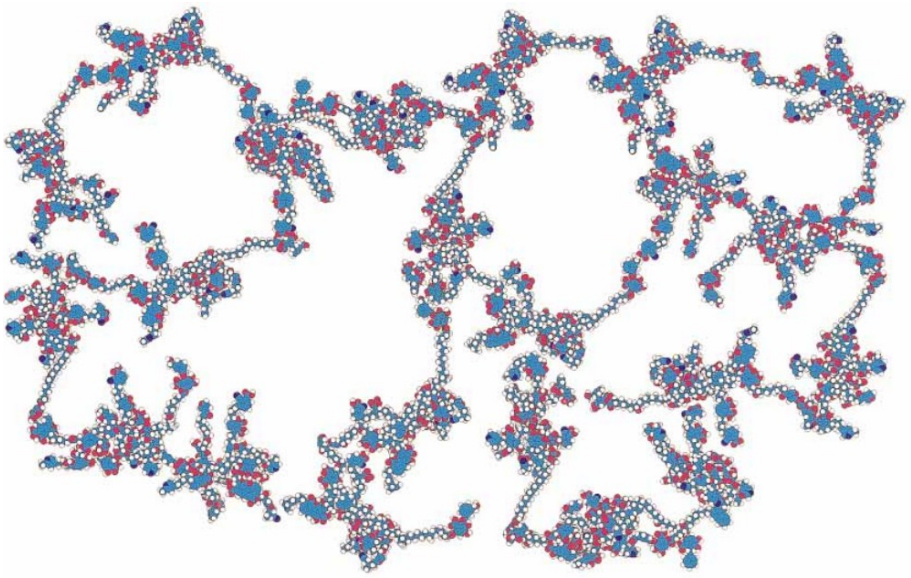

Fig.1.2. Structure model of humic substances proposed by Schlten and Leinweber (2000)

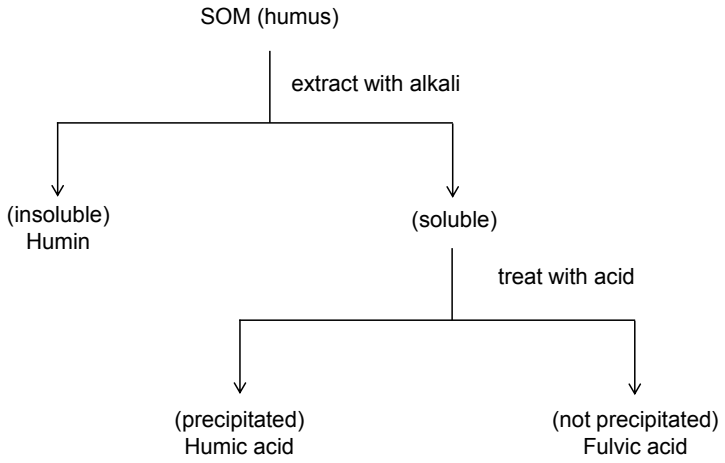

Fig.1.3. Chemical fractionation scheme of SOM based on solubility characteristics.

The progress of humification is evaluated on the basis of increases in the degree of darkness, particularly for HAs (Kumada 1987). In general, less altered components in HAs that have light color, such as amino acids, aliphatic acids, lignin derivatives and carbohydrates can be easily decompose to H_2O and CO_2 by microorganisms. Contrastingly, altered dark color components in HAs are more stable in soil due to their chaotic chemical structure (Yanagi et al. 2003). The degree of darkness of HAs increases with increasing aromatic C content (including aromatic C in condensed aromatic components), with increasing carboxyl group content, and with decreasing O-alkyl C and alkyl C content (Ikeya et al. 2007; Watanabe and Takada 2006; Yonebayashi and Hattori 1988). As darkening progresses, HAs become more structurally stable and thus highly resistant to biodegradation (Yanagi et al. 2003), and their residence time exceeds 10,000 years (Yamada 1986). Among Japanese soil HAs, Andisol HAs show the highest degree of darkness (Kumada 1987).

Andisols cover only 0.8 % of the earth's surface, but they contain approximately 1.8 % of the global soil C due to the high stability of the SOM against biodegradation (Lal 2004). This is due to the high stability of the SOM against decomposition. It is generally considered that (1) the SOM stabilizes in the form of clay–humus complexes and/or aluminum (Al)/iron (Fe)–humus complexes (Wada and Higashi 1976, Wagai et al. 2011), and (2) low soil pH (Tonneijck et al. 2010), and (3) high level of Al toxicity (Dorea and Clarke 2008; Kraal et al. 2009) inhibit the microbial activity.

Andisols in Japan have very thick and dark color A horizons (melanic epipedon) with large amount of SOM. The dark color has inspired many soil scientists to study the humus composition, and the dark color is attributed to the existence of HAs with high degree of darkness which called Type-A HAs (Shoji et al., 1993). However, Type A HAs is not always the presence for Andisols from other countries. For example, New Zealand Andisols had a high content of FAs and the HAs was dominated by P type HAs (Shoji et al 1987). Also in New Zealand Andisols, grass vegetation contributes to the formation of Type A HAs while forest vegetation promotes formation of Type P HAs (Sase 1986). C stable isotope ratio analysis revealed that melanic epipedon developed under grassland vegetation in Japan (Hiradate et al., 2004). In Japan, the climax vegetation is forest and artificial burning or wildfire is needed to maintain the grassland vegetation for long period (Yamane, 1973). In fact, a lot of charred plant fragments which provided evidence for fires were found in those A horizon (Shindo et al., 2004). Shindo et al. (1986) compared optical properties, IR spectra and X-ray diffraction patterns of HAs from Andisols with those from plant charred materials and concluded that plant charred materials could be one of the possible sources for the Type-A HAs.

1.3. Effects of fire on the carbon cycle in terrestrial ecosystems

Wildfire has been a natural disturbance factor in most ecosystems. It has been estimated that more than 30% of the land surface is subjected to a significant frequency of fires (Chuvieco et al., 2008). Approximately 10 million (M) hectares (M ha) are annually affected by fires in boreal forests, 5 M ha in North America forests, 25 M ha in tropical forest, 3M ha in Asia, and around 50,000 wildfires affected annually 0.6M ha of forest in Europe, being mainly the Mediterranean Basin the most affected. At the end of the 20^{th} and beginning of the 21^{th} century, global fire emissions of C ranged from 1.5 to 4.0 Pg/year, equivalent to half of global fossil fuel emissions (Bowman et al., 2009). Of these fire-based emissions, grasslands and savannas contributed the greatest proportion (44 %) and tropical peat fires the smallest (3 %), and forest fires accounted for 15 % of global fire emissions of C (Van der Werf et al., 2010). Furthermore, owing to ongoing global changes, it is expected that fire regimes will immediately respond to climate change in terms of frequency, size, seasonality, recurrence and fire intensity and severity, with direct and indirect effects on soil, water and vegetation (Bento-Gonçalves et al. 2012).

Wildfires and prescribed burning dramatically alter the ecosystem C cycle and storage (Wadle et al., 2003). Forest fires release significant amounts of CO_2 into the atmosphere, but also convert a fraction of the burning vegetation to charred black carbon. Black carbon is hard to break down, and formation of this reserve therefore creates a long-term soil carbon sink (Lehmann et al., 2008). Wildfires can also strongly modify the abiotic and biotic characteristics of soil, altering its structure, chemical and physicochemical properties, C content and macronutrient levels (Knicker 2007). The degree of the alteration depends on the factors such as the type of fire, vegetation, climate, and topography, and all these modifications being particularly important in the surface horizons.

The transformations in HAs and FAs during wildfire have been modeled and studied. Some previous works about fire effects, as well in situ as in laboratories, have mainly shown an increase in aromaticity and the removal of oxygen-containing functional groups of HAs (Almendros et al., 1990; González-Pérez et al., 2004). The more recalcitrant and aromatic structures formed by fires derive from the alteration of carbohydrates (Almendros et al., 1997; González-Vila et al., 2001), lipids, alkylated macromolecules and peptides (Almendros et al., 2003). Those recalcitrant organic compounds are important because it determines the long-term SOM content and C-sequestration capacity of the soil (Knicker et al., 2012). On the other hand, the decrease in oxygen-containing functional groups leads to changes in the sorptive interactions with other soil components, which negatively affects the water repellency (Mataix-Solera et al., 2011; Rodríguez-Alleres et al., 2012).

Some of these newly formed structures can become extractable like the HA fractions

(Almendros et al., 1990; Fernandez et al., 1997). Simultaneously, initial HAs and FAs present a loss for solubility, leading to a decrease of the respective extraction yields. Actually, fires transform HAs into alkali-insoluble compounds and of FA into acid-insoluble compounds (Almendros et al., 1990). Some authors (Miltner and Zech, 1997; Ponomarenko and Anderson, 2001) suggested that fire is a factor for humification due to its ability to accentuate polycondensation reactions.

1.5. Objective of this study

The objective of this study is to develop and apply novel analytical method to determine thermal denaturation process of soil organic matter. This thesis is composed of five chapters. Chapter 1 is a general introduction of this study. Chapter 2 and 3 propose new analytical methods for soil HAs. Stable isotope analytical techniques are applied to HAs study in Chapter 2. To relate the isotopic composition of soil HAs to their source plants and their degree of humification (as indicated by the degree of darkening), as well as to soil type, we determine the $\delta^{13}C$ and $\delta^{15}N$ of HAs extracted from 26 virgin soil samples (14 Andisols and 12 non-Andisols) and from leaf samples from ten C3 plants and seven C4 plants. In Chapter 3, stacking nanostructure properties of 12 soil HAs extracted from Japanese Andisols, Inceptisols and Entisols are evaluated by analysis of the 002 band of their XRD profiles. Chapter 4 gives topics on the effects of heating for humic substances. The objective of the Chapter 4 was to examine how the properties of humic substances in two different soils hosting different vegetation (an Entisol from a paddy field and an Inceptisol from a coniferous forest) were affected by heating at temperatures ranging from relatively low to high. I determined the effects of heating on the quantity and quality of soil humic substances by analyzing their composition and chemical structure by means of conventional methods, as well as by a new technique developed by Chapter 2 and 3.

Chapter 2. Relationship between stable carbon and nitrogen isotope ratios of humic acids extracted from Andisols and non-Andisols

2.1. Introduction

Stable carbon isotope ratios have been used to determine the source plants of soil organic matter since 1980's (Schwartz et al., 1986; von Fischer and Tieszen, 1995). The stable carbon isotope ratio ($\delta^{13}C$) of a plant is determined primarily by its mode of photosynthesis: the $\delta^{13}C$ values of plants that use the C_3 pathway, which include terrestrial forest vegetation, range from –34‰ to –25‰ whereas the values of C_4 plants, such as Japanese pampas grass (*Miscanthus sinensis*), range from –16‰ to –11‰. Mean $\delta^{13}C$ values of –27.1 ± 2.0‰ for C_3 plants and –13.1 ± 1.2‰ for C_4 plants have been calculated from data for many species (O'Leary, 1988).
Stable carbon and nitrogen isotope ratios are also used to estimate the degree of decomposition and humification of soil organic matter. Comparing to tree waste, soil organic matter is slightly enriched in ^{13}C, and $\delta^{13}C$ values increase downward in the soil profile (Nadelhoffer and Fry, 1988; Tiunov, 2007; Wang et al., 2008). The carbon isotope composition of soil organic matter reflects that of the plant material from which it originated, making $\delta^{13}C$ a useful indicator of the photosynthetic mode of vegetation grown on that soil. Carbon isotopes in soil organic matter can be used to distinguish changes in vegetation patterns; for example, $\delta^{13}C$ was used to study the spatially distinct distributions of present and past vegetation communities in a subtropical savanna ecosystem (Boutton et al., 1998).

The changes in stable nitrogen isotope ratios ($\delta^{15}N$) during the degradation of plant residues are much more pronounced than the changes in $\delta^{13}C$ values. Soil microorganisms strongly fractionate nitrogen isotopes during litter decomposition (Connin et al., 2001). The biochemical reactions of the nitrogen cycle (such as ammonification, nitrification, and denitrification) can produce considerable changes in $\delta^{15}N$ because ^{15}N is concentrated in the residual substrate after these reactions. A considerable increase in $\delta^{15}N$ downward in the soil profile is common (Marin-Spiotta et al., 2009; Nadelhoffer and Fry, 1988; Pardo et al., 2007; Tiunov, 2007) and reflects the increase in the degree of decomposition and humification of soil organic matter.

There have been a few reports on the use of the $\delta^{13}C$ values of HAs to investigate the contribution of C_4 plants to organic matter in Andisols (Hiradate et al., 2004; Iimura et al. 2010;

Shindo et al., 2005). However, there are few data on the $\delta^{15}N$ values of soil HAs (Balieiro et al., 2012; Iimura et al., 2013).

In the present study, to relate the isotopic composition of soil HAs to their source plants and to soil type, we determined the $\delta^{13}C$ and $\delta^{15}N$ values of HAs extracted from a wide range of Andisols and non-Andisols, and we also determined the $\delta^{13}C$ and $\delta^{15}N$ values of selected C_3 and C_4 plants. Changes in the $\delta^{13}C$ and $\delta^{15}N$ values with humification (as indicated by darkening) of Andisol and non-Andisol HAs were studied. The contributions of C_3 and C_4 plant–derived carbon to Andisol HA carbon were estimated. We also determined the $\delta^{13}C$ and $\delta^{15}N$ values for the bulk soils.

2.2. Materials and methods

2.2.1. Extraction of HAs from soil samples

HAs were extracted from 26 surface samples of virgin soils collected in Japan (Table 2.1): 14 Andisols, 10 Inceptisols, 1 Oxisol, and 1 Histosol. Andisols were sampled from grasslands or forests in nine prefectures, and Inceptisols were sampled from forests or grasslands in eight prefectures. The Oxisol and Histosol were collected from a forest and grassland, respectively.
The soil samples were air-dried, sieved (2 mm mesh), and then extracted with an aqueous solution containing 0.1 mol L^{-1} NaOH and 0.1 mol L^{-1} $Na_4P_2O_7$ (300 mL g^{-1} soil C) overnight under N_2 at 60°C (Fig. 2.1). This alkaline extraction was repeated until the extract was pale in color. The combined humic extracts were acidified with 6 mol L^{-1} H_2SO_4 to pH 1.5 and then allowed to stand overnight at room temperature. The resulting precipitate, which included the HAs, was separated by centrifugation at 4,000*g* for 15 min. The recovered solids (the HA fraction) were purified by redissolution in the NaOH/$Na_4P_2O_7$ solution, reprecipitation with 6 mol L^{-1} H_2SO_4, and subsequent centrifugation. This purification of the HA fraction was repeated until the acidic supernatant was light yellow. The solid HAs were dissolved in a small amount of 0.1 mol L^{-1} NaOH and centrifuged at 20,000 *g* for 2 h to remove coarse-grained materials. To remove fine-grained materials, we acidified the HAs to pH 1.5, added a solution of HF (0.3 mol L^{-1}) and HCl (0.1 mol L^{-1}), and stirred the resulting suspension for 5 h at room temperature. The suspension was then centrifuged, and the solid was collected and washed with deionized water, dissolved in a small amount of 0.1 mol L^{-1} NaOH, dialyzed (BioDesign Dialysis Tubing, MWCO 3500; BioDesign Inc., Carmel, NY, USA) against distilled water, passed through Amberlite IR-120 resin (H^+ form), and then freeze-dried (Yonebayashi and Hattori, 1988).

Table 2.1 Charactarisitcs of soil sampled for this study

Sample name	Site name	Location	Soil type	Altitude (m)	MAT (°C)	MAP (mm)	Land use	Vegetation*
SGG	Sugadaira G	Ueda, Nagano Pref.	Andisol	1,315	6.5	1,226	Grassland	Ms
GS	Gyoseizan	Shiso, Hyogo Pref.	Andisol	980	13.7	1,756	Grassland	Ss
SN	Soni	Soni, Nara Pref.	Andisol	720	13.0	1,892	Grassland	Ss
DS	Daisen	Houki, Tottori Pref.	Andisol	646	10.9	2,547	Forest	Pd
HB	Hachibuse	Kami, Hyogo Pref.	Andisol	1,179	8.0	2,193	Grassland	Ss
MK	Makino	Taka, Hyogo Pref.	Andisol	213	13.4	1,639	Grassland	Ms, Ss
MYK	Myoko	Myoko, Niigata Pref.	Andisol	547	10.4	1,899	Grassland	Ms
SGM	Sugadaira M	Ueda, Nagano Pref.	Andisol	1,315	6.5	1,226	Forest	Qc, Ss
HNK	Hinakura	Sayo, Hyogo Pref.	Andisol	659	10.6	1,912	Forest	Pd, Cj, Ss
YGD	Yatsugadake	Minamimaki, Nagano Pref.	Andisol	1,433	7.1	1,454	Forest	Qc, Ss
SA	Aburahi	Koka, Shiga Pref.	Andisol	230	13.0	1,529	Forest	Pt
MZ13	Miyakonojyo 13	Miyakonojyo, Miyazaki Pref.	Andisol	n.d.	n.d.	n.d.	Forest	nd
ND0-20	Nodayama	Kanazawa, Ishikawa Pref.	Andisol	170	13.3	2,434	Forest	Mo, Qa
TK-05	Tomuraushi 05	Shintoku, Hokkaido	Inceptisol	620	6.7	1,086	Forest	Pj, Qc
KRS	Kirishima	Kobayashi, Miyazaki Pref.	Inceptisol	650	16.2	2,957	Forest	Cj, Ss
SZK	Suzukitadake	Higashiomi, Shiga Pref.	Inceptisol	1,182	9.7	2,144	Grassland	Ss
KYG	Kyogamine	Kamikitamura, Nara Pref.	Inceptisol	1,476	7.3	3,111	Forest	Fc
KRZ	Keirozan	Tatsuno, Hyogo Pref.	Inceptisol	155	14.3	1,270	Forest	EBF
YSG	Yashagaike	Minamiechizen, Fukui Pref.	Inceptisol	1,130	7.8	2,705	Forest	Fc
TGD	Togadani	Kobe, Hyogo Pref.	Inceptisol	633	12.1	1,611	Forest	Qs
HO-99	Hanaoreyama 99	Kobe, Hyogo Pref.	Inceptisol	539	12.9	1,640	Forest	EBF
NG	Nagamine, Rokko	Kobe, Hyogo Pref.	Inceptisol	678	12.8	1,548	Grassland	Ss
KT	Kuta	Kyoto, Kyoto Pref.	Inceptisol	480	10.0	2,500	Forest	Cj
YON	Yona, Kunigami	Kunigami, Okinawa Pref.	Oxisol	120	23.2	2,624	Forest	Pr, Cs
IJ	Ichijima	Tanba, Hyogo Pref.	Histosol	84	13.8	1,495	Grassland	Pa

Mean annual temperature (MAT) and Mean annual precipitation (MAP) are averaged value for 1971-2014 (Japan Meteorogical Agency)

*vegetation: Cj; Cryptomeria japonica, Cs; Castanopsis sieboldii, EBF; Evergreen broadleaf forest, Fc; Fagus crenata, Mo; Magnola obovata, Ms; Miscanthus sinensis, Pa; Phragmites australis, Pd; Pinus densiflora, Pj; Picea jezoensis, Pr; Psychotria rubra, Pt; Pinus thunbergii, Qa; Quercus acutissima, Qc; Quercus crispula, Qs; Quercus serrata, Ss; Sasa spp.,

n.d.: no data

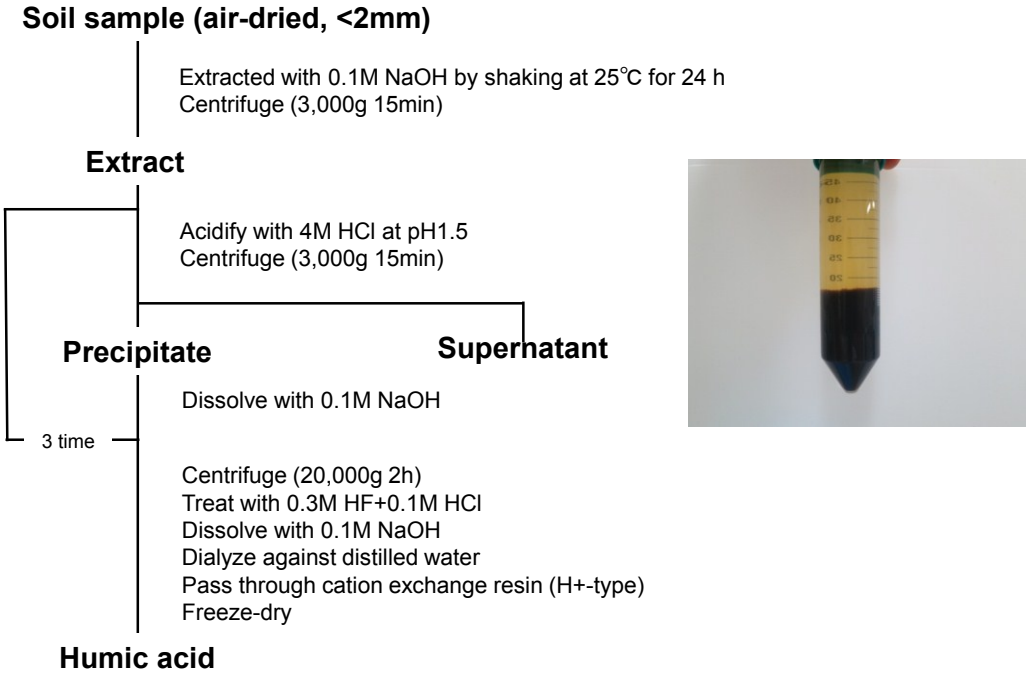

Fig. 2.1 Procedure of extraction and purification of humic acids.

2.2.2. Visible spectroscopy

A 5-mg portion of each freeze-dried HA sample was dissolved in 50 mL of 0.1% NaOH solution, and the absorbance of the solution at 600 nm was measured with a spectrophotometer (UVmini-1240, Shimadzu, Kyoto, Japan) within 2 h of dissolution. The absorbance was used to calculate the absorption coefficient E for a 1% HA solution at 600 nm ($E_{600}^{1\%}$; Yonebayashi, 1989). All the values are expressed on a moisture- and ash-free basis. The moisture content of each HA sample was determined by heating the sample at 105°C for 24 h, and then the ash content was determined by igniting the sample in a microceramic crucible at 550°C for 6 h.

2.2.3. Elemental analysis

The amounts of carbon, hydrogen and nitrogen in the extracted HAs were determined with an elemental analyzer (2400 Series II, Perkin-Elmer Japan, Yokohama, Japan). Oxygen content (O%) was calculated by subtracting C% + H% + N% + ash% from 100%. All the results are expressed on a moisture- and ash-free basis. The elemental compositions are expressed as H/C, O/C, C/N, and O/H atomic ratios, to clarify the stoichiometric relationships between the elements.

2.2.4. Liquid-state ^{13}C nuclear magnetic resonance spectroscopy

Liquid-state ^{13}C nuclear magnetic resonance spectra were recorded at 125.76 MHz on an Avance 500 spectrometer (Bruker GmbH, Karlsruhe, Germany) using 5-mm-diameter sample tubes. Specifically, each HA sample (ca. 30–50 mg) was dissolved in 0.4 mL of 0.5 mol L^{-1} NaOD in D_2O (Iimura et al., 2013). Chemical shifts are reported relative to sodium 3-(trimethylsilyl)propionate-2,2,3,3-D_4 (Euriso-Top, Saint-Aubin, France). For integration of the ^{13}C spectra, we proton-decoupled the ^{13}C signal by the inversed-gated decoupling technique with a pulse width of 45°, an acquisition time of 0.839 s, and a total repetition time of 2.5 s. Scans from 10,000 to 20,000 were accumulated. Resonance areas were calculated by electronic integration. To obtain quantitative information, we divided the spectra into the following six regions (Fujitake and Kawahigashi, 1999; Iimura et al., 2013): alkyl C, 5–48 ppm; O-alkyl C, 48–110 ppm; aryl C, 110–145 ppm; O-aryl C, 145–165 ppm; carboxylic C, 165–190 ppm; and carbonyl C, 190–230 ppm. As proposed by Watanabe and Fujitake (2008), aromaticity was expressed as the ratio of the sum of aryl C and O-aryl C to the sum of alkyl C, O-alkyl C, aryl C, and O-aryl C.

2.2.5. Preparation of plant leaf samples

Leaf samples (from ten C_3 plant and seven C_4 plants) were gathered at the sites where the soil samples were collected or at a hilly site in Ishikawa Prefecture. The plant leaves were oven-dried at 70°C for 2 days and ground to fine powder in a grinder mill.

2.2.6. Determination of $\delta^{13}C$ and $\delta^{15}N$ values of HAs, pulverized bulk soil samples, and plant leaf samples

The $\delta^{13}C$ and $\delta^{15}N$ values of the HAs, pulverized bulk soil samples, and plant leaf samples were determined with an isotope ratio mass spectrometer (IsoPrime IRMS, GV Instruments, UK) linked to an elemental analyzer (EA3000, EuroVector, Italy). The results are expressed as relative δ values calculated as follows:

$$\delta X = [(R_{Xsample}/R_{Xstandard}) - 1] \times 1000\ (‰), \quad (1)$$

where X = C and N, and $R_{Xsample}$ and $R_{Xstandard}$ represent the $^{13}C/^{12}C$ and $^{15}N/^{14}N$ ratios of the sample and the standard, respectively. An L-glutamic acid reference material (USGS40, U.S. Geological Survey, Reston, VA, USA) with a $\delta^{13}C$ value of –26.2‰ and a $\delta^{15}N$ value of –4.5‰ was used as a secondary standard, calibrated relative to the primary standards for carbon (Cretaceous Pee Dee belemnite, Pee Dee, SC, USA) and nitrogen (atmospheric N_2). The experimental errors in the $\delta^{13}C$ and $\delta^{15}N$ values were ≤0.1‰. Each sample was analyzed in triplicate. If the standard deviation was greater than 0.2‰, measurements were repeated until the standard deviation of all the replicates was <0.2‰.

Hiradate et al. (2004) showed that the contributions of C_4 plant–derived and C_3 plant–derived carbon to Andisol HA carbon (CR_{C4} and CR_{C3}, respectively) were calculated from the following equations:

$$\delta^{13}C = (\delta^{13}C_4)(CR_{C4}) + \delta^{13}C_3(1 - CR_{C4}), \quad (2)$$

$$CR_{C3} = 1 - CR_{C4}, \quad (3)$$

where $\delta^{13}C_4$ and $\delta^{13}C_3$ are the $\delta^{13}C$ values of carbon derived from C_4 and C_3 plants, respectively. The contribution percentages were calculated from CR_{C4} and CR_{C3} as $CR_{C4} \times 100$ and $CR_{C3} \times 100$, respectively.

2.3. Results and discussion

2.3.1. Chemical properties of extracted HAs

The carbon, hydrogen, nitrogen, and oxygen contents of the 26 HAs ranged from 51.8% to 60.2%, from 3.10% to 5.71%, from 1.86% to 4.77%, and from 30.9% to 38.5%, respectively (Table 2.2). In all the HAs, the content of each element was within the range of commonly accepted values for soil HAs (Kuwatsuka et al., 1978; Yonebayashi and Hattori, 1988). The average carbon content of the Andisol HAs was significantly higher than that of the non-Andisol HAs. The average hydrogen content and the average nitrogen content of the Andisol HAs were significantly lower than the corresponding averages of the non-Andisol HAs (Table 2.4).

The H/C, O/C, O/H, and C/N atomic ratios and the $E_{600}^{1\%}$ values of the 26 HAs ranged from 0.63 to 1.27, from 0.38 to 0.56, from 0.34 to 0.74, from 14.7 to 41.3, and from 9.5 to 67.5, respectively (Table 2.2). The average H/C ratio of the Andisol HAs was significantly lower than that of the non-Andisol HAs, whereas the average O/H and C/N ratios and the average $E_{600}^{1\%}$ value of the Andisol HAs were significantly higher than the corresponding averages of the non-Andisol HAs (Table 2.4).

The alkyl C, O-alkyl C, aryl C, O-aryl C, carboxylic C, and carbonyl C contents and the aromaticity ranged from 6.05% to 28.4%, from 8.44% to 32.9%, from 16.6% to 49.7%, from 4.37% to 10.3%, from 11.4% to 23.4%, from 1.74% to 5.80%, and from 0.29 to 0.79, respectively (Table 2.3). The average alkyl C and O-alkyl C contents of the Andisol HAs were significantly lower than the corresponding averages of the non-Andisol HAs, whereas the average aryl C content and aromaticity of the Andisol HAs were significantly higher than the corresponding averages of the non-Andisol HAs (Table 2.5).

The $\delta^{13}C$ and $\delta^{15}N$ values of the 26 HAs ranged from –29.1‰ to –16.2‰ and from 0.18‰ to 5.97‰, respectively (Table 2.3). The average $\delta^{13}C$ and $\delta^{15}N$ values of the Andisol HAs were significantly higher than the corresponding averages of the non-Andisol HAs (Table 2.5).

The high $E_{600}^{1\%}$ values, low hydrogen and nitrogen contents, low H/C ratios, low alkyl C and O-alkyl C contents, high O/H and C/N ratios, and high aryl C content and high aromaticity of the Andisol HAs indicate a high degree of humification. These results agree with previously reported results (Fujitake and Kawahigashi, 1999; Kumada, 1987; Kuwatsuka et al., 1978; Yonebayashi and Hattori, 1988). The high $\delta^{13}C$ and $\delta^{15}N$ values of the Andisol HAs also suggest a high degree of humification.

Table 2.2. Elemental compositions, ash contents, and $E_{600}^{1\%}$ values for extracted humic acids.

Humic acid designation	Elemental composition (%)				Ash	Atomic ratios				$E_{600}^{1\%}$
	C	H	N	O	%	H/C	O/C	O/H	C/N	
SGG	59.4	4.14	3.40	33.0	2.59	0.84	0.42	0.50	23.3	35.3
GS	55.0	3.87	3.46	37.7	2.82	0.84	0.51	0.61	21.2	46.8
SN	55.9	3.85	4.02	36.3	2.17	0.83	0.49	0.59	18.5	41.3
DS	59.3	3.48	2.83	34.4	1.65	0.70	0.44	0.62	27.9	42.3
HB	55.4	3.97	3.61	37.0	1.23	0.86	0.50	0.58	20.4	53.4
MK	58.7	3.50	2.09	35.7	0.28	0.72	0.46	0.64	37.5	40.2
MYK	55.5	4.75	4.51	35.2	0.59	1.03	0.48	0.46	16.4	30.9
HZ	57.5	3.60	1.86	37.0	0.22	0.75	0.48	0.64	41.3	64.8
SGM	53.6	4.65	3.74	38.0	2.66	1.04	0.53	0.51	19.1	24.9
HNK	57.4	4.00	3.99	34.6	2.68	0.84	0.45	0.54	19.2	42.3
YGD	58.9	3.10	3.29	34.7	2.86	0.63	0.44	0.70	23.9	61.2
SA	56.7	3.82	2.09	37.4	0.31	0.81	0.49	0.61	36.2	53.2
MZ13	56.6	4.03	3.07	36.3	0.30	0.85	0.48	0.56	24.5	53.5
ND0-20	57.3	3.19	1.96	37.5	0.37	0.67	0.49	0.74	39.0	67.5
TK-05	54.6	5.42	3.79	36.2	0.87	1.19	0.50	0.42	19.2	10.8
KRS	51.8	5.09	4.70	38.5	1.32	1.18	0.56	0.47	14.7	12.1
SZK	54.8	4.81	4.74	35.6	4.77	1.05	0.49	0.46	15.4	19.8
KYG	53.2	5.47	4.71	36.6	0.03	1.23	0.52	0.42	15.1	9.5
KRZ	55.0	5.18	3.87	35.9	0.58	1.13	0.49	0.43	18.9	9.8
YSG	54.5	4.83	4.12	36.6	0.03	1.06	0.50	0.47	17.6	20.1
TGD	54.1	5.38	4.25	36.3	0.27	1.19	0.50	0.42	17.0	21.5
HO-99	60.2	5.68	3.16	30.9	1.95	1.13	0.38	0.34	25.4	14.4
NG	53.4	5.39	4.77	36.4	1.98	1.21	0.51	0.42	14.9	14.1
KT	54.1	5.71	3.30	36.9	1.00	1.27	0.51	0.40	21.9	16.1
YON	52.0	4.90	4.64	38.5	1.36	1.13	0.56	0.49	14.9	19.1
IJ	58.4	4.77	2.15	34.6	1.10	0.98	0.44	0.45	36.2	19.0

Table 2.3. Distributions of carbon species (%), aromaticity values, and $\delta^{13}C$ and $\delta^{15}N$ values for extracted humic acids.

Humic acid designation	Carbon species [a]						Aromaticity	$\delta^{13}C$ (‰)	$\delta^{15}N$ (‰)
	C_{Al} (5–48)	C_{OMe} (48–110)	C_{Ar} (110–145)	C_{Ph} (145–165)	C_{COOH} (165–190)	C_{CO} (190–230)			
SGG	6.05	13.0	49.7	6.87	19.2	5.26	0.75	−19.6	4.41
GS	7.18	19.4	46.3	5.99	18.4	2.79	0.66	−17.6	5.48
SN	11.2	23.1	34.8	7.90	19.2	3.80	0.55	−19.7	3.91
MZ13	18.0	21.2	38.6	4.37	13.7	4.14	0.52	−21.3	5.97
HB	9.70	14.1	44.2	8.80	19.1	4.20	0.69	−17.6	4.26
MK	6.31	8.44	47.0	9.90	23.4	4.91	0.79	−26.2	5.12
MYK	19.4	26.5	30.2	6.94	13.9	3.13	0.45	−23.0	3.48
HZ	14.3	25.8	38.0	7.70	11.4	2.69	0.53	−17.8	4.05
SGM	19.4	17.9	35.0	6.82	17.9	2.94	0.53	−22.6	5.18
HNK	14.6	18.5	36.7	7.40	19.6	3.20	0.57	−24.9	3.44
YGD	8.96	16.2	47.3	6.90	18.9	1.74	0.68	−23.3	5.72
SA	18.1	18.8	42.4	5.78	12.7	2.20	0.57	−25.4	3.97
DS	10.2	15.1	39.7	8.40	21.3	5.30	0.66	−21.8	4.77
ND0-20	12.2	21.0	44.6	4.97	14.6	2.67	0.6	−16.2	4.28
TK-05	22.3	29.3	19.5	5.00	18.3	5.60	0.32	−26.7	0.37
KRS	22.4	26.1	23.9	7.06	16.6	3.91	0.39	−25.7	1.33
KT	22.3	29.4	19.4	5.00	18.1	5.80	0.32	−26.8	0.56
KYG	22.0	30.0	20.5	5.42	17.8	4.32	0.33	−26.7	1.78
KRZ	22.4	26.1	23.9	7.06	16.6	3.91	0.39	−27.8	0.18
YSG	17.8	26.2	29.2	5.90	19.2	1.80	0.44	−26.8	2.26
TGD	27.1	24.3	18.3	7.40	18.2	4.70	0.33	−27.2	0.59
HO-99	28.4	27.1	18.7	4.54	16.9	4.41	0.29	−27.2	3.85
NG	17.7	27.7	24.5	7.90	18.9	3.20	0.42	−25.5	2.54
SZK	17.8	26.2	29.2	5.90	19.2	1.80	0.44	−23.9	3.45
YON	21.3	32.9	16.6	5.64	18.8	4.85	0.29	−29.1	0.36
IJ	16.9	21.5	35.9	10.3	13.0	2.70	0.55	−27.2	1.95

[a] C_{Al}, alkyl C; C_{OMe}, *O*-alkyl C; C_{Ar}, aryl C; C_{Ph}, *O*-aryl C; C_{COOH}, carboxylic C; C_{CO}, carbonyl C; aromaticity: (aryl C + *O*-aryl C)/(alkyl C + *O*-alkyl C + aryl C + *O*-aryl C). The values in the parentheses in the column headings indicate ranges of chemical shift values (δ, ppm).

Table 2.4. Average elemental compositions, atomic ratios, and $E_{600}^{1\%}$ values for humic acids extracted from Andisols and non-Andisols.

Soil type	Elemental composition (%)				Atomic ratios				$E_{600}^{1\%}$
	C	H	N	O	H/C	O/C	O/H	C/N	
Andisols (n = 14)	56.9	3.85	3.14	36.1	0.815	0.476	0.593	26.3	47.0
Non-Andisols (n = 12)	54.7	5.22	4.02	36.1	1.15	0.497	0.433	19.3	15.5
	**	***	***	—	***	—	***	*	***

* Significant at the 5% level. ** Significant at the 1% level. *** Significant at the 0.1% level.

Table 2.5. Average carbon species, and aromaticity, $\delta^{13}C$, and $\delta^{15}N$ values for humic acids extracted from Andisols and non-Andisols.

Soil type	Carbon species [a]						Aromaticity	$\delta^{13}C$ (‰)	$\delta^{15}N$ (‰)
	C_{Al} (5–48)	C_{OMe} (48–110)	C_{Ar} (110–145)	C_{Ph} (145–165)	C_{COOH} (165–190)	C_{CO} (190–230)			
Andisols (n = 14)	12.5	18.5	41	7.05	17.4	3.5	0.68	−21.2	4.57
Non-Andisols (*n* = 12)	21.5	27.2	23.3	6.43	17.6	3.92	0.38	−26.7	1.6
	***	***	***	—	—	—	***	***	***

[a] C_{Al}, alkyl C; C_{OMe}, *O*-alkyl C; C_{Ar}, aryl C; C_{Ph}, *O*-aryl C; C_{COOH}, carboxylic C; C_{CO}, carbonyl C; aromaticity: (aryl C + *O*-aryl C)/(alkyl C + *O*-alkyl C + aryl C + *O*-aryl C). The values in the parentheses in the column headings indicate ranges of chemical shift values (δ, ppm). *** Significant at the 0.1%

Plots of H/C versus O/C have been used for analyzing coalification (van Krevelen, 1950) and for characterizing HAs (Fujitake et al., 1999; Kuwatsuka et al., 1978; Yonebayashi and Hattori, 1988). We prepared a plot of H/C versus O/C for the 26 HAs samples analyzed in this study (Fig. 2.2); in the plot, demethanation, dehydration, and decarboxylation are indicated by the gray arrows (van Krevelen, 1950). The Andisol HAs were more demethanated and dehydrated than the non-Andisol HAs, indicating that aliphatic moieties split off from the humic molecules in the early stage of humification and that dehydrative condensation may have occurred as humification proceeded (Yonebayashi and Hattori, 1988). Many investigators have reported that the number of carboxyl and carbonyl groups of HAs increases during the late stage of humification, and that the number of alcoholic hydroxyl group of HAs decreases during the early stage of humification (Kumada, 1987; Kuwatsuka et al., 1978; Yonebayashi and Hattori, 1988). Estimation of the seeming dehydration from the atomic ratio was hindered by the competition between changes in these functional groups (Yonebayashi and Hattori, 1988): these structural changes are reflected in the elemental composition of Andisol HAs (Fujitake and Kawahigashi, 1999; Ikeya et al., 2004; Yonebayashi and Hattori, 1988).

Generally, the increase of the $E_{600}^{1\%}$ value is attributed to the increase of the degree of humification (darkening) of HAs, and the decrease of the H/C ratio is ascribed to the increase of the saturated bond content of HAs. We observed a strong negative correlation between H/C ratio and $E_{600}^{1\%}$ (r = –0.908, significant at the 0.1% level, Fig. 2.3b), which is in agreement with previously reported results (Fujitake et al., 1999; Kumada, 1987; Yonebayashi and Hattori, 1988).

In contrast, the O/H ratio is an effective index of the degree of HA oxidation. We prepared a plot of H/C ratio versus O/H ratio (Fig. 2.3a); such plots have been used to analyze the progress of HA humification (Kumada, 1987). A highly significant correlation coefficient between H/C ratio and O/H ratio was observed (r = –0.919, significant at the 0.1% level), in agreement with previously reported results (Fujitake et al., 1999). Humification of Andisol HAs occurs in a more oxygen-rich soil environment than humification of non-Andisol HAs (Kumada, 1987), and thus Andisol HAs show a higher degree of oxidation (Fujitake et al., 1999).

The aryl C content of HAs is an effective index of their degree of humification (Kögel-Knabner et al., 1991; Watanabe and Fujitake, 2008). We observed a strong negative correlation between aryl C content and H/C ratio (r = –0.906, significant at the 0.1% level, Fig. 2.3c). At the same time a strong correlation (r = 0.817) between H/C ratio and alkyl C content was found to be significant at the 0.1% level. These results suggest that the decrease in the saturated aliphatic C content directly reflects the increase in the aryl C content (Fujitake and Kawahigashi, 1999) as humification (darkening) proceeds.

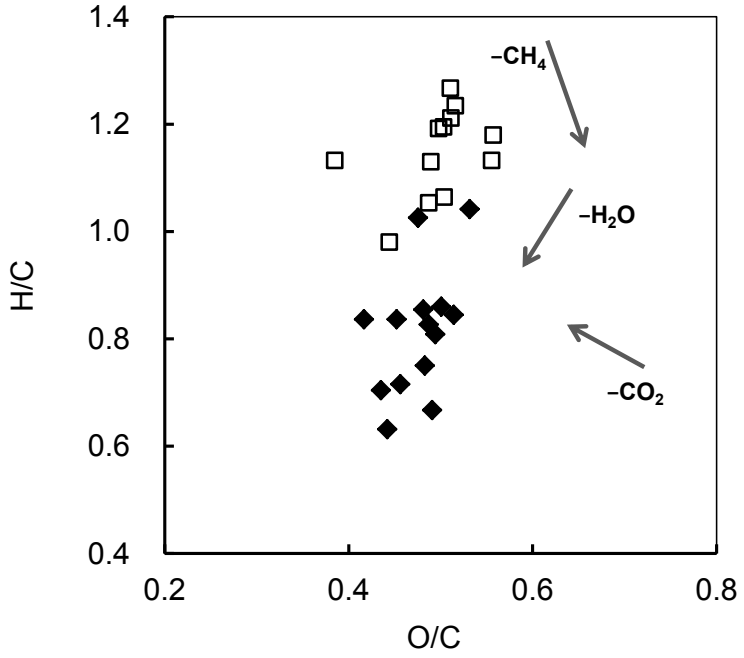

Fig. 2.2. Plots of H/C versus O/C for the 26 humic acids extracted from ◆, Andisols and □, non-Andisols.

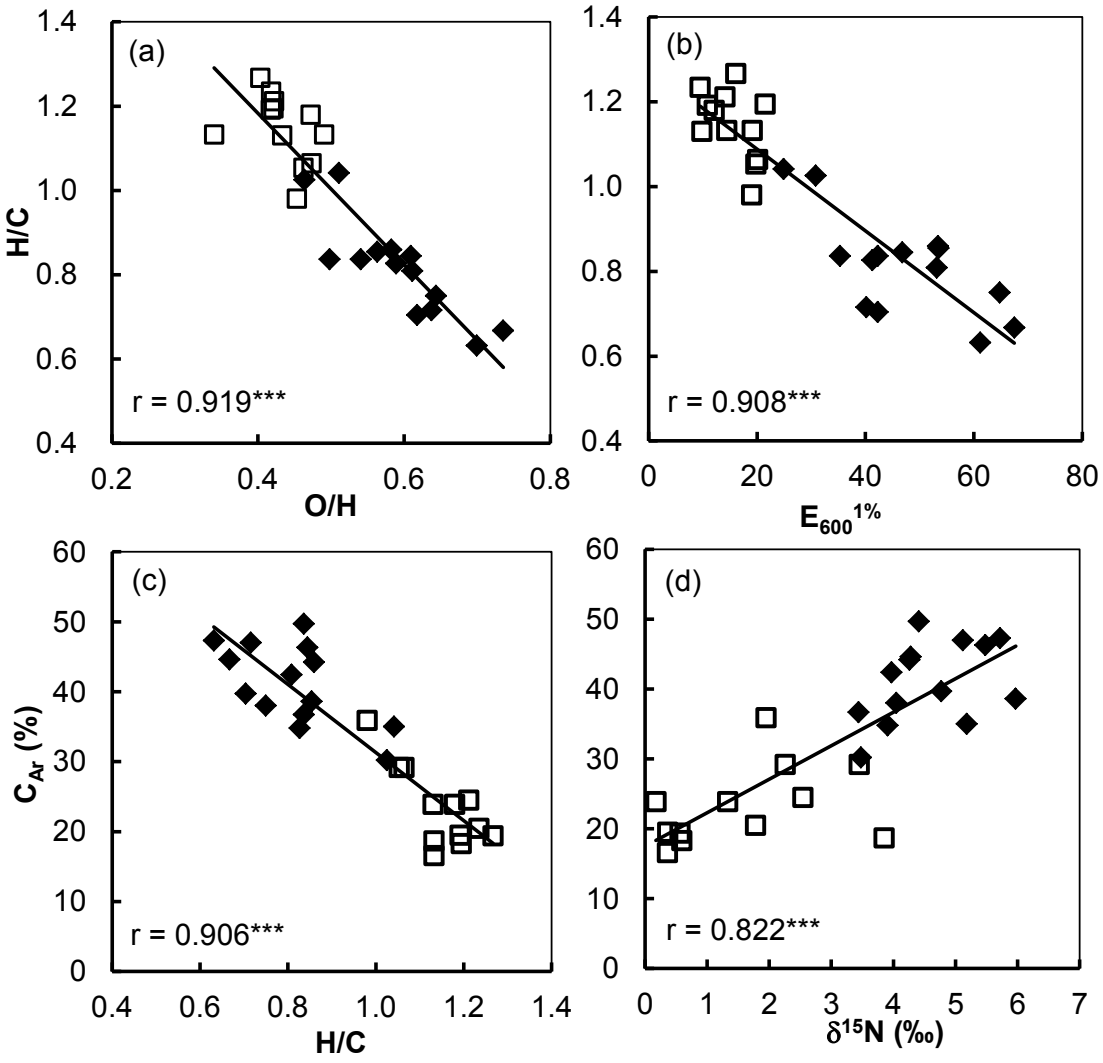

Fig. 2.3. Plots of (a) H/C vs O/H, (b) H/C vs $E_{600}^{1\%}$, (c) aryl C (C_{Ar}) content vs H/C, and (d) aryl C (C_{Ar}) content vs $\delta^{15}N$ for the 26 humic acids. *** Significant at the 0.1% level. See the caption of Fig. 2.1 for a key to the symbols.

The $\delta^{15}N$ values of soil organic matter depend on the degree of decomposition of the source plants and alteration of soil organic matter during humification (Marin-Spiotta et al., 2009). A plot of aryl C content versus $\delta^{15}N$ (Fig. 2.3d) revealed a strong correlation between aryl C content and $\delta^{15}N$ value (r = 0.822, significant at the 0.1% level). In addition, significant positive correlations between $\delta^{15}N$ and aromaticity and between $\delta^{15}N$ and $E_{600}{}^{1\%}$ (r = 0.770 and 0.743, respectively, significant at the 0.1% level) were observed. Significant negative correlation between $\delta^{15}N$ and alkyl C, *O*-alkyl C content, and H/C ratio (r = –0.680, –0.720, and –0.792, respectively, significant at the 0.1% level) were observed. These results suggest that the increase in $\delta^{15}N$ reflects the increase in the degree of HA humification, which is in agreement with previously reported results (Balieiro et al., 2012). Rivas et al. (2012) reported significant relationship was not observed between bulk soil $\delta^{15}N$ values and any of the physicochemical properties. The samples they used were Andisols but we used Andisols and Inceptisols. We suspect the difference in the soil types have influence on the results.

2.3.2 $\delta^{13}C$ and $\delta^{15}N$ values of extracted HAs and C_3 and C_4 plant samples

We determined the $\delta^{13}C$ and $\delta^{15}N$ values of 17 plant samples (10 C_3 samples and 7 C_4 samples; Table 2.6) to investigate the relationships between $\delta^{13}C$ and $\delta^{15}N$ for the plant samples and the HAs. The $\delta^{13}C$ and $\delta^{15}N$ values of the C_3 plants ranged from –32.2‰ to –26.7‰ (average, –29.3‰) and from –4.39‰ to 0.29‰ (average, –1.38‰), respectively. The $\delta^{13}C$ and $\delta^{15}N$ values of the C_4 plants ranged from –14.2‰ to –11.7‰ (average, –12.8‰) and from –2.92‰ to –0.60‰ (average, –1.38‰), respectively. There was no significant difference between the $\delta^{13}C$ and $\delta^{15}N$ values we determined in this study and the previously reported values (Akamatsu et al., 2004; Inagaki et al., 2004; Yoneyama et al., 2001). There are no previously published $\delta^{15}N$ data for C_4 plants in Japan for comparison with our data for *M. sinensis*. The $\delta^{15}N$ values that we determined for *M. sinensis* leaves were low because symbiotic nitrogen-fixing bacteria are present in the leaves, stems, and roots of this species (Miyamoto et al., 2004).

We plotted $\delta^{13}C$ against $\delta^{15}N$ for the non-Andisol HAs, along with the average value for the C_3 plant leaves (Fig. 2.4). The difference between the $\delta^{13}C$ values for the HAs and the C_3 plant leaves ranged from 0.2‰ to 5.4‰. Peri et al. (2012) showed that the difference in $\delta^{13}C$ between foliar samples and surface soil in native forests varies between 2‰ and 6‰. We observed a significant correlation coefficient between the $\delta^{13}C$ and $\delta^{15}N$ values of the non-Andisols and the average of C_3 plant leaves (r = 0.683, significant at the 5% level); the regression line is shown in Fig. 2.3 ($\delta^{13}C = 0.672(\delta^{15}N) - 27.8$). The data for the non-Andisol HAs and C_3 plant leaves were distributed along this line, where $\delta^{13}C$ increases by 0.67‰ for every 1‰ increase in $\delta^{15}N$. According to Marin-Spiotta et al. (2009), ^{13}C and ^{15}N enrichment in soil organic matter often

Table 2.6. Values of $\delta^{13}C$ and $\delta^{15}N$ for leaves of C_3 and C_4 plants sampled for this study.

	Plant species	Sampling location	$\delta^{13}C$ (‰)	$\delta^{15}N$ (‰)
C_3 plants	*Sasa* sp.	Noda, Kanazawa, Ishikawa	−29.7	0.14
	Sasa sp.	Nukadani, Ishikawa	−26.7	−4.39
	Sasa sp.	Nomi, Ishikawa	−29.6	−1.99
	Quercus serrata	Nonoichi, Ishikawa	−28.7	−0.74
	Quercus serrata	Noda, Kanazawa, Ishikawa	−27.0	−1.03
	Cryptomeria japonica	Noda, Kanazawa, Ishikawa	−28.1	−2.95
	Zelkova serrata	Nonoichi, Ishikawa	−32.2	0.29
	Zelkova serrata	Thurugi, Ishikawa	−30.1	−0.94
	Fagus crenata	Thurugi, Ishikawa	−30.3	−0.06
	Deciduous hardwood	Noda, Kanazawa, Ishikawa	−30.9	−2.12
	Average		−29.3	−1.38
C_4 plants	*Miscanthus sinensis*	Hakusan, Ishikawa	−12.5	−0.97
	Miscanthus sinensis	Noda 1, Kanazawa, Ishikawa	−12.6	−0.60
	Miscanthus sinensis	Noda 2, Kanazawa, Ishikawa	−13.0	−1.37
	Miscanthus sinensis	Noda 3, Kanazawa, Ishikawa	−14.2	−1.10
	Miscanthus sinensis	Kigo, Kanazawa, Ishikawa	−13.1	−2.10
	Miscanthus sinensis	Kawatabi 1, Miyagi	−11.7	−0.61
	Miscanthus sinensis	Kawatabi 2, Miyagi	−12.3	−2.92
	Average		−12.8	−1.38

reflects the degree of biodegradation and humification. Connin et al. (2001) reported that $\delta^{15}N$ clearly increases relative to $\delta^{13}C$ with microbial degradation of litter that is easily decomposed by microorganisms. Iimura et al. (2013) reported that $\delta^{13}C$ for a size-separated HA fraction increases with increasing $\delta^{15}N$ and that the $\delta^{13}C$:$\delta^{15}N$ ratios for these HAs fall along two lines, a 1:1 line and a 1:3 line. These investigators suggested that the HAs that fall along the 1:1 line may be more resistant to microbial attack than those that fall along the 1:3 line. Because the non-Andisol HAs that we extracted were whole HAs, and were not HAs size-separated as Iimura et al. (2013) did, the 0.67:1 $\delta^{13}C$:$\delta^{15}N$ ratio that we observed lies between the 1:1 and 1:3 ratios observed in the study of Iimura et al. (2013).

We also plotted $\delta^{13}C$ versus $\delta^{15}N$ for the Andisol HAs, as well as the average value for the C_4 plants (Fig. 2.4). The $\delta^{13}C$ and $\delta^{15}N$ values of the Andisol HAs ranged from –26.2‰ to –16.2‰ and from 3.44‰ to 5.97‰, respectively, and there was no correlation between the $\delta^{13}C$ and $\delta^{15}N$ values of the Andisol HAs. The $\delta^{13}C$ values of the Andisol HAs were generally higher than the $\delta^{13}C$ values of the non-Andisol HAs and fell between the values for the C_3 and C_4 plants. These results clearly indicate that the Andisol HAs were derived from both C_4 and C_3 plants (Yoneyama et al., 2001). The contributions of C_4 plant–derived and C_3 plant–derived carbon to HA carbon (CR_{C4} and CR_{C3}, respectively) were calculated from Eq. 2.

Yoneyama et al. (2001) expressed that equation 2 is based on the assumption that microbial degradation of plant material is not associated with appreciable isotopic fractionation. However, Wang et al. (2008) determined $\delta^{13}C$ values of soil organic matter for 14 soil profiles at three sites and found that the isotopic difference between vegetation and soil organic matter was 1.8‰ for surface soil; that is, isotopic fractionation during plant decomposition resulted in ^{13}C-enrichment of the soil organic matter. These investigators suggested substituting $\delta^{13}C - 1.8$ for $\delta^{13}C$ in Eq. 2.

As described above, the $\delta^{13}C$ and $\delta^{15}N$ values of the non-Andisol HAs increased with the progress of humification of C_3 plant–derived HAs. Because isotopic fractionation during plant decomposition resulted in ^{13}C and ^{15}N enrichments of the HAs, the $\delta^{15}N$:$\delta^{13}C$ ratio for Andisol HAs should be 1:0.67, as was the case for the non-Andisol HAs. To calculate CR_{C4}, we could not substitute the $\delta^{13}C$ values of the HAs into Eq. 2. In Fig. 2.4, we drew a line corresponding to $\delta^{15}N$:$\delta^{13}C$ = 1:0.67 from point A (the data point for one of the HAs) to the line linking the average $\delta^{15}N$ and $\delta^{13}C$ values for the C_3 and C_4 plants; these two lines intersect at point A′. The line that includes point A and has a slope of 0.67 can be expressed by Eq. 4:

$$\delta^{13}C = 0.67(\delta^{15}N) + b. \quad (4)$$

By substituting the values of point A ($\delta^{13}C_A$, $\delta^{15}N_A$) into Eq. 4, we obtained the value of b. By

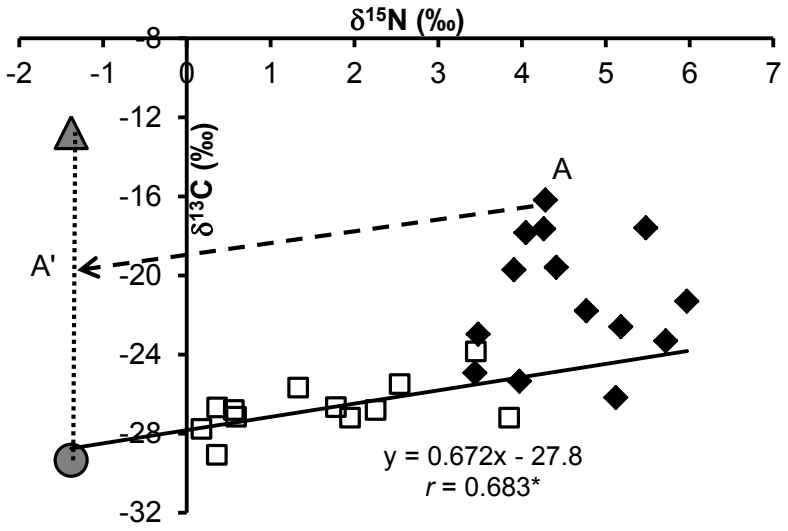

Fig. 2.4. Plots of $\delta^{13}C$ vs $\delta^{15}N$ for the 26 humic acids, as well as the average values for C_3 plant and C_4 plant . *Significant at the 5% level. See the caption of Fig. 2.1 for a key to the symbols for the humic acids. The solid line is the regression line for the non-Andisol HAs. Point A is the data point for one of the HAs. Point A′ is a plant $\delta^{15}N$ value with a correction for the $\delta^{15}N$ value at point A. The dashed line is the line that includes point A and corresponds to $\delta^{15}N$:$\delta^{13}C$ = 1:0.67.

Table 2.7. Contribution ratios of C_4 plant-derived C to humic acid C (CR_{C4}) for Andisol humic acids calculated by the usual method (uncorrected) and the proposed method (corrected).

Humic acid designation	Corrected CR_{C4}	Uncorrected CR_{C4}	Difference
SGG	0.37	0.59	0.22
GS	0.45	0.71	0.26
SN	0.38	0.58	0.20
MZ13	0.21	0.48	0.27
HB	0.50	0.71	0.21
MK	-0.05	0.19	0.24
MYK	0.20	0.38	0.18
HZ	0.49	0.69	0.20
SGM	0.16	0.41	0.24
HNK	0.08	0.27	0.18
YGD	0.10	0.36	0.26
SA	0.04	0.24	0.20
DS	0.23	0.45	0.23
ND0-20	0.58	0.79	0.21

calculating the $\delta^{13}C$ value for $\delta^{15}N = -1.38‰$ (average $\delta^{15}N$ value for the C_3 and C_4 plants), we were able to obtain the coordinates for point A′. Substituting the $\delta^{13}C_{A'}$ value of point A′ into Eq. 2 allowed us to calculate the corrected contribution ratio of C_4 plant–derived carbon at point A. We used the average $\delta^{13}C_4$ and $\delta^{13}C_3$ values of –12.8‰ and –29.3‰, respectively (Table 2.6), to determine corrected CR_{C4} values for the Andisol HAs, which are shown in Table 2.7, along with the uncorrected CR_{C4} values obtained by means of the usual method. The corrected CR_{C4} values (–5% to 58%) were approximately 22% lower than the uncorrected CR_{C4} values (19%–79%). As a result of performing a sensitivity analysis on the calculation method of the CR_{C4}, the standard deviation of the model case was admitted that sufficiently small with respect to the average value (data not shown). CR_{C4} is acceptable for the objective of this study, although CR_{C4} contains the small errors. Yoneyama et al. (2001) reported that the $\delta^{13}C$ values for organic carbon in cropland soil range between –25‰ and –17‰, indicating that up to 70% of the soil organic carbon originates from C_4 plants (presumably *M. sinensis*). Hiradate et al. (2004) reported that HAs in Japanese volcanic ash soils originate from both C_3 and C_4 plants and that the CR_{C4} values range from 18% to 52%. In this study, we found that the corrected CR_{C4} value for Andisol HAs was less than 58%, indicating that the proportion of HA carbon that originated from C_4 plants was not particularly high.

The source plants of soil HAs can be estimated by means of plant opal phytolith analysis of soil samples (Sase and Hosono, 1996). Phytolith analysis (data not shown) suggests that dwarf bamboo (*Sasa* spp.) and *M. sinensis* were the predominant C_3 and C_4 plants, respectively, contributing to the Andisol HAs.

2.3.3. $\delta^{13}C$ and $\delta^{15}N$ values of bulk soils

We also determined the $\delta^{13}C$ and $\delta^{15}N$ values of the bulk soils (surface soils) from which the HAs were extracted (Fig. 2.5). Regression analysis revealed a significant positive correlation between the $\delta^{13}C$ values of the HAs and those of the bulk soils (r = 0.983, significant at the 0.1% level; Fig. 2-5a). The difference between the two sets of $\delta^{13}C$ values was not significant (t = 0.265, no significance at 5% level). Hiradate et al. (2004) reported a strong positive correlation between the $\delta^{13}C$ values of HAs and those of bulk soil organic matter in surface volcanic ash soils, and they observed no significant difference between the two sets of values. Watanabe and Takada (2006) reported significant differences between the $\delta^{13}C$ values of humus fractions and bulk soil organic matter with buried humic layers in volcanic ash soil profiles; however, the $\delta^{13}C$ values of the HAs and bulk soil organic matter in surface soils were almost the same. Balieiro et al. (2012) reported that the values of $\delta^{13}C$ for bulk soils and for HAs were similar (no significance at the 5% level) for 17 surface soils (non-Andisol). These results

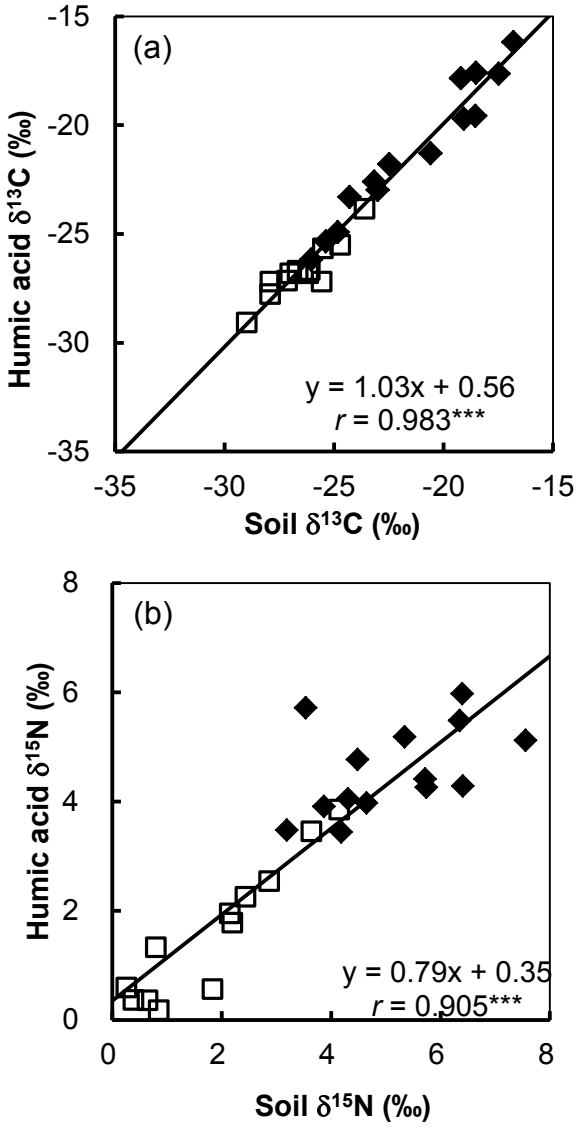

Fig. 2.5. Plots of (a) $\delta^{13}C$ values of humic acids vs $\delta^{13}C$ values of crude soils and (b) $\delta^{15}N$ values of humic acids vs $\delta^{15}N$ values of crude soils. ***Significant at the 0.1% level. See the caption of Fig. 2.1 for a key to the symbols.

suggest that HAs and other fractions contained in soil organic matter have the same origin. Regression analysis also revealed a significant positive correlation between the $\delta^{15}N$ values of the HAs and those of the bulk soils (r = 0.905, significant at the 0.1% level; Fig. 2.5b). The $\delta^{15}N$ values of the HAs were significantly lower than those of the bulk soils (t = 2.363, significant at the 5% level). Balieiro et al. (2012) reported that the $\delta^{15}N$ values obtained for bulk soils and for HAs were not significantly different (no significance at the 5% level) for 17 surface soils (non-Andisol). Additional data are necessary to reveal the complex factors affecting ^{15}N in soil organic matter during humification processes.

Chapter 3. Evaluation of stacking nanostructure in soil humic acids by analysis of the 002 band of their X-ray diffraction profiles

3.1. Introduction

The use of XRD to analyze the stacking nanostructure of humic substances has a long history; XRD profiles of FAs and HAs were measured in the late 1950s (Kobo and Tatsukawa 1959). HAs have turbostratic structure, as indicated by the 002 band at around 25° (2θ for Cu Kα) and the 10 band at around 42° in the XRD profile of soil HAs (Yamane et al. 1978). The 002 band provides information about the degree of stacking of C-layer planes and the distance between C-layer planes (Iwashita et al. 2004). Furthermore, the 11 band at around 80°, which is derived from the C planes in the turbostratic structure, has been observed in the XRD profile of soil HAs (Ikeya et al. 2011). Turbostratic carbon structure is built up from randomly stacked C planes. Calculation of the diffraction patterns in terms of the random stacking networks model shows 00*l*-type reflections with a symmetric peak (e.g., the 002 band) and *hk*-type reflections with an asymmetric peak (e.g., the 10 and 11 bands), which are the characteristics of stacking structure and C-layer plane structure, respectively, in turbostratic carbon structure (Reshetenko et al. 2003). Carbon black is a typical turbostratic carbon structure.

Several previous structural analyses of soil HAs by means of XRD have been published (Ikeya et al. 2011; Matsui et al. 1984; Schnitzer et al. 1991; Xing and Chen 1999). Ikeya et al. (2011) analyzed the 11 band, and their analysis indicated that the size of the condensed aromatic rings along the *a* axis (L_a) in HAs ranges from 0.48 to 1.68 nm, corresponding to condensed aromatic components with 4 to 37 rings. Xing and Chen (1999) suggested that HAs have stacking structure, as indicated by the presence of 002 bands at around 25° and 10 bands at around 42° in their XRD profiles. Another peak has been detected at around 20° (γ band; distance between two adjacent layers, 0.43 nm) in the XRD profile of HAs, and this peak has been attributed to aliphatic compounds or lignin (Matsui et al. 1984; Schnitzer et al. 1991; Xing and Chen 1999). Schnitzer et al. (1991) separated the 002 and γ bands by curve fitting and calculated HA aromaticity from the areas of the two peaks. Fourier transform analysis of the 002 band by Matsui et al. (1984) indicated that stacked structures are present in darkly colored Andisol HAs, but the method used is applicable only to Andisol HAs and not to the other soil HAs, because the γ band interferes with the 002 band. Therefore, the stacking nanostructures of

HAs from soils other than Andisols have not been determined. Development of models for the chemical structure of humic substances, including HAs, would improve our understanding of their behavior in the environment.

In the present study, I used XRD analysis to evaluate the turbostratic structure of Andisol, Inceptisol, and Entisol HAs (12 soil samples in total) using a new method involving waveform separation. I analyzed the relationship between the stacking nanostructure properties of the HAs and their chemical structure properties, which were determined by ^{13}C NMR spectroscopy.

3.2. Materials and Methods

3.2.1. Samples

I collected samples of six Andisols, three Entisols, and three Inceptisols from various regions in Japan (Table 1). The soil samples were air-dried and passed through a 2-mm-mesh sieve. Fine roots and litter were removed from the sieved samples with tweezers. To obtain humus extracts, an extractant (1:1 mixture of aqueous 0.1 mol L^{-1} NaOH and 0.1 mol L^{-1} $Na_4P_2O_7$) was added to each soil sample at a concentration of 300 mL per g soil C, and the resulting suspension was allowed to stand for 24 h at 25 °C under a N_2 atmosphere with intermittent shaking. This alkaline extraction was repeated until the extract was pale in color. The combined humic extracts were acidified with 6 mol L^{-1} H_2SO_4 to pH 1.5 and then allowed to stand overnight at room temperature. The resulting precipitate, which included the HAs, was separated by centrifugation at 4,000*g* for 15 min. The recovered solids (the HA fraction) were purified by redissolution in the NaOH/$Na_4P_2O_7$ solution, reprecipitation with 6 mol L^{-1} H_2SO_4, and subsequent centrifugation. This purification of the HA fraction was repeated until the acidic supernatant was light yellow. The solid HAs were dissolved in a small amount of 0.1 mol L^{-1} NaOH and centrifuged at 20,000 *g* for 2 h to remove coarse-grained materials. To remove fine-grained materials, we acidified the HAs to pH 1.5, added a solution of HF (0.3 mol L^{-1}) and HCl (0.1 mol L^{-1}), and stirred the resulting suspension for 5 h at room temperature. The suspension was then centrifuged, and the solid was collected and washed with deionized water, dissolved in a small amount of 0.1 mol L^{-1} NaOH, dialyzed (BioDesign Dialysis Tubing, MWCO 3500; BioDesign Inc., Carmel, NY, USA) against distilled water, passed through Amberlite IR-120 resin (H^+ form), and then freeze-dried (Yonebayashi and Hattori, 1988).

3.2.2. Characterization of HAs

The elemental compositions of the HAs (%C, %H, and %N) were determined with an

elemental analyzer (2400 II, Perkin-Elmer Japan, Yokohama, Japan); %O was calculated by subtracting (%C + %H + %N + %ash) from 100%. The elemental compositions are expressed as H/C, O/C, and O/H atomic ratios, to clarify the stoichiometric relationships between the elements.

The degree of darkness (A_{600}/C, where A_{600} is the absorbance at 600 nm and C is the organic C concentration in milligrams of C per milliliter) of the HAs was determined according to the method of Ikeya and Watanabe (2003). The absorbance at 600 nm of HAs dissolved in alkali was measured with a UV–vis spectrophotometer (UVmini-1240, Shimadzu) within 2 h after dissolution. Organic C concentration was determined with a total organic carbon analyzer (TOC-V_{CSH}, Shimadzu, Kyoto, Japan).

Liquid-state ^{13}C NMR spectra were recorded at 100.5 MH_Z on a JEOL ECX 400 spectrometer (JEOL, Tokyo, Japan). Each HA (50 mg) was dissolved in 0.5 mL of 0.5 mol L^{-1} NaOD in D_2O in a 5-mm-diameter sample tube. Chemical shifts were referenced to sodium 3-trimethylsilylpropionate-2,2,3,3-D_4 (0 ppm). To quantify the ^{13}C NMR spectra, ^{13}C signals were proton-decoupled by means of the inverse-gated decoupling technique under the following operating conditions: pulse width, 4.9 μs; acquisition time, 1.04 s; pulse delay, 2.5 s. A total of 15,000 to 20,000 scans were accumulated, and line broadening was set at 50 Hz. Resonance areas were calculated by means of electronic integration. The spectra were divided into the following six regions (Fujitake and Kawahigashi 1999): alkyl C, 0–48 ppm; O-alkyl C, 48–110 ppm; aryl C, 110–145 ppm; O-aryl C, 145–165 ppm; carboxylic C, 165–190 ppm; and carbonyl C, 190–230 ppm. Aromaticity as determined by NMR ($f_{a\text{-}NMR}$) was given by the ratio of (aryl C + O-aryl C) to (alkyl C + O-alkyl C + aryl C + O-aryl C) (Watanabe and Fujitake 2008). The O-aryl C content was very small and was classified as aromatic C, along with aryl C (110–165 ppm).

3.2.3. Analysis of the 002 band of the XRD profile

Forty to fifty milligrams of each sample (freeze-dried HA, carbon black, or lignin) was packed into a 0.2-mm-deep hole on a nonreflecting silicon holder (20 (W) × 18 (H) × 0.2 (T) mm) (Rigaku, Tokyo, Japan), and XRD patterns were measured with a diffractometer (MiniFlex, Rigaku, Tokyo, Japan) with Cu Kα radiation (wavelength, 0.154 nm). The generator was set at 30 kV and 15 mA. Samples were scanned over a 2θ range from 5° to 90° with a step size of 0.1° and a scanning speed of 2° min^{-1}. Aburahi HAs (sample designation SA, Table 1) were analyzed in triplicate to estimate the experimental error, whereas a single data set was obtained for the other soil HAs. The XRD profiles were corrected with the Lorentz factor, the polarization factor, and the adsorption factor (Iwashita et al. 2004). After those corrections, the smoothing treatment

was done using a weighted mean method (smoothing number, 11). The areas covering the 2θ range from 5° to 60° were separated into four peaks by calculation of the second derivative and comparison of the profiles of the reference and HA samples; and least-squares iterative curve fitting was carried out with the Voigt function using PeakFit (ver. 4.12, SeaSolve Software Inc., Framingham, MA, USA). The peak positions, widths, and areas were determined. The validity of the profile fitting can be evaluated from the *R*-factor, which is defined as follows:

$$R\text{-factor} = [\Sigma_{2\theta}|I(2\theta) - P_r(2\theta)|)/\Sigma_{2\theta}I(2\theta)] \times 100 \quad (1)$$

where $I(2\theta)$ is the experimentally observed intensity profile, and $P_r(2\theta)$ is the profile fitted by calculation. The value of the *R*-factor should be as small as possible. The spacing between C planes (d_{002}) in the HAs was calculated from the the position of the peak for the separated 002 band by means of Bragg's equation:

$$d_{002} = \lambda/(2 \sin \theta) \quad (2)$$

where λ is the wavelength of the X-rays in nanometers (0.154 nm for Cu Kα), and θ is Bragg's angle at a diffraction line. The mean thickness of the stacking nanostructure along the *c* axis (L_c) was calculated from the the full-width at half maximum and the position of the peak for the 002 band by means of Scherrer's equation (Iwashita et al. 2004):

$$L_c = K\lambda/(\beta \cos \theta) \quad (3)$$

where β is the full-width at half maximum of the 002 band, and *K* is Scherrer's constant (0.91). The average number of C planes in the stacking nanostructure (N_c) was estimated from d_{002} and L_c by means of the following equation:

$$N_c = L_c/d_{002} + 1 \quad (4)$$

3.2.4. Statistical analysis

When one-way analysis of variance, which was used to evaluate the significance of differences among variables, indicated a significant difference, mean comparisons were performed with Tukey's honestly significant difference test. All statistical analyses were carried out with IBM SPSS Statistics 21 (IBM Corporation, Armonk, NY, USA).

3.3. Results and Discussion

3.3.1. Characterization of HAs

The elemental compositions and optical properties of the HAs are shown in Table 3.1. The A_{600}/C values and atomic ratios of all the HAs were within the range of commonly accepted values for soil HAs (Ikeya and Watanabe 2003; Kuwatsuka et al. 1978; Yonebayashi and Hattori 1988). The average H/C ratio of the Andisol HAs was significantly lower than that of the Inceptisol and Entisol HAs, whereas the average O/H ratio and the average A_{600}/C value of the Andisol HAs were significantly higher than those of the Inceptisol and Entisol HAs. Increases in A_{600}/C are generally attributed to increases in the degree of humification of HAs, and decreases in H/C are ascribed to increases in the unsaturated bond content of HAs (Yonebayashi and Hattori 1988).

The peaks in the liquid-state ^{13}C NMR spectra of the HAs (Fig. 3.1) were assigned according to the reports of Fujitake and Kawahigashi (1999), Kögel-Knabner (1997), and Schnitzer and Preston (1986). The major peaks appeared at around 32, 58, 72, 130, 150, and 170 ppm. The peak at 32 ppm was attributed to methylene C in long-chain aliphatic compounds, such as lipids, suberin, and cutin; the peak at 58 ppm was assigned to lignin-derived methoxyl C; and the peak at 72 ppm was ascribed to polysaccharides. The peaks at 130 and 150 ppm were attributed to C-substituted and H-substituted aromatic C and phenolic C, respectively. The peak at 170 ppm was assigned to carboxyl C. Methylene C was the dominant peak in the spectra of the Inceptisol and Entisol HAs. Methoxyl C and phenolic C were observed clearly in the spectra of the Inceptisol and Entisol HAs, which suggests that those HAs contained altered lignin-like structure. In contrast, aromatic C and carboxyl C were the dominant peaks in the spectra of the Andisol HAs, and the peaks for methylene C, methoxyl C, and polysaccharides were minor peaks.

The relative contents of the various functional groups were determined by integrating over the standard chemical shift range (Table 3.2). In the Andisol HAs, the major C species were aromatic C (aryl C + O-aryl C; 37.1–63.9% of total intensity). The aromatic C of Andisol HAs consists mainly of C in condensed aromatic components (Ikeya et al. 2004, 2007; Kramer et al. 2004). The aromatic C content and aromaticity of the Andisol HAs were significantly higher than those of the Inceptisol and Entisol HAs ($P < 0.01$). In the Andisol HAs, alkyl C contributed <20% of the total intensity. In contrast, alkyl C and O-alkyl C in the Inceptisol and Entisol HAs were the major C species (alkyl C, 33.5–43.1% of total intensity; O-alkyl C, 20.8–28.9% of total intensity). Aromatic C content was strongly positively correlated with A_{600}/C ($r = 0.978$, $P < 0.01$) and negatively correlated with H/C ($r = –0.982$, $P < 0.01$). These results indicate that

Table 3.1. Characteristics of soil humic acids used in this study.

sample	Soil order	Land use	Horizon	Location	Atomic ratios of humic acids			Degree of darkness
					H/C	O/C	O/H	A_{600}/C †
ND	Andisols	Forest	A2	Kanazawa, Ishikawa Pref.	0.67	0.51	0.70	12.0
HZ ‡	Andisols	Grassland	A1	Hiruzen, Tottori Pref.	0.75	0.48	0.64	11.3
MZ	Andisols	Grassland	2A1	Miyakonojou, Miyazaki Pref.	0.85	0.49	0.57	9.5
SA ‡	Andisols	Forest	A	Aburahi, Shiga Pref.	0.81	0.49	0.61	9.4
KGY	Andisols	Grassland	Bw	Kanazawa, Ishikawa Pref.	0.84	0.58	0.68	8.9
MK ‡	Andisols	Grassland	A1	Myoko, Niigata Pref.	1.03	0.48	0.46	5.6
H12	Entisols	Paddy field	Ap	Nayoro, Hokkaido	1.18	0.48	0.41	3.8
GF	Entisols	Paddy field	Ap	Gifu, Gifu Pref.	1.22	0.50	0.41	2.8
OKY	Entisols	Paddy field	Ap	Okayama, Okayama Pref.	1.26	0.48	0.38	2.6
KT ‡	Inceptisols	Forest	A	Kuta, Kyoto Pref.	1.27	0.52	0.41	2.8
ASU	Inceptisols	Forest	A	Asu, Kyoto Pref.	1.22	0.47	0.38	2.7
TRG	Inceptisols	Forest	A	Hakusan, Ishikawa Pref.	1.22	0.56	0.46	2.3

H, hydrogen; C, carbon; O, oxygen

†: A_{600} is the absorbance at 600 nm and C is the organic C concentration (mg C mL^{-1})

‡: These samples were also used in study in Katsumi et al. (2015)

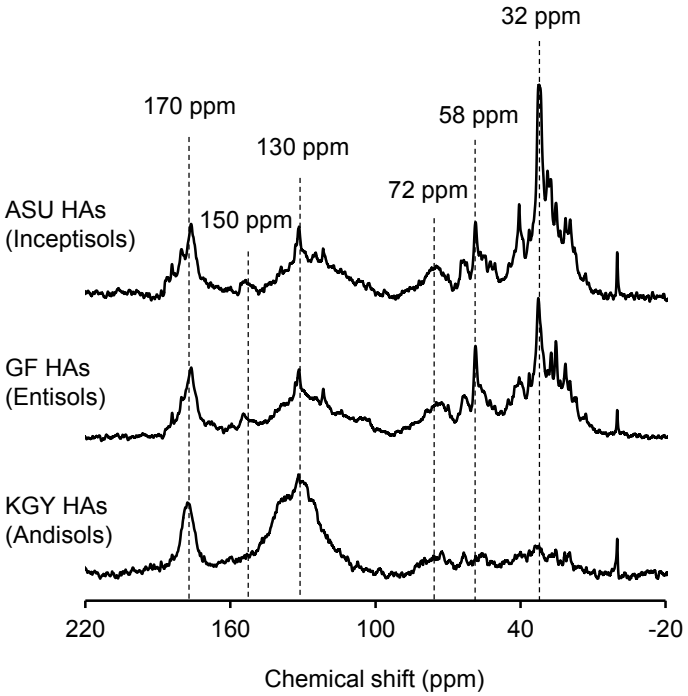

Fig. 3.1. ^{13}C NMR spectra of humic acids (HAs).

Table 3.2. Distribution of carbon species and aromaticity estimated by 13C NMR

	Alkyl C (0-48 ppm)	*O*-alkyl C (48-110 ppm)	Aromatic C (110-165 ppm)	Carboxyl C (165-190 ppm)	$f_{a\text{-}NMR}$†
ND	10.1	10.6	63.9	13.0	0.76
HZ	10.3	14.9	58.3	13.2	0.70
MZ	18.0	21.2	43.0	13.7	0.52
SA	13.5	17.6	54.6	13.0	0.64
KGY	14.4	15.5	50.2	15.0	0.63
MK	19.4	26.5	37.1	13.9	0.45
H12	33.5	25.1	27.7	11.7	0.32
GF	37.6	22.6	25.3	12.2	0.30
OKY	39.2	20.8	26.1	10.7	0.30
KT	37.6	23.9	23.3	11.2	0.27
ASU	43.1	23.0	21.1	10.7	0.24
TRG	35.9	28.9	24.6	10.0	0.28
Mean value					
Andisol HAs (n = 6)	14.3 ± 1.6 b	17.7 ± 2.2	51.2 ± 4.0 a	13.6 ± 0.3	0.61 ± 0.05 a
Entisol HAs (n = 3)	36.7 ± 1.7 a	22.8 ± 1.2	26.4 ± 0.7 b	12.9 ± 0.5	0.31 ± 0.01 b
Inceptisol HAs (n = 3)	38.9 ± 2.2 a	25.3 ± 1.8	23.0 ± 1.0 b	11.5 ± 0.3	0.26 ± 0.01 b
ANOVA	**	NS	**	NS	**

Values are mean ± standard error

ANOVA: analysis of variance. Asterisks (**) indicate statistical significance at $P < 0.01$. NS indicates no significant difference.

Different lowercase letters indicate statistically significant differences at $P < 0.01$ (Tukey honestly significant difference test).

†: $f_{a\text{-}NMR}$ = aromatic C / (alkyl C+*O*-alkyl C+aromatic C)

aromatic C was responsible for the dark color of the HAs.

3.3.2. XRD profiles of HAs and related substances

The XRD profiles of HAs and related substances are shown in Fig. 3.2. The XRD profile of carbon black exhibited four peaks, at 26°, 42°, 54°, and 80°, which were assigned to the 002, 10, 004, and 11 bands, respectively. The XRD profile of lignin showed a peak at 22°, two shoulders (at 32° and 42°), and a small peak at 80°; these four peaks correspond to the so-called γ band (Matsui et al. 1984).

The XRD profiles of the HAs showed an asymmetric peak at 22–26°, a shoulder at 42°, and a small peak at 80°, which were attributed to the 002, 10, and 11 bands, respectively (Fig. 3.2). The asymmetry of the peak at 22–26° suggests the coexistence of another band (the γ band) to the left of the 002 band. In the profiles of the Entisol and Inceptisol HAs in particular, the overlap of the 002 and γ bands markedly broadened the peak with a maximum at around 22°. Matsui et al. (1984) and Schnitzer et al. (1991) attributed the γ band at 22° to lignin or saturated compounds. In contrast, the shapes of the peaks for the Andisol HAs were similar to those of carbon black, suggesting that Andisol HAs have a chemical structure similar to that of carbon black. All the HAs, as well as carbon black, exhibited turbostratic structure, as indicated by the presence of the 002, 10, and 11 bands (Ikeya et al. 2011; Matsui et al. 1984). The 002 band of the Andisol HAs was sharper than the 002 bands of the Inceptisol and Entisol HAs, which indicates that, among the three types of HAs, the Andisol HAs had the most-developed turbostratic structure.

3.3.3. Analysis of stacking nanostructure in HAs

The XRD profiles of the HAs after waveform separation are shown in Fig. 3.3. The *R*-factors were <3 for all samples, confirming the accuracy of the fitting. The XRD profile of the HAs were separated into four peaks, at around 21°, 25°, 32°, and 42°, which were attributed to the γ_1, 002, γ_2, and 10 bands, respectively. The peaks at around 21° and 32° were specific to the XRD profile of lignin and were thus not present in the XRD profile of carbon black (Fig. 3.2). Waveform separation allowed us to define the new peaks at around 21° and 32° as the γ_1 and γ_2 bands, respectively.

We investigated the relationship between the ratio of the area of each band to the sum of the areas of the γ_1, 002, and γ_2 bands and the relative contents of the various C species (calculated by integrating the standard chemical shift range in the ^{13}C NMR spectra). The proportion of the γ_1 band area ($A_{\gamma 1}$) was positively correlated with relative alkyl C content (r =

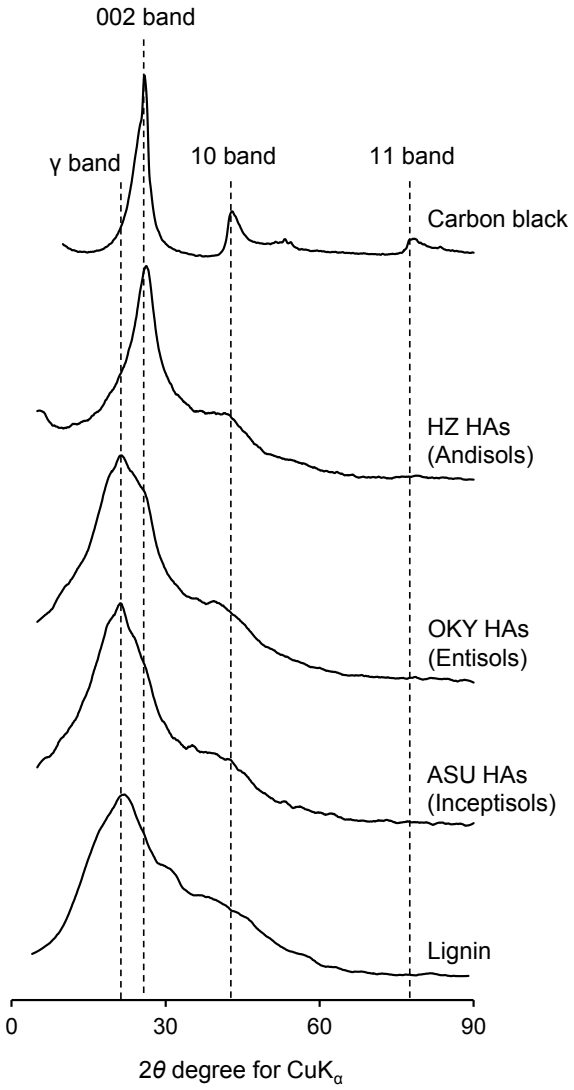

Fig. 3.2. X-ray diffraction profiles of humic acids (HAs) and related substances.

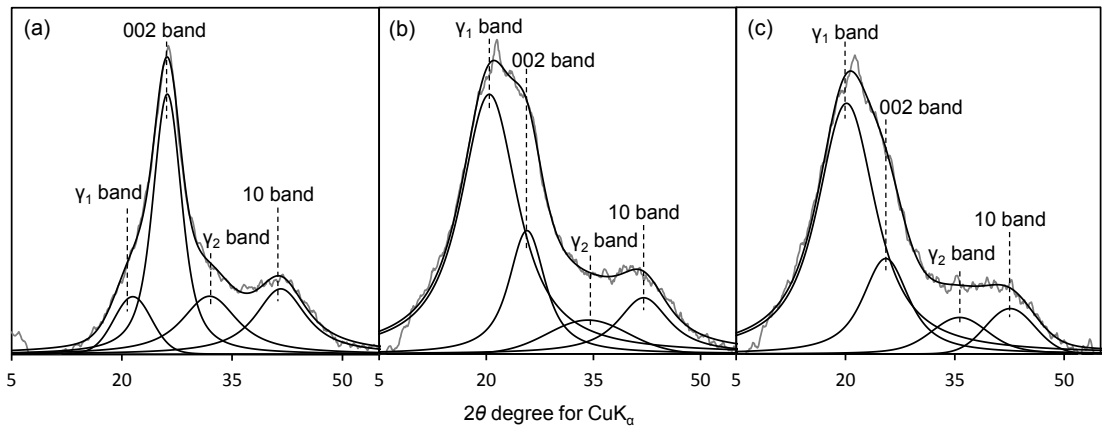

Fig. 3.3. X-ray diffraction profiles of (a) HZ (Andisols), (b) OKY (Entisols), and (c) ASU (Inceptisols) humic acids after waveform separation.

Table 3.3. Stacking structure properties of soil humic acids estimated from the 002 band of the X-ray diffraction profile

	$A_{\gamma 1}/A_{002}$†	Lc‡	d_{002}§	Nc¶	$f_{\text{a-XRD}}$
			nm		
ND	0.24	1.84	0.340	5.40	0.81
HZ	0.61	1.79	0.344	5.21	0.62
MZ	0.52	1.72	0.341	5.05	0.66
SA	0.32	1.70	0.343	4.95	0.76
KGY	0.62	1.67	0.345	4.85	0.62
MK	1.38	1.55	0.346	4.48	0.42
H12	3.15	1.40	0.342	4.10	0.24
GF	2.66	1.30	0.348	3.72	0.27
OKY	2.57	1.20	0.344	3.50	0.28
KT	5.95	1.17	0.343	3.40	0.14
ASU	3.37	1.14	0.349	3.28	0.23
TRG	4.34	1.04	0.345	3.01	0.19
Mean value					
Andisol HAs (n = 6)	0.61 ± 0.17 b	1.71 ± 0.04 a	0.343 ± 0.001	5.00 ± 0.13 a	0.65 ± 0.06 a
Entisol HAs (n = 3)	2.79 ± 0.18 a	1.30 ± 0.06 b	0.345 ± 0.002	3.77 ± 0.18 b	0.26 ± 0.01 b
Inceptisol HAs (n = 3)	4.55 ± 0.75 a	1.12 ± 0.04 b	0.346 ± 0.002	3.23 ± 0.11 b	0.19 ± 0.02 b
ANOVA	**	**	NS	**	**

Values are mean ± standard error

ANOVA: analysis of variance. Asterisks (**) indicate statistical significance at $P < 0.01$. NS indicates no significant difference. Different lowercase letters indicate statistically significant differences at $P < 0.01$ (Tukey honestly significant difference test).

†:$A_{\gamma 1}/A_{002}$ = area ratio of 002 band / area ratio of γ_1 band.

‡: mean stacking structure length along the c axis

§: spacing between carbon planes in humic acid

¶: Number of stacked carbon plane

$f_{\text{a-XRD}}$ = area ratio of 002 band / (area ratio of 002 band + area ratio of γ_1 band)

0.931, $P < 0.01$) and negatively correlated with relative aromatic C content ($r = –0.968$, $P < 0.01$). Thus, we attributed the γ_1 band to aliphatic components in the HAs. In contrast, there was no association between the proportion of the γ_2 band area ($A_{\gamma 2}$) and the relative contents of any of the C species. Because the 002 band was attributed to the spacing between the C planes, the proportion of the 002 band area (A_{002}) was positively correlated with aromatic C content ($r = 0.872$, $P < 0.01$) and negatively correlated with alkyl C content ($r = −0.884$, $P < 0.01$).

The stacking nanostructure properties of the soil HAs estimated from the XRD 002 band are listed in Table 3. Relative standard deviation obtained from SA HAs (n = 3) was ± 11.4% for the $A_{\gamma 1}/A_{002}$, ± 1.2% for L_c, ± 0.1% for the d_{002}, ± 1.3% for the N_c and ± 2.8% for the $f_{\text{a-XRD}}$, which exhibited low variability. The area ratios of the γ_1 and 002 bands ($A_{\gamma 1}/A_{002}$) ranged from 0.24 to 5.95. The $A_{\gamma 1}/A_{002}$ ratios for the Andisol HAs were lower than those for the Inceptisol and Entisol HAs ($P < 0.01$). This result indicates that the Andisol HAs were richer in aromatic components and poorer in aliphatic components than the Inceptisol and Entisol HAs. In fact, $A_{\gamma 1}/A_{002}$ was negatively correlated with aromatic C content (Spearman's rank correlation test, $\rho = –0.923$, $P < 0.01$) and positively correlated with H/C (Spearman's rank correlation test, $\rho = 0.853$, $P < 0.01$). Therefore, $A_{\gamma 1}/A_{002}$ provides a good indication of the structural features of the HAs.

Theoretically, the areas of the 002 and γ_1 bands are proportional to the number of aromatic C atoms (C_{ar}) and the number of aliphatic C atoms (C_{al}), respectively (Lu et al. 2000; Sonibare et al. 2010; Yen et al. 1961). According to Schnitzer et al. (1991) and Lu et al. (2000), the aromaticity determined by XRD ($f_{\text{a-XRD}}$) can be expressed by the following equation using the separated peak areas of the XRD profile:

$$f_{\text{a-XRD}} = C_{\text{ar}}/(C_{\text{ar}} + C_{\text{al}}) = A_{002}/(A_{002} + A_{\gamma 1}) \quad (5)$$

Aromaticities calculated from XRD and ^{13}C NMR ranged from 0.14 to 0.81 and from 0.24 to 0.76, respectively, and $f_{\text{a-XRD}}$ was highly correlated with $f_{\text{a-NMR}}$ ($r = 0.958$, $P < 0.01$). Linear regression analysis of the HA aromaticity data obtained by the two methods yielded the following equation:

$$f_{\text{a-NMR}} = 0.752\, f_{\text{a-XRD}} + 0.122 \quad (6)$$

The regression model explained 92% of the variability in $f_{\text{a-NMR}}$, and $f_{\text{a-NMR}}$ can be estimated from $f_{\text{a-XRD}}$. The slope of the regression equation (0.752) indicates that the aromaticity obtained by XRD was larger than that obtained by ^{13}C NMR. The $f_{\text{a-XRD}}$ has often been used to characterize coal and carbon black (e.g., Lu et al., 2000), which are composed mainly of

aromatic C and contain a small amount of aliphatic C. In contrast, HAs consist of aromatic C and aliphatic C as well as polysaccharides and lignin derivatives, as indicated by the ^{13}C NMR spectra of the HAs, especially for the Inceptisol and Entisol HAs (Fig. 3.1). Therefore, the overestimation of aromaticity by means of XRD is due to the fact that C derived from polysaccharides and lignin derivatives is not included in the denominator of eq. (5).

The d_{002} values of the HAs ranged from 0.340 to 0.349 nm (Table 3.3) and were slightly larger than the value of graphite (0.335 nm). The d_{002} values of the HAs from the three soil orders did not differ substantially from one another. The L_c and N_c values ranged from 1.04 to 1.84 nm and from 3.01 to 5.40, respectively (Table 3.3). The L_c and N_c values of the Andisol HAs were higher than those of the Inceptisol and Entisol HAs ($P < 0.01$) but lower than the values of the carbon black used in this study (L_c, 2.70 nm; N_c, 8.86). Takagi et al. (2004) reported L_c and N_c values for seven types of raw coal ranging from 0.71 to 1.89 nm and from 2.99 to 6.43, respectively. These results suggest that the degree of stacking nanostructure in the HAs we studied was in the same range as that in raw coal. We observed significant relationships between the proportions of the various carbon species and the stacking nanostructure properties measured by XRD (Fig. 3.4). The proportion of aromatic C was positively correlated with L_c, whereas the sum of the alkyl C and O-alkyl C contents was negatively correlated with L_c; furthermore, L_c was positively correlated with A_{600}/C (Fig. 3.4). These findings suggest that the formation and accumulation of building blocks containing layered C planes contribute to the darkening of HAs in soil. The presence of HAs with the highest degree of darkness is believed to be the reason for the darkness of Japanese Andisols (Iimura et al. 2013). Therefore, the formation of stacking nanostructures in HAs plays a role in the darkening of soils, especially for Japanese Andisols.

Ikeya et al. (2011) reported that the average L_a values for Andisol HAs ($n = 5$) and Inceptisol HAs ($n = 3$) range from 0.80 to 0.96 nm and from 0.81 to 0.91 nm, respectively, and that the value for Entisol HAs ($n = 1$) is 0.86 nm. These results taken together with ours suggest that the average stacking nanostructure models shown in Fig. 3.5 were present in the HAs analyzed in this study.

The process by which stacking nanostructures form in HAs is largely unknown. The L_a of Andisol HAs is larger than that of polynuclear quinones, such as dihydroxyperylenequinones in Type P HAs, produced by fungi (Kumada and Hurst 1967). Because the mean L_a of charred plant fragments in Andisols ranges from 1.26 to 1.37 nm (Sultana et al. 2010), they can be expected to contribute to condensed aromatic components in Japanese volcanic ash soils (Shindo et al. 2004). Fresh char contains very small amounts of HAs (Shindo and Honma 1998). However, partial degradation and oxidation of char are necessary to produce HAs with a high degree of darkness (Trompowsky et al. 2005). Furthermore, Nishimura et al. (2006) extracted

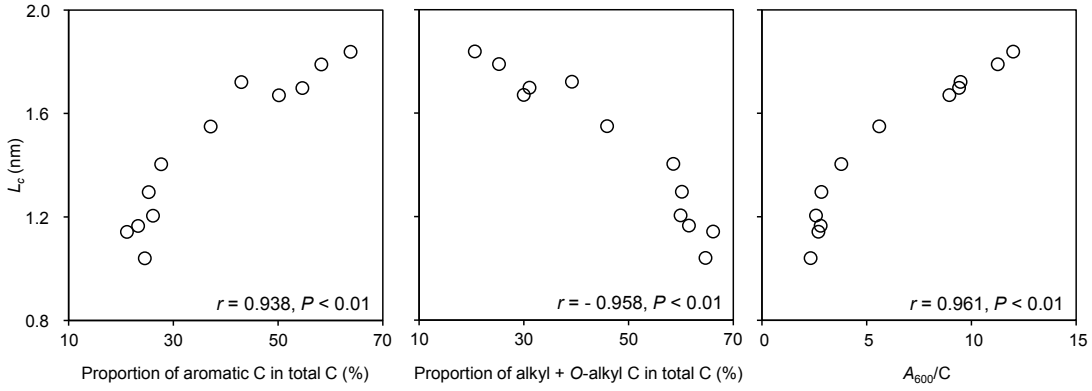

Fig. 3.4. Relationships between mean stacked structure length along *c* axis (L_c) and proportion of aromatic C (%), (alkyl C + O-alkyl C) (%), and A_{600}/C.

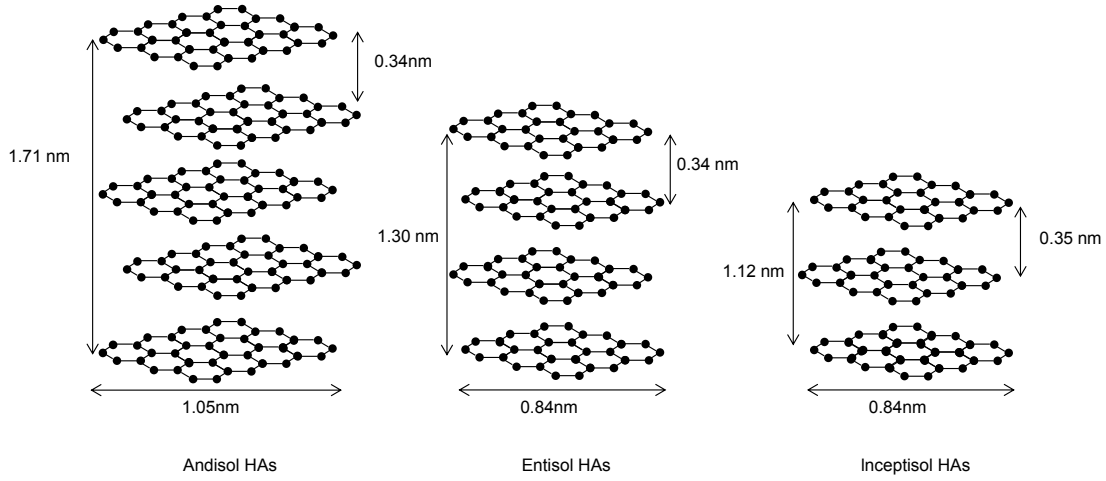

Fig. 3.5. Proposed average stacking nanostructure models for humic acids analyzed in the present study. These nanostructure models used theoretical values for La and approximate value for Nc.

HAs with a high degree of darkness from charred plant fragments that had naturally oxidized in the field. The mean L_a values of HAs extracted from HNO_3- and H_2O_2-oxidized char are 1.29 and 1.05 nm, respectively (Sultana et al. 2011), and the mean L_a of the latter HAs is about the same as that of Andisol HAs. These results suggest that the stacking nanostructure of the Andisol HAs was well-developed. Moreover, we confirmed that the L_c of HAs is increased, from 1.29 to 1.67 nm, by heating soils at 250 °C (Katsumi et al. 2014). Therefore, char and heating are likely to be important factors in the formation of turbostratic structures in HAs.

Chapter 4. Effects of heating on composition, degree of darkness, and stacking nanostructure of soil humic substances

4.1. Introduction

Wildfires and prescribed burning dramatically alter C cycling and storage in the ecosystem (Wadle et al., 2003). Fire alters the physical, chemical, and biological properties of soil (DeBano, 2000; Hart et al., 2005); the most commonly reported effects of fire are qualitative and quantitative changes in SOM (González-Pérez et al., 2004; Knicker, 2007). SOM undergoes pyrolysis, charring, and oxidation during burning (Certini, 2005). The transformations of HAs and FAs during wildfires have been modeled and studied in detail in the laboratory by Almendros et al. (1990) and González-Vila and Almendros (2003). These investigators heated HAs or FAs at 350 ºC for various durations and made the following observations: heating results in (1) increased aromatic C content owing to aromatization of carbohydrates, (2) removal of oxygen-containing functional groups, (3) formation of heterocyclic N compounds, (4) reduction in the chain length of alkyl compounds, and (5) decreases in the amounts of FAs and HAs accompanied by increases in the amounts of humins and black carbon. These changes lead to the formation of weakly colloidal organic substances with enhanced resistance to chemical and biological degradation (Knicker et al., 2005). Such recalcitrant substances are important because they determine the long-term SOM content and C-sequestration ability of soils (Egli et al., 2012).

Forest fires typically produce temperatures ranging from 200 to 400 ºC in the region from the soil surface down to a few centimeters below the surface (Gimeno-Garcia et al., 2004). However, previous laboratory studies of the effects of heating on soil humic substances (Almendros et al., 1990, 2003; González-Vila and Almendros, 2003) have been carried out only at 350 ºC, and the effects of temperatures of <350 ºC on the quantity and quality of humic substances is not clear. Furthermore, how soil type and vegetation affect the changes in HA chemical structure due to thermal denaturation is also largely unknown.

The objective of the present study was to examine how the properties of humic substances in two different soils hosting different vegetation (an Entisol from a paddy field and an Inceptisol from a coniferous forest) were affected by heating at temperatures ranging from relatively low to high. We determined the effects of heating on the quantity and quality of soil

humic substances by analyzing their composition and chemical structure by means of conventional methods, as well as by a new technique developed by Katsumi et al. (2015a, 2015b).

4.2. Materials and methods

4.2.1. Soil samples and heating treatment

Soil samples were collected from the A horizon of two mineral soils in Japan. One sample, an Entisol, was collected from a paddy field at the Experimental Farm of Yamagata University (YGU). This area has been used as a paddy field for at least 300 years. The other sample, an Inceptisol, was collected from a coniferous forest at the Ishikawa Forest Experiment Station (TRG), where vegetation has been dominated by Japanese cedar (*Cryptomeria japonica*) over the past 80 years. Soil samples were air-dried and passed through a 2-mm-mesh sieve. Fine roots and litter were removed from the soil samples with tweezers. The characteristics of the soils are listed in Table 5.1.

A portion (50 g) of each of the soil samples was placed in a ceramic crucible with a lid, and the crucibles were placed inside a muffle furnace (FO300, Yamato Scientific Co., Tokyo, Japan) and heated in a controlled process at 200, 250, and 300 °C for 1, 3, 5, or 12 h. After the heating interval was completed, the samples were allowed to cool to room temperature (ca. 25 ºC) in a desiccator, and the weight losses of the samples were determined by comparing sample weights before and after heating. The total carbon (TC) contents of the heat-treated soils were determined in triplicate by dry combustion with an elemental analyzer (2400, Perkin-Elmer Japan, Yokohama, Japan).

4.2.2. Composition of humic substances and degree of darkness

The HA and FA contents of the soil samples before and after heating and the A_{600}/C values of the HAs were determined according to the methods of Ikeya and Watanabe (2003); A_{600} is the absorbance at 600 nm, and C is the organic C concentration (mg C mL^{-1}). To obtain the HAs and FAs, 45 mL of 0.1 mol L^{-1} NaOH was added to a soil sample containing 150 mg of C, and the mixture was continuously shaken for 24 h at room temperature under a N_2 atmosphere. The suspension was centrifuged at 2000*g* for 10 min and then filtered through a Whatman GF/B glass fiber filter (nominal pore size, 1.0 μm; Whatman International, Maidstone, England). To remove coarse-grained materials, the filtrate was centrifuged at 20,000*g* for 20 min. The extract

Table 5.1. Characteristics of the soils

Sample	Location	Soil order	Horizon	Depth	Land use	pH		TC
						H_2O [a]	NaF [b]	g kg^{-1}
TRG	Tsurugi, Ishikawa Prefecture	Inceptisols	A	0-5 cm	Forest	4.6	9.0	107.9
YGU	Tsuruoka, Yamagata Prefecture	Entisols	Ap	0-15 cm	Paddy field	4.1	9.4	22.0

[a] soil : water ratio = 1 : 2.5

[b] mixture of 1g of soil and 25 mL of 1 mol L^{-1} NaF shaking for 2 min.

was acidified to pH 1.5 with 4 mol L^{-1} H_2SO_4 and allowed to stand overnight. HAs and FAs were separated by centrifugation at 2000*g* for 10 min. The organic carbon contents of the FAs were determined with a TOC analyzer (TOC-V_{CSH}, Shimadzu, Kyoto, Japan) under acidic conditions after bubbling with N_2 gas. HAs were redissolved in 0.1 mol L^{-1} NaOH, and the absorbance at 600 nm was measured with a UV–vis spectrophotometer (UVmin-1240, Shimadzu). The HA solution was diluted with 0.7 mol L^{-1} KH_2PO_4, and its organic carbon content was determined with a TOC analyzer. The concentration of the alkali-insoluble fraction (AIF) was calculated as the difference between the TC of the bulk soil and the HA and FA carbon contents. Subsequently, the HA solution was purified as follows: 0.3 mol L^{-1} HF /0.1 mol L^{-1} HCl was added to the HA solution, and the mixture was stirred for 5 h at room temperature to remove fine-grained minerals. The suspension was centrifuged at 2000*g*, and the precipitated fraction was collected, washed with deionized water, and redissolved in a small amount of NaOH solution. The redissolved fraction was dialyzed using a dialysis tube (molecular weight cutoff, 3500; CelluSep T1, Membrane Filtration Products, Inc., Seguin, TX, USA) until the electrical conductivity of the equilibrated outer solution was 10 μS cm^{-1} or less; the dialyzed solution was passed through a column of cation-exchange resin (Amberlite IR-120, H^+ form, Organo Corporation, Tokyo, Japan) and freeze-dried.

4.2.3. Elemental analysis and isotope ratio mass spectrometry

The elemental compositions of the HAs (%C, %H, and %N) were determined with an elemental analyzer (2400 II, Perkin-Elmer Japan, Yokohama, Japan). Elemental compositions are expressed as H/C ratios to clarify the stoichiometric relationships among the elements.

The $\delta^{13}C$ and $\delta^{15}N$ values of the HAs were determined with an isotope ratio mass spectrometer (IsoPrime IRMS, GV Instruments, Manchester, UK) linked to an elemental analyzer (EA3000, EuroVector, Milan, Italy) according to the methods of Katsumi et al. (2015a). The results are expressed as relative δ values, calculated as follows:

$$\delta X = [(R_{Xsample}/R_{Xstandard}) - 1] \times 1000\ (‰), \quad (1)$$

where X = C or N and $R_{Xsample}$ and $R_{Xstandard}$ represent the $^{13}C/^{12}C$ and $^{15}N/^{14}N$ ratios of the sample and the standard, respectively. An L-glutamic acid reference material (USGS40, U.S. Geological Survey, Reston, VA, USA) with a $\delta^{13}C$ value of –26.2‰ and a $\delta^{15}N$ value of –4.5‰ was used as a secondary standard, calibrated relative to the primary standards for carbon (Cretaceous Pee Dee belemnite, Pee Dee, SC, USA) and nitrogen (atmospheric N_2). The

experimental errors in the $\delta^{13}C$ and $\delta^{15}N$ values were ≤0.1‰. Each sample was analyzed in triplicate. If the standard deviation was greater than 0.2‰, measurements were repeated until the standard deviation of all the replicates was <0.2‰.

4.2.4. Liquid-state ^{13}C nuclear magnetic resonance spectroscopy

Liquid-state ^{13}C nuclear magnetic resonance (NMR) spectra were recorded at 100.5 MHz on a JEOL ECX 400 spectrometer (JEOL, Tokyo, Japan). Each HA (50 mg) was dissolved in 0.5 mL of 0.5 mol L^{-1} NaOD in D_2O in a 5-mm-diameter sample tube. Chemical shifts were referenced to sodium 3-(trimethylsilyl)propionate-*2,2,3,3-d*$_4$ (0 ppm). To quantify the ^{13}C NMR spectra, ^{13}C signals were proton-decoupled by means of the inverse-gated decoupling technique under the following operating conditions: pulse width, 4.9 μs (45°); acquisition time, 1.04 s; pulse delay, 2.5 s. A total of 10,000–60,000 scans were accumulated, and line broadening was set at 50 Hz. The peaks in the ^{13}C NMR spectra of the HAs were assigned according to the reports of Fujitake and Kawahigashi (1999), Kögel-Knabner (1997), and Schnitzer and Preston (1986). Resonance areas were calculated by means of electronic integration. The spectra were divided into the following five regions (Fujitake and Kawahigashi, 1999): alkyl C, 0–48 ppm; O-alkyl C, 48–110 ppm; aryl C, 110–145 ppm; O-aryl C, 145–165 ppm; and carboxylic C, 165–190 ppm. Aromaticity as determined by ^{13}C NMR was given by the ratio of (aryl C + O-aryl C) to (alkyl C + O-alkyl C + aryl C + O-aryl C) (Watanabe and Fujitake, 2008). The O-aryl C content was very small and was classified as aromatic C, along with aryl C (110–165 ppm).

4.2.5. X-ray diffraction

Because the changes of weight loss, degree of darkness, and NMR spectra were relatively small after 5 h of heating, the HAs extracted from soil samples after 5 h of heating were analyzed by X-ray diffraction (XRD). Forty to fifty milligrams of sample was packed into a 0.2-mm-deep hole on a nonreflecting silicon holder (20 (W) × 18 (H) × 0.2 (T) mm) (Rigaku, Tokyo, Japan), and XRD patterns were obtained with a Rigaku MiniFlex diffractometer (Cu Kα radiation, 0.154-nm wavelength). The generator was set at 30 kV and 15 mA. Samples were scanned over a 2θ range from 10° to 90° with a step size of 0.01° and a scanning speed of 2° min^{-1}. After the XRD patterns were corrected with the Lorentz polarization and absorption factors, smoothing was performed using a weighted mean method (smoothing number, 15).

Properties of the stacked nanostructures were analyzed according to the methods of Katsumi et al. (2015b). The areas covering the 2θ range from 10° to 60° were separated into four peaks by calculating the second derivative and comparing the profiles of the reference and

HA samples, and least-squares iterative curve fitting was carried out with the Voigt function using PeakFit (ver. 4.12, SeaSolve Software Inc., Framingham, MA, USA). The peak positions, widths, and areas were determined. The validity of the profile fitting was evaluated from the *R* factor, which is defined as follows:

$$R = [\Sigma_{2\theta}|I(2\theta) - P_r(2\theta)|)/\Sigma_{2\theta}I(2\theta)] \times 100 \quad (2)$$

where $I(2\theta)$ is the experimentally observed intensity profile and $P_r(2\theta)$ is the profile fitted by calculation. The value of the *R* factor should be as small as possible. The spacing between C planes (d_{002}) in the HAs was calculated from the position of the peak for the separated 002 band by means of Bragg's equation:

$$d_{002} = \lambda/(2 \sin \theta) \quad (3)$$

where λ is the wavelength of the X-rays in nanometers (0.154 nm for Cu Kα radiation) and θ is Bragg's angle at a diffraction line. The mean thickness of the stacking nanostructure along the *c* axis (L_c) was calculated from the full width at half-maximum and the position of the peak for the 002 band by means of Scherrer's equation:

$$L_c = K\lambda/(\beta \cos \theta) \quad (4)$$

where β is the full width at half-maximum of the 002 band and *K* is Scherrer's constant (0.91). The average number of C planes in the stacking nanostructure (N_c) was estimated from d_{002} and L_c by means of the following equation:

$$N_c = L_c/d_{002} + 1 \quad (5)$$

4.3. Results

4.3.1. Total carbon and weight loss of bulk soil

For all heating temperatures (200, 250, and 300 °C), the weight losses for the YGU and TRG samples rapidly increased during the initial 3 h of heating and then gradually increased until 12 h (Table 4.2). The values of TC for the TRG and YGU samples decreased with heating time for the various heating conditions (Table 4.2).

Table 4.2. Changes in composition and H/C atomic ratios of HAs in soil samples with heating treatment

	Temperature	Time	Weight loss	Total carbon	HAs	FAs	AIF	H/C atomic ratio of HAs
	(°C)	(h)	(%)	(mg kg^{-1})		(mg kg^{-1})		
YGU	Control	0	0.0	22.0	2.7	2.9	16.3	1.22
	200	1	2.0	21.5	2.9	3.9	14.7	1.12
		3	2.6	20.2	4.8	2.5	12.8	1.04
		5	3.0	17.9	6.0	2.5	9.4	0.94
		12	3.3	16.1	7.3	2.3	6.5	0.92
	250	1	2.9	18.6	2.4	3.0	13.3	0.92
		3	3.6	18.7	2.1	1.4	15.2	0.84
		5	4.1	16.7	4.0	1.2	11.5	0.68
		12	4.7	14.2	4.6	1.2	8.4	0.67
	300	1	4.3	21.5	1.6	1.3	18.6	0.87
		3	4.6	15.4	1.0	0.9	13.5	0.75
		5	4.2	13.5	1.0	0.8	11.6	0.62
		12	4.8	6.0	0.6	0.6	4.8	0.62
TRG	Control	0	0.0	107.9	23.2	16.0	68.7	1.29
	200	1	8.1	110.6	22.1	16.0	72.5	1.00
		3	9.8	113.6	24.3	12.3	77.0	1.05
		5	9.9	105.1	25.2	12.0	67.9	0.93
		12	12.5	100.3	24.8	11.1	64.3	0.91
	250	1	10.6	109.2	22.6	14.9	71.7	0.98
		3	11.6	103.3	14.3	9.6	79.5	0.92
		5	13.2	101.0	13.2	8.5	79.3	0.85
		12	15.4	77.6	12.7	7.3	57.6	0.85
	300	1	13.2	116.0	15.6	9.9	90.5	0.87
		3	14.0	102.6	11.2	7.8	83.6	0.85
		5	15.9	98.1	7.1	6.1	84.9	0.84
		12	16.7	78.0	5.8	4.8	67.5	0.78

4.3.2. Quantitative changes of humic substances

The relationships between heating temperature and FA, HA, and AIF contents are shown in Table 2. The initial proportions of FAs, HAs, and AIF in TC were within the range of commonly accepted values for soil humic substances (Watanabe and Kuwatsuka, 1991). Heating altered the initial proportions of FAs, HAs, and AIF in TC (Fig. 5.1). The proportion of FAs in TC decreased with increasing heating temperature and time, and heating at 300 °C for 12 h provided the maximum reduction. For the TRG sample, the proportion of HAs in TC increased with increasing heating time at 200 °C but decreased with increasing heating time at 250 and 300 °C. For the YGU sample, the proportion of HAs in TC increased markedly with increasing heating time at 200 and 250 °C but decreased with increasing heating time at 300 °C. For the TRG sample, the proportion of AIF in TC increased with increasing heating time at 250 and 300 °C. In contrast, for the YGU sample, the proportion of AIF in TC decreased with increasing heating time at 200 and 250 °C. The FA contents in soil negatively correlated with weight loss (TRG sample: $r = -0.94$, $p < 0.01$, $n = 12$; YGU sample: $r = -0.95$, $p < 0.01$, $n = 12$), whereas no such correlation was observed for the AIF and HA contents, except for the TRG sample HAs ($r = -0.86$, $p < 0.01$, $n = 12$). These results suggest that FAs are more likely than HAs and AIF to undergo degradation by heating.

4.3.3. Degree of darkness

The degree of darkness (A_{600}/C) of the HAs increased with increasing heating temperature, and the highest value of A_{600}/C for the HAs was recorded at 300 °C for 12 h (Fig. 4.2). Similarly, Kumada (1988) and Shindo and Urabe (1993) reported a progression of humification (darkening process of HAs) with increasing heating temperature. The A_{600}/C values for the TRG sample increased rapidly during the initial 3 h of heating and then gradually increased until 12 h. In contrast, the A_{600}/C values for the YGU sample increased rapidly during the initial 3 h of heating and then became constant after 5 h. The TRG data conformed to two-compartment first-order kinetics, whereas the YGU data conformed to first-order kinetics. Kumada (1988) classified HAs into four types (Type A, Type B, Type P, and Type Rp) on the basis of their optical properties and degree of darkness, the latter increasing in the order Type A, Type B, Type P, Type Rp. Under the conditions in this study (50 g of soil sample in a 100-mL-capacity ceramic crucible heated in a muffle furnace), the following heating treatments produced Type A HAs ($A_{600}/C > 5$): 24 min at 300 °C, 33 min at 250 °C, and 96 min at 200 °C for the YGU sample; 8 min at 300 °C, 25 min at 250 °C, and 79 min at 200 °C for the TRG sample, obtained by first-order kinetic curves.

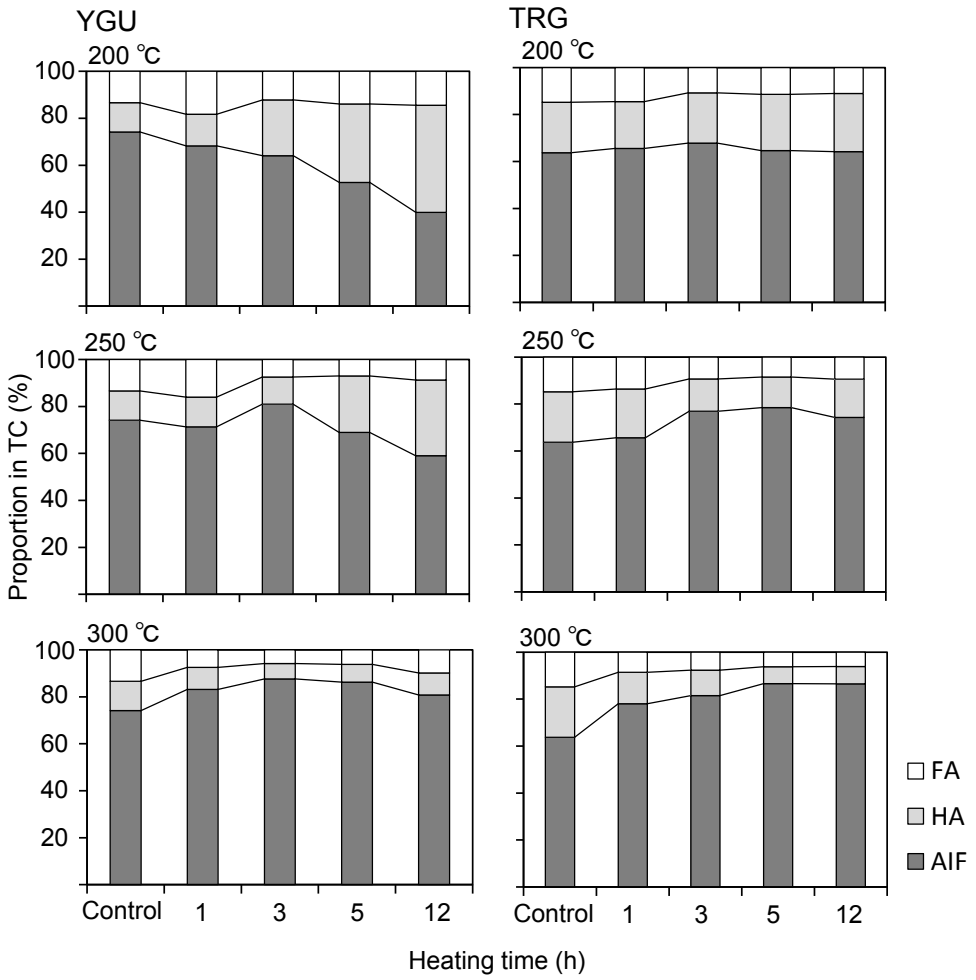

Fig. 4.1. Changes in proportion of each fraction in TC for the Inceptisol (TRG) and Entisol (YGU) samples after heating for 200, 250, or 300 °C at 0, 1, 3, 5, or 12 h. Alkali soluble: 0.1 mol L^{-1} NaOH soluble; alkali insoluble: 0.1 mol L^{-1} NaOH insoluble, FA: fulvic acids, HA: humic acids; AIF: alkali-insoluble fraction

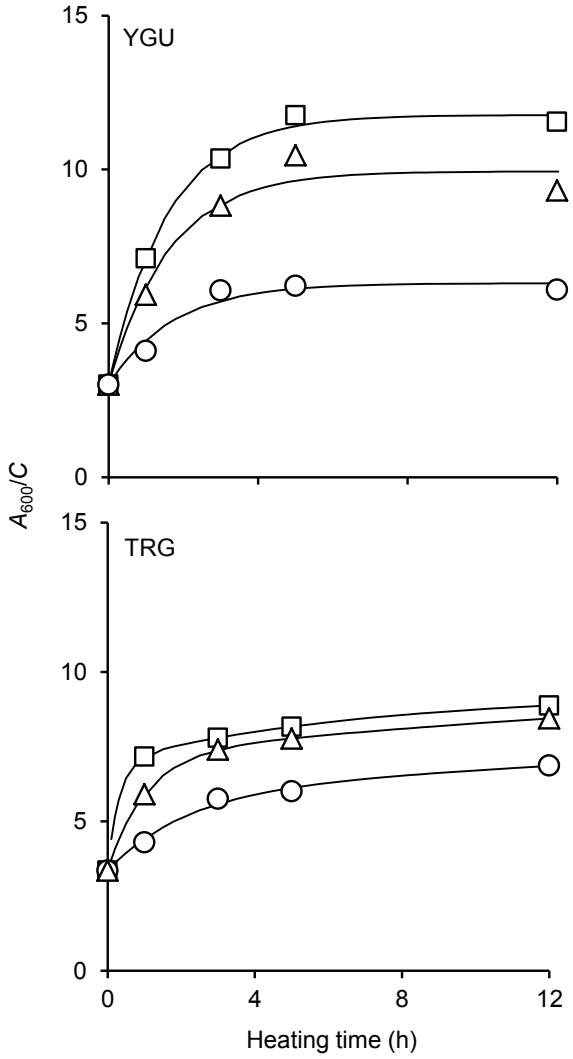

Fig. 4.2. Relationship between A_{600}/C of HAs and heating time at various temperatures. A_{600}/C is the absorbance at 600 nm per mg of C per mL of HA in 0.1 mol L^{-1} NaOH. YGU: Entisol sample; TRG: Inceptisol sample. (○) 200 °C; (Δ) 250 °C; (□) 300 °C.

4.3.4. Elemental composition and stable isotope ratios

The elemental compositions of the HAs are shown in Table 4.2. Heating led to a decrease in H/C ratio, and this tendency was especially pronounced in the YGU sample. In general, a decrease in H/C ratio reflects a decrease in the saturated bond content (Yonebayashi and Hattori, 1988). Therefore, heating led to a loss of polysaccharides and hydroxylated aliphatic moieties in the HA structures. This was confirmed by ^{13}C NMR spectroscopy.

The $\delta^{13}C$ and $\delta^{15}N$ values for the HAs increased with heating temperature (Table 4.3). In studies on the carbonization of plants, Czimczik et al. (2002) and Poole et al. (2002) found that the incremental change of $\delta^{13}C$ at the initial stage of the carbonization process (<300 °C) was due to loss of isotopically lighter extractives, trapping of isotopically heavier cellulose-derived C in the charcoal structure, or both. Above a heating temperature at 300 °C, the $\delta^{13}C$ value decreased by 1–2‰ in charcoal (Turney et al., 2006; Bird and Ascough, 2012). The incremental changes of the $\delta^{13}C$ values of the HAs during heating appear to be due either to the total disappearance of the isotopically lighter fraction or to transfers of ^{13}C from other fractions (FAs and humin) that are more enriched in ^{13}C, such as cellulose-derived C.

In contrast, the factors controlling the incremental $\delta^{15}N$ changes in SOM during heating are not well understood. Saito et al. (2007) hypothesized that the $\delta^{15}N$ values for SOM would increase with increasing temperature due to volatilization of lighter isotopes. In the present study, similar phenomena may occur. Furthermore, litter or humic material subjected to fire produces black N, which consists mostly of pyrrole/indole-type N with minor contributions from pyridine N, possibly 2.5-diketopiperazines, pyrroline, and pyrrolidine (Knicker et al., 2008), and these heterocyclic N compounds are likely to be involved in ^{15}N enrichment.

4.3.5. ^{13}C NMR spectra

^{13}C NMR spectra of HAs are shown in Figs. 4.3 and 4.4 for various heating treatments. HAs extracted from the control sample have high alkyl and O-alkyl C contents and low aromatic and carboxyl C contents, whereas HAs extracted from heated soil have high aromatic and carboxyl C contents and low alkyl and O-alkyl C contents. These results suggest that alkyl and O-alkyl C correspond to heat-labile compounds, in agreement with the elemental composition results.

Major peaks for the control sample appeared at 32, 58, 72, 130, 150, and 170 ppm. In the alkyl and O-alkyl C regions, the peak at 32 ppm was attributed to methylene C in long-chain aliphatic compounds such as lipids, suberin, and cutin (Kögel-Knabner, 1997); the peak at 58 ppm was assigned to a lignin-derived methoxyl group; and the peak at 72 ppm was ascribed to

Table 4.3. Changes in $\delta^{13}C$ and $\delta^{15}N$ with heating treatment for 5 h

	Temperature	$\delta^{13}C$	$\delta^{15}N$
	(°C)	(‰)	
YGU	Control	-27.8	0.32
	200	-27.3	0.58
	250	-27.1	0.80
	300	-26.6	1.04
TRG	Control	-27.5	1.29
	200	-27.3	1.69
	250	-27.1	2.02
	300	-26.8	2.27

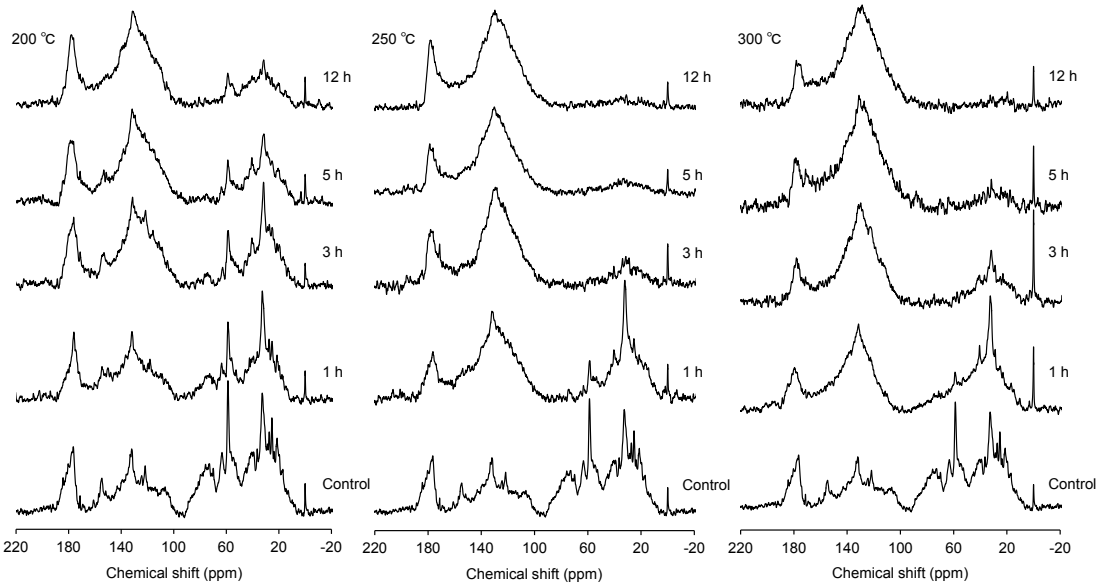

Fig. 5.3. Changes in ^{13}C NMR spectra of Entisol (YGU) HAs with heating treatment.

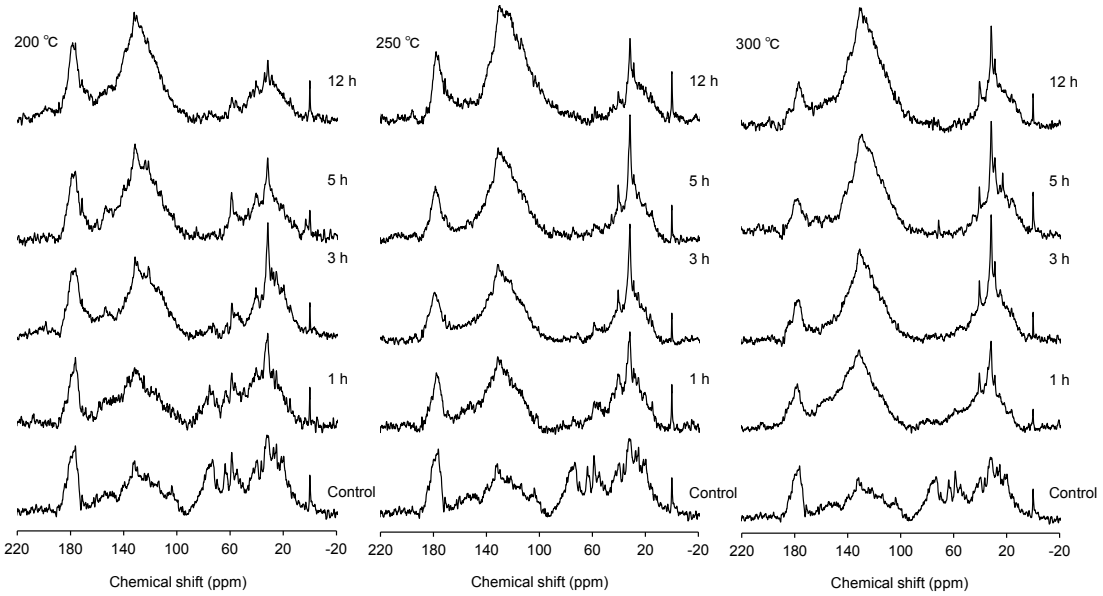

Fig. 4.4. Changes in ^{13}C NMR spectra of Inceptisol (TRG) HAs with heating treatment.

polysaccharides. In the aromatic and carboxyl C regions, the peaks at 130 and 150 ppm were attributed to C-substituted and H-substituted aromatic C and phenolic C, respectively, and the peak at 170 ppm was assigned to carboxyl C.

For the YGU sample (Fig. 4.3), the methylene chain and methoxyl group peaks decreased with increasing heating temperature and time, and heating at 200 °C for 3 h led to disappearance of the polysaccharide peak. In addition, heating at 200 °C for 12 h led to disappearance of the phenolic C peak. After 3 h of heating at 250 °C, the methylene chain, methoxyl group, and polysaccharide peaks disappeared, whereas the aromatic and carboxyl C peaks remained. These spectral properties are similar to those of HAs extracted from *Terra preta de Indio* (anthropogenic dark earths formed by addition of charcoal) and Japanese Andisols (Araujo et al., 2014; Fujitake and Kawahigashi, 1999).

For the TRG sample (Fig. 4.4), the methoxyl group peak decreased and the aromatic C peak increased with increasing heating time, and the polysaccharide peak disappeared after 3 h at 200 °C, as with the YGU sample. These results suggest that the altered lignin and cellulose structures in Entisol (YGU) and Inceptisol (TRG) HAs are easily cracked by heating. In contrast, the sharp peaks at 32 ppm attributed to $(CH_2)_n$ in long-chain aliphatic components in lipids, suberin, or cutin remained in the spectrum of the TRG sample after heating at 300 °C for 12 h.

The relationships between the proportions of C species in the samples and the heating time are shown in Fig. 4.5. In both soils, an increase in heating temperature and time led to an increase in the proportion of aromatic C species and a decrease in the proportions of alkyl C and O-alkyl C species. Heating treatment had little effect on the proportion of carboxyl C species. Although González-Pérez et al. (2004) reported that oxygen-containing functional groups, including carboxylic C, are unstable during heating, we found that carboxylic C was relatively stable at heating temperatures below 300 °C. The proportion of alkyl C species in the YGU sample declined sharply after 3 h of heating at 250 and 300 °C. In contrast, the proportion of alkyl C species in the TRG sample declined slightly at all temperatures.

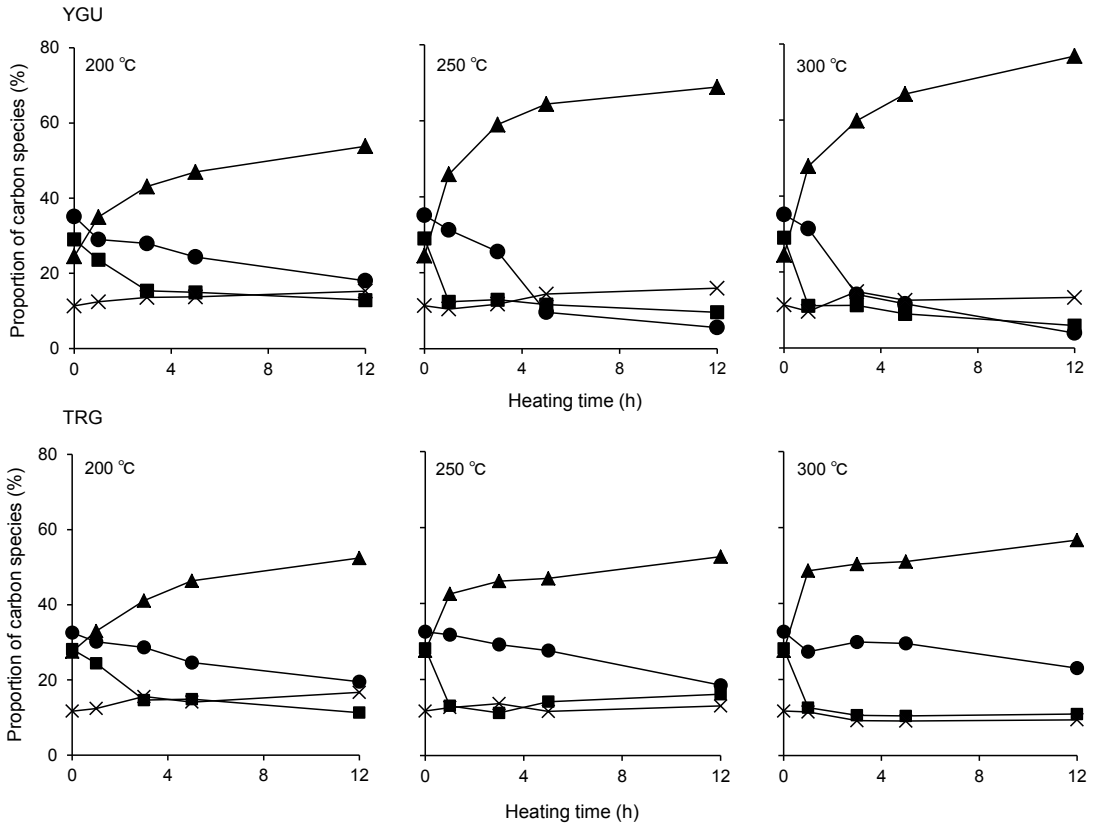

Fig.4.5. Transition of carbon species of HAs with heating treatment. (▲) Aromatic C species; (●) alkyl C species; (■) O-alkyl C species; (×) carboxyl C species.

4.3.6. XRD

XRD patterns of HAs and after waveform separation of those patterns are shown in Fig. 4.6 and 4.7. Gray lines are observed patterns, and black lines are fitted curves. *R* factors were less than 3 for all samples, and the accuracy of the fitting was confirmed. The XRD patterns were separated into four peaks, at 21°, 25°, 32°, and 40° 2θ, and these peaks were attributed to the γ_1, 002, γ_2, and 10 bands, respectively (Katsumi et al., 2015b). Simultaneous appearance of the 002 and 10 bands at these 2θ values is a typical feature of a graphite-like structure (Fujimoto, 2003). The γ_1 and 002 bands were assigned to aliphatic components and a stacked carbon plane, respectively (Katsumi et al., 2015b). The 002 bands became sharper with increasing temperature, and the 002 band was the dominant peak at temperatures above 250 °C. Meanwhile, the peak intensity of the γ bands decreased with increasing temperature. In other words, heating resulted in an increase in the proportion of aromatic C species and a decrease in the proportion of the aliphatic component. These results are in agreement with the elemental composition and ^{13}C NMR results. The stacking nanostructure properties of the HAs are shown in Table 4. The d_{002} value of the HAs was similar to that of graphite (0.335 nm). The d_{002} values for the YGU sample decreased with increasing temperature (0.352 nm to 0.340 nm), whereas no similar pattern was evident for the TRG sample. The N_c and L_c values of the HAs increased with heating temperature. Japanese Andisol HAs have a developed stacking nanostructure (Katsumi et al., 2015b), and the stacking nanostructures of HAs extracted from heated Entisols (YGU) are similar to those extracted from Japanese Andisols. In contrast, HAs extracted from heated Inceptisols (TRG) had poorly developed nanostructures relative to those extracted from heated Entisols.

4.4. Discussion

4.4.1. Effect of heating on the composition of humic substances

Our results showed that heating drastically changed the solubility properties of humic substances. For the TRG sample, temperatures above 250 °C resulted in an increase of the AIF and decreases of the HA and FA fractions, and AIF was the main organic component. These findings are similar to the results of previous laboratory heating experiments (Almendros et al., 1990; Fernandez et al., 2001) and are consistent with the quantitative decreases of the HA and FA fractions found after natural fires (Vergnoux et al., 2011). González-Vila and Almendros (2003) showed that HAs are rapidly transformed into AIF at 350 °C by carbonization. Japanese pampas grass (*Miscanthus sinensis*) and Japanese cedar (*Cryptomeria japonica*) were rapidly

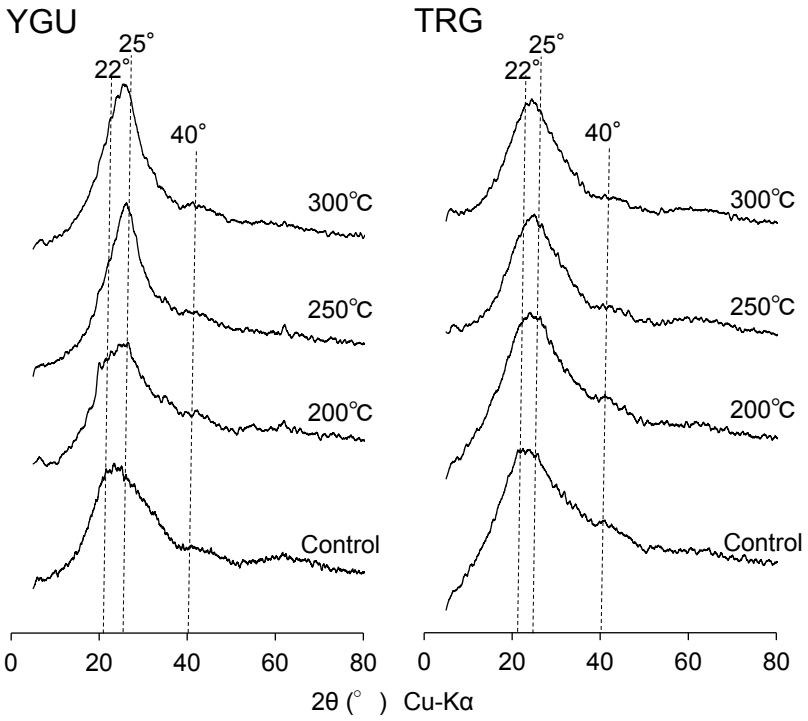

Fig. 4.6. Changes in XRD patterns of HAs with heating treatment

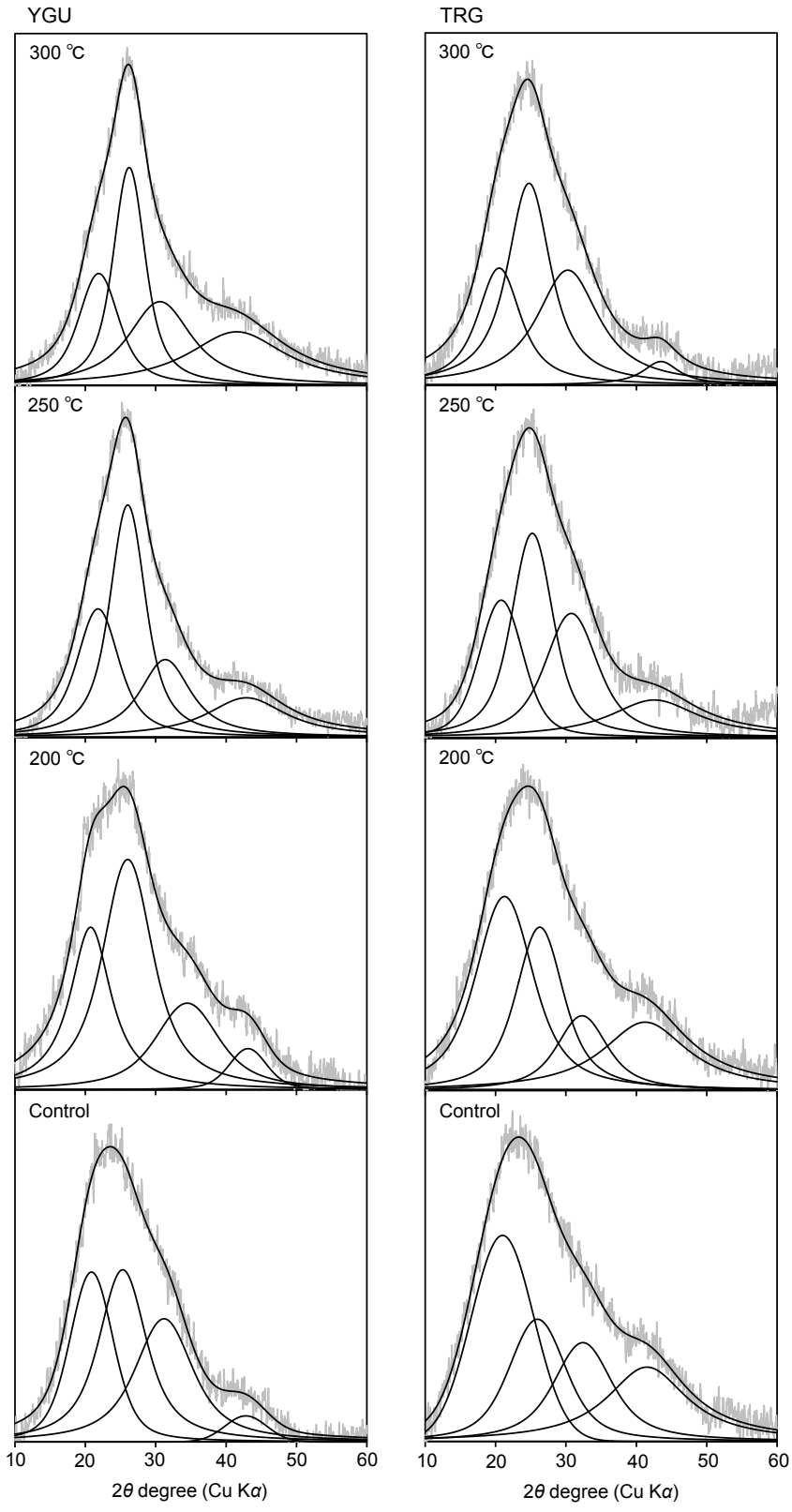

Fig.4.7. Changes in deconvoluted XRD patterns of HAs with heating treatment

Table 4.4. Changes in stacking nanostructure properties of HAs with heating treatment for 5 h

	Temperature (°C)	d_{002} (nm)	L_c	N_c
YGU	Control	0.352	1.06	3.02
	200	0.342	1.12	3.26
	250	0.342	1.41	4.12
	300	0.340	1.57	4.64
TRG	Control	0.345	1.04	3.01
	200	0.345	1.06	3.07
	250	0.345	1.17	3.38
	300	0.343	1.22	3.55

carbonized at temperatures above 250 °C under the conditions of our study (data not shown). Therefore, part of the HA and FA fractions can be transformed into AIF by carbonization at temperatures above 250 °C.

In contrast, for the YGU sample, the proportion of HA fraction increased 2- to 3-fold with increasing heating duration owing to the decrease of AIF and FA fraction, and HAs were the main organic component after heating. It appears that AIF turned into HAs, because there is no correlation between the HA content and the FA content. For the YGU sample, two hypotheses can be considered: (1) some components of AIF are chemically transformed into HAs by ongoing polymerization or depolymerization reactions during heating and (2) heat-induced alteration leads to an increase in the extractability of the fraction that is tightly bound to the mineral phase. The first hypothesis is likely because fire is a factor in the thermal condensation of soil organic compounds (Tinoco et al., 2006) and in forming new macromolecular structures in HAs (Fernandez et al., 2004; González-Pérez et al., 2004). The second hypothesis requires that the thermal conductivities of different types of minerals and possible catalyst effects be taken into account, which is beyond the scope of the present study. Further studies are needed to confirm this hypothesis.

4.4.2. Importance of type of vegetation in the heating-induced chemical structure alterations of HAs

González-Pérez et al. (2004) reported that heating SOM led to decreases in alkyl C and O-alkyl C and an increase in aromatic C. These results suggested that heating induced production of new aromatic material from O-alkyl C species of carbohydrates through Maillard reactions. In the present study, ^{13}C NMR spectra showed that the newly formed HAs were rich in aromatic C and poor in O-alkyl C, suggesting that these HAs also could be formed by Maillard reactions. HAs newly formed by heating are not present in biomass or SOM unaffected by fire. Such increases in molecular diversity could be related to progressively chaotic structures not readily recognized by soil enzymes, which could play a role in the resistance of post-fire SOM to biodegradation (Knicker, 2007).

For the YGU sample, the methylene chain peaks at 32 ppm in the ^{13}C NMR spectra disappeared after heating; in contrast, methylene chains were protected selectively in the TRG sample. Thermogravimetric analysis of a Japanese Entisol paddy soil revealed that lipids and carbohydrates in the soil were thermally decomposed at 250 °C (Yonebayashi et al., 1974). In contrast, lipids and carbohydrates in Japanese forest soils decompose above 300 °C (Sato, 1984). The long-chain unsaturated fatty acids cutin and suberin, commonly found as organic C in forest

soils, are highly resistant to biodegradation (Kögel-Knabner et al., 1992), and the amounts of cutin and suberin in forest soils are higher than the amounts in grassland soils. Because the aliphatic C–H stretching vibration appears in Fourier transform infrared spectra until 350 °C during incomplete combustion of *C. japonica* (Sultana et al., 2011), these components are relatively stable under moderate heating conditions, but a reduction of chain length may occur. These results suggest that, under moderate heating conditions, structural changes of HAs differ depending on the source of the plant species (grass plant or woody plant). Under moderate heating conditions (<300 °C), the major structural components of HAs derived from grass plants become aromatic C and carboxyl C, whereas aliphatic components remain in HAs derived from woody plants. These remaining aliphatic components may play a key role in inhibiting the development of stacking nanostructures in Inceptisol HAs.

4.4.3. New insights into the thermal denaturation of humic substances

Previous studies (Almendros and González-Vila, 2012; González-Pérez et al., 2004) have demonstrated that the main structural changes in HAs exposed to a relatively high temperature (350 °C) are (1) an increase in aromatic C content with aromatization of O-alkyl and alkyl C, (2) removal of oxygen-containing functional groups, (3) formation of heterocyclic N compounds, and (4) reduction of chain length of alkyl compounds. In the present study, we have demonstrated four new important features: (1) high temperatures lead to an increase in the $\delta^{13}C$ and $\delta^{15}N$ values of the HAs, (2) a stacking aromatic nanostructure develops when HAs are exposed to high temperatures, (3) the proportion of carboxyl groups increases due to condensation or addition under moderate heating, and (4) changes in the chemical structure features of HAs during heating depend on their end members. The L_c value for the control was essentially the same as that at 200 °C, whereas L_c increased sharply at 250 °C. As described above, heating at 250 °C led to carbonization. This result suggests that stacking aromatic nanostructures are developed by partial carbonization of HAs. These aspects can be strong factors for producing dark soils.

Chapter 5. General Discussion

5.1. Development for the analytical methods of HAs to reveal the environmental behavior.

Renovation of analysis technique during the past three decades makes a major contribution to the understanding of structure and properties of humic substances. Stacking nanostructure of HAs, a stable form of carbon in soil, consisted from lots of condensed aromatic C plane in nanometre-scale has been studied for a long time (Matsui et al. 1984). However, those environmental behaviors remained to be explained due to the analytical method was not defined. Therefore, I developed the new methods which evaluated the stacking nanostructure in HAs extracted from Japanese Andisols, Inceptisols, and Entisols using XRD in Chapter 3.

To reveal the environmental behavior of stacking nanostructure in HAs, I will discuss the relationship between stacking nanostructure properties and C dating using soil profile of nonalophanic Andisols in Ishikawa, Japan from the following sentences. Soil samples were collected from Nodayama, Ishikawa Japna (Fig. 5.1) and chemical properties of soil samples are shown in Table 5.1 and 5.2. Soil samples were collected from the A horizons (A1: 0 to 20 cm, A2: 20 to 40 cm, A3: 40 to 60 cm). The median ^{14}C cal yr BP of bulk soil and HAs ranged from 1,317 to 5,418 and 1,595 to 5,790, respectively. The $\delta^{13}C$ of HAs extracted from those soil samples ranged from −15.4 to −17.0 ‰, suggesting contribution of C4 plant (grass plant) derived C to TC reached more than 70%. In Japan, the climax vegetation is forest, and artificial burning or wildfire is needed to maintain the grassland vegetation for long period (Yamane 1973). Therefore, the vegetation of this site is secondary forest now, but grassland (Japanese pampas grass) vegetation had been maintained by human activity before 6,000 years.

The relationship between stacking nanostructure properties and C dating are shown in Fig. 5.2. The L_c and N_c of HAs increased with increment of C dating and soil depth. In this case, two hypotheses could be considered; (1) stacking nanostructure is more stable than aliphatic component and carbohydrate in HAs chemical structure, which remains and accumulates selectively in soil profile; (2) the qualitative changes of HAs from upper horizon is caused by changes in microbiota with the succession from grass to forest.

The first hypothesis comes from the classical belief proposed by Kumada (1987). Humification is the process of darkening for HAs, and HAs transform into stabilized phase with progress of humification. Changes in the chemical composition with progress of humification are as follows; 1) increase of A_{600}/C, 2) decrease of H/C ratio, 3) decrease of alkyl and O-alkyl C and 4) increment of aromatic C (Fujitake et al., 2012). Those changes are reflected the process which transformed to chemically stable state for SOM. Actually, the proportion of

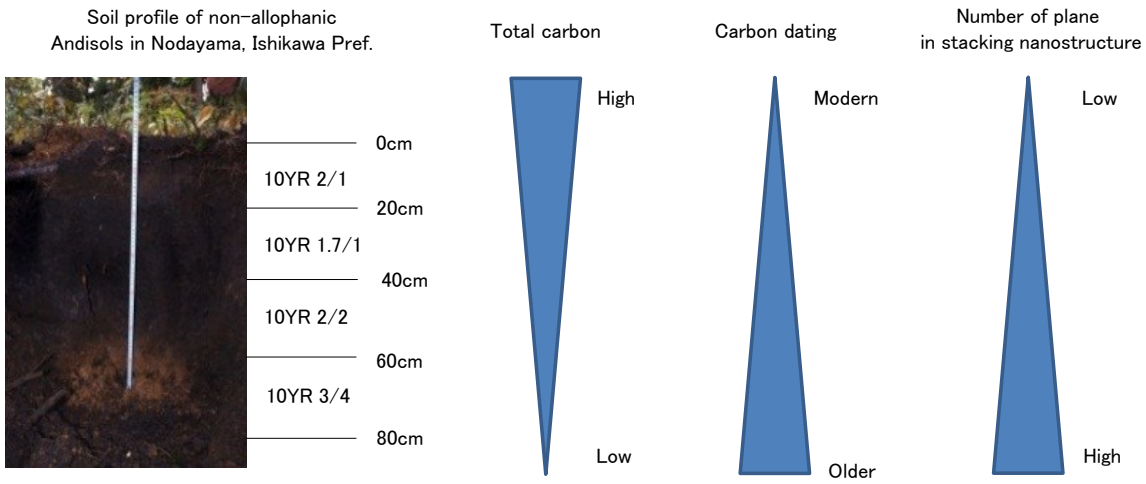

Fig.5.1. Soil profile of nonallphanic Andisols in Nodayama, Ishikawa Pref. Central Japan and characteristics of those HAs.

Table 5.1. Chemical properites of soil samples from Nodayama, Ishikawa Japnan

Horizon	Depth	pH		TC	TN	CEC	Texture	Acid-oxalate				Stable isotope ratio	
	cm	H_2O	NaF	mg kg^{-1}		cmolc kg^{-1}		Alo	Feo	Sio	Alo+1/2Feo	$\delta^{13}C$	$\delta^{15}N$
A1	0-20	4.9	11.5	104.3	4.7	54.5	LiC	20.0	15.0	0.5	27.5	-16.2	4.3
A2	20-40	4.7	11.7	97.1	4.2	58.5	LiC	20.5	15.5	0.5	28.2	-17.0	5.8
A3	40-60	4.9	11.7	72.8	3.0	46.8	LiC	19.3	16.2	0.6	27.3	-15.4	3.8
Bw	60-70	4.7	10.8	17.9	1.4	29.4	LiC	17.0	14.4	1.8	24.2	-	-

Table 5.2. ^{14}C age of soil and their HAs.

	Depth	^{14}C age	^{14}C cal yr BP			Labo Code
	cm	yr BP	2σ range	median	probability(%)	
Soil	0-20	1405 ± 25	1290-1344	1317	100.0	NUTA2-20466
	20-40	2495 ± 25	2489-2644	2567	77.1	NUTA2-20467
			2651-2670	2661	3.0	
			2675-2723	2699	19.9	
	40-60	4640 ± 25	5310-5333	5322	17.6	NUTA2-20468
			5348-5352	5350	0.6	
			5372-5463	5418	81.7	
Humic acids	0-20	1710 ± 25	1554-1635	1595	72.0	NUTA2-19499
			1648-1695	1672	28.0	
	20-40	2745 ± 25	2776-2884	2830	97.8	NUTA2-19498
			2909-2919	2914	2.2	
	40-60	5115 ± 25	5753-5826	5790	55.0	NUTA2-19500
			5860-5922	5891	45.0	

aromatic C and A_{600}/C increased, whereas the proportion of alkyl and O-alkyl C decreased from the surface (< 1,000 yBP) toward to the older layers (30,000 yBP) in buried Andisols profile (Watanabe and Takata, 2006). This result indicates that stacking nanostructure in HAs also develop from the surface toward to the older layers in buried Andisols profile.

As to second hypothesis, changes in the microbial flora with ecological succession may play an important role in the regulation to the transformation of HAs chemical structure in soil profile. Melanic epipedon that contained a large amount of Type-A HAs develops under grassland vegetation in Japan. Golchin et al. (1997) demonstrated that ecological succession from Japanese pampas grass to deciduous broad-leaf forest via pine forest over a time-span of a hundred years resulted in the gradual disappearance of the melanic epipedon with decreasing aromatic C and increasing alkyl C proportions in the bulk soil and HAs detected by ^{13}C CPMAS NMR. Iimura et al. (2010; 2013) concluded that changes in chemical properties of HAs in that study site could be due to extraordinary microbial degradation processes through accelerated plant N uptake along with ecological succession from grassland to forest in earlier stages. There is an interesting report on soil microbial respiration in a Chilean volcanic ash soil with reforestation. Dube et al. (2009) reported significantly higher soil microbial respiration in pine forests at depths below 10 cm compared to an adjacent grassland site, and hypothesized that this may be due to the presence of mycorrhizae. Alfredsson et al. (1998) also reported that the decrease in soil C and N with afforestation on temperate grassland may be attributed to changes in soil macro- and micro-flora associated with the root/ rhizosphere systems in forests, compared with grassland. Ectomycorrhizal fungi associated with tree roots have been found to increase the mineralization of organic forms of N in soil via the production of extracellular hydrolase enzymes such as proteinase (Marschner and Dell, 1994; George and Marschner, 1996). The decrease in stacking nanostructure of HAs in our study site could also be result of changes in microbial properties with ecological succession (grassland to secondary forest).

(a)

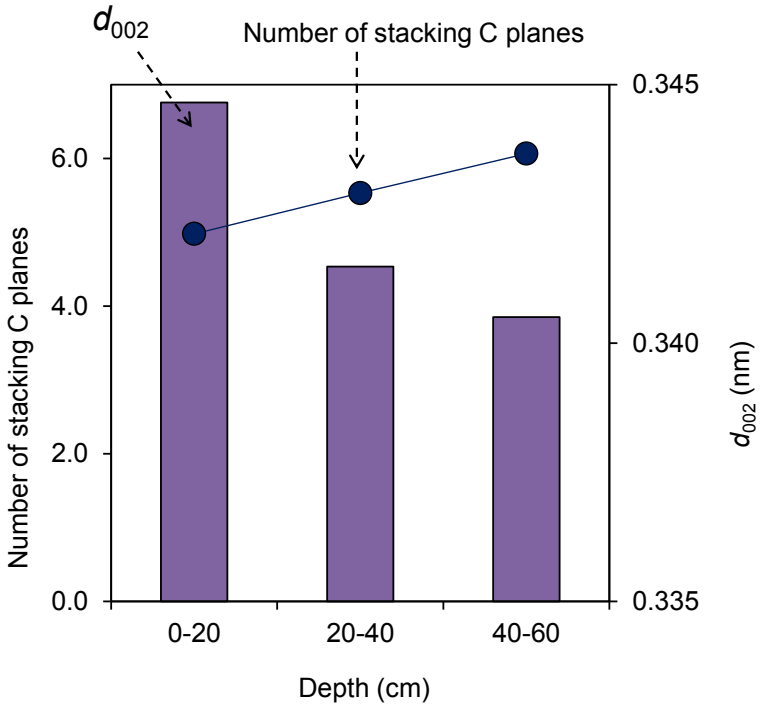

(b)

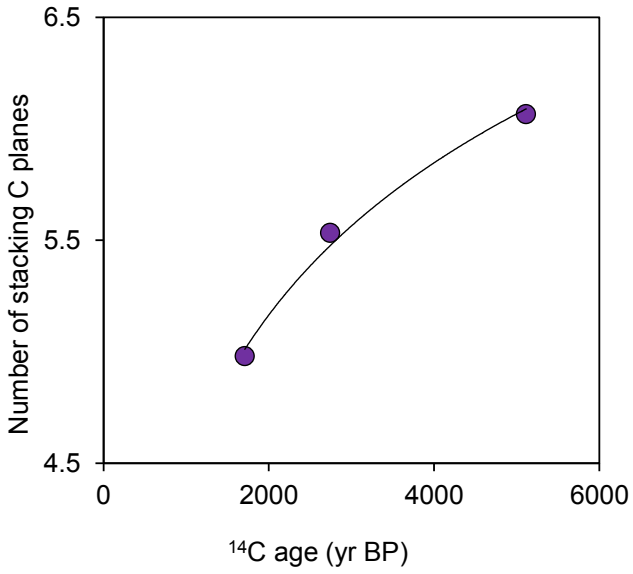

Fig. 5.2. Environmental behavior of Stacking nanostructure in soil HAs.
(a) The relationship between soil depth and properties of stacking nanostructure.
(b) The relationship between ^{14}C age and number of C planes.

5.3. Implication for genesis of Type-A HAs

Previous studies (Almendros and González-Vila, 2012; González-Pérez et al., 2004) have demonstrated that the main structural changes in HAs exposed to a relatively high temperature (350 °C) are (1) an increase in aromatic C content, due to aromatization of O-alkyl and alkyl C, (2) removal of oxygen-containing functional groups, (3) formation of heterocyclic N compounds, and (4) reduction of the chain length of alkyl compounds. In the present study, we demonstrated four important new features: (1) changes in the chemical structure of HAs during heating depended on their end members, (2) high temperatures led to an increase in the $\delta^{13}C$ and $\delta^{15}N$ values of the HAs, (3) a stacking aromatic nanostructure developed when HAs were exposed to high temperatures (>250 °C), and (4) the proportion of carboxyl groups increased, owing to condensation or addition, during heating at moderate temperatures. These features contributed to the darkening of HAs, suggesting that fire accelerates humification.

Andisols in Japan have A horizons (melanic epipedon) that are very thick and dark in color and contain a large amount of SOM. The dark color has spurred many soil scientists to study the humus composition, and the dark color has been attributed to the existence of highly humified HAs, referred to as Type-A HAs (Shoji et al., 1993). Type-A HAs are characterized by high aromatic C content, low alkyl C and O-alkyl C contents (Fujitake et al., 2012), and turbostratic structure (Katsumi et al., 2015b). Ikeya et al. (2011) analyzed the XRD profile of Type-A HAs and found that the size of the condensed aromatic rings along the *a* axis (L_a) in Type-A HAs ranges from 0.48 to 1.68 nm, corresponding to condensed aromatic components with 4 to 37 rings. The content of the carbon planes corresponding to 14-, 19- and 30-ring condensed aromatic structures correlates positively with degree of darkness. The L_a value of the condensed aromatic components is larger than that of polynuclear quinones, such as the dihydroxyperylenequinones (4 rings) in Type-P HAs, produced by fungi (Kumada and Hurst 1967). Therefore, the condensed aromatic structures may be produced by abiotic oxidation (Ikeya et al., 2015). There are two theories about the formation of Type-A HAs: (1) they originate from oxidized charred plant materials or (2) they originate from decay and denaturation of plants without the formation of charred materials.

Shindo et al. (2004a) suggest that charred plant materials in Andisols are one source of Type-A HAs, on the basis of the fact that the physicochemical and spectroscopic properties of HAs obtained from treatment of charred grasses with nitric acid or H_2O_2 are similar to the properties of Type-A HAs. In addition, the ^{13}C NMR spectra of HAs extracted from terra preta de indio soil are similar to the spectra of Type-A HAs (Araujo et al., 2014). Therefore, charred plant materials could be an important source of Type-A HAs. However, the contribution of charred plant materials to organic C in Andisols ranges from 3.4% to 32.7% (median value,

8.5%) in Japan (Shindo et al., 2004b) and from 0.3% to 6.9% (median value, 1.8%) in Chile (Rivas et al., 2012). In contrast, the contribution of HAs to organic C in Andisols is approximately 30% (Watanabe and Kuwatsuka, 1991). Thus, charred plant materials may be only a minor source of HAs, even if all the charred plant materials are extracted as HAs.

The following experiment, which supports the second of the two theories mentioned above, resulted in the formation of Type-A HAs from plant residues by means of thermal incubation without charring. When plant residues of Japanese pampas grass (*M. sinensis*), dwarf bamboo (*Sasa nipponica*), and Japanese emperor oak (*Quercus dentata*) were incubated separately at 60, 75, or 90 °C with or without fresh volcanic ash in the presence of water, three important results were observed: (1) the formation of Type-A HAs was temperature dependent; (2) the grass plants were most likely to be converted to Type-A HAs; and (3) fresh volcanic ash catalytically accelerated darkening of the test materials (Otsuka et al., 1994).

In present study, I showed that the degree of darkness of HAs increased with increasing heating temperature and time, and heating treatments produced Type-A HAs from Entisols and Inceptisols which were categorized to be Type-B HAs. In addition, the heating provided the increment of aromatic C and decrease of alkyl and O-alkyl C with development of stacking structure, and the ^{13}C NMR spectra and XRD profile of heated soil samples were similar to those of Type-A HAs. Those finding raise the possibility that soil heating could be one of the synthesis pathway to formed Type-A HAs. Melanic epipedon develop under grassland vegetation in Japan. In Japan, the climax vegetation is forest and artificial burning or wildfire is needed to maintain the grassland vegetation for long period (Yamane, 1973). Moreover, melanic epipedon were generated after wildfires in Northern California, USA and Hachinohe Aomori, Japan without grassland vegetation (Takahashi et al, 1994, Hosono et al. 1995). Forest fires produce temperatures typically ranging from 200 to 400ºC at the soil surface to a few centimeters below the soil surface (Gimeno-Garcia et al., 2004). Those HAs in Andisols may be created by repletion of heating with wildfire (Fig. 5.3).

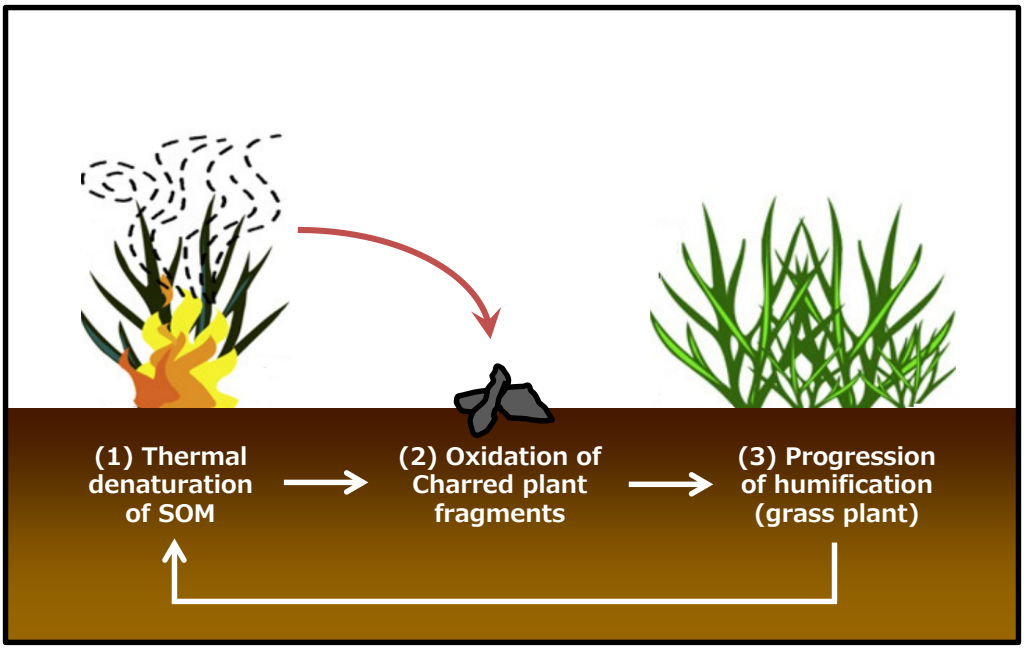

Fig.5.3. Concept for the formation process of Type-A HAs in melanic epipedon proposed in this Ph.D thesis.

Summary

The objective of this study is to develop and apply novel analytical method to determine thermal denaturation process of soil organic matter. This thesis is composed of five chapters. Chapter 1 is a general introduction of this study.

To relate the isotopic composition of soil HAs to their source plants and their degree of humification (as indicated by the degree of darkening), as well as to soil type, I determined the stable isotope ratios for carbon ($\delta^{13}C$) and nitrogen ($\delta^{15}N$) of HAs extracted from 26 virgin soil samples (14 Andisols and 12 non-Andisols) and from leaf samples from ten C_3 plants and seven C_4 plants in Chapter 2. The high absorption coefficients (estimated at 600 nm for 1% solutions), low hydrogen and nitrogen contents, low H/C ratios, low alkyl C and *O*-alkyl C contents, high O/H and C/N ratios, high aryl C contents, and high aromaticity of the Andisol HAs indicated a high degree of humification. The $\delta^{13}C$ and $\delta^{15}N$ values of the non-Andisol HAs increased along with the progression of humification of C_3 plant–derived HAs. A significant correlation was observed between the $\delta^{15}N$ and $\delta^{13}C$ values of the non-Andisol HAs, but not for the Andisol HAs. Most of the Andisol HA $\delta^{13}C$ values were higher than the highest non-Andisol HA $\delta^{13}C$ value, and $\delta^{13}C$ values were distributed between the $\delta^{13}C$ values for the C_3 and C_4 plants. The contributions of C_4 plant–derived carbon to total Andisol HA carbon (CR_{C4}) are usually calculated on the assumption that the $\delta^{13}C$ values are not substantially altered during the decomposition of plant materials and the formation of soil organic matter. However, if ^{13}C enrichment occurs during organic matter decomposition, CR_{C4} will be overestimated. Therefore, we suggest a new method to calculate CR_{C4} values of Andisol HAs with a correction for isotopic fractionation associated with microbial degradation; the corrected CR_{C4} values ranged from –5% to 58% and were approximately 22% lower than the uncorrected values.

In chapter 3, I used X-ray diffraction (XRD) to develop models for the stacking nanostructure of 12 humic acids (HAs) extracted from Japanese Andisols, Inceptisols, and Entisols. In the XRD profiles of the HAs, the γ band, which was attributed to aliphatic side chains, and the 002 band were separated by means of curve fitting with the Voigt function. The interlayer spacing of the carbon (C) planes (d_{002}) and the mean thickness of the stacking nanostructure along the *c* axis (L_c) were calculated from the position of the peak for the 002 band and the full-width at half maximum by means of Bragg's and Scherrer's equations, respectively. The average number of C planes in the stacking nanostructure (N_c) was estimated from d_{002} and L_c. The L_c and N_c values ranged from 1.04 to 1.84 nm and from 3.01 to 5.40, respectively. The mean L_c and N_c values of the Andisol HAs were larger than those of the Inceptisol and Entisol HAs ($P < 0.01$). The d_{002} value of the HAs was approximately 0.34 nm,

which was slightly larger than that of graphite (0.335 nm). The L_c value positively correlated with aromatic C content ($r = 0.938$, $P < 0.01$) and negatively correlated with the sum of alkyl C and O-alkyl C contents ($r = -0.958$, $P < 0.01$), which were estimated from the liquid-state ^{13}C nuclear magnetic resonance spectra. Furthermore, the degree of darkness of the HAs positively correlated with L_c ($r = 0.961$, $P < 0.01$). Analysis of the 002 band of the XRD profile clarified the number of C planes in the stacking nanostructure and the thickness of the stacking layer unit of the HAs. Our results indicate that the accumulation of polynuclear aromatic C with stacking nanostructures contributed to the darkening of HAs in soil.

In chapter 4, I investigated qualitative and quantitative changes of soil humic substances in two different soils (an Entisol from a paddy field and an Inceptisol from a cedar forest) under several controlled heating conditions. Soil samples were heated in a muffle furnace at 200, 250, or 300 °C for 1, 3, 5, or 12 h. The HA and FA contents of the soil samples prior to and after heating were determined. The degree of darkness, elemental composition, carbon and nitrogen stable isotope ratios, ^{13}C nuclear magnetic resonance spectra, and XRD patterns of HAs extracted from the soils before and after heating were measured. The proportion of HAs in total carbon decreased with increasing heating time at high temperature (300 °C), but increased with increasing heating time at ≤ 250 °C. The degree of darkness of the HAs increased with increasing heating time and temperature. During darkening, the H/C atomic ratios, the proportion of aromatic C, and the carbon and nitrogen stable isotope ratios increased, whereas the proportions of alkyl C and O-alkyl C decreased. XRD analysis verified that a stacking nanostructure developed by heating. Changes in the chemical structure of the HAs from the heated soils depended on the type of soil. The major structural components of the HAs from the heated Entisol were aromatic C and carboxylic C, whereas aliphatic C, aromatic C, and carboxylic C structural components were found in the HAs from the heated Inceptisol. These results suggest that the heat-induced changes in the chemical structure of the HAs depended on the source plant.

In Chapter 5, I discussed about the genesis of dark colored HAs in Andisols based on the results of this study. I concluded that fire play an important role in the genesis of dark colored HAs in Andisols.

要旨

日本には黒くて厚い A 層を有する黒ボク土が存在する。これらの土壌における黒味の発現には、極めて黒色度が高い腐植物質が関与していると考えられているが、それらの黒色化プロセスは未解明のままである。本論文では黒色度が高い腐植物質の生成には火が関与しているという作業仮説のもと、安定同位体比と XRD を用いて黒ボク土の腐植物質が受けてきた火の履歴を直接的/間接的に評価し、それらの情報に基づいて腐植物質の黒色化と熱変性の関係を解析した。本論文は次の各章から成っている。

第 1 章は序論であり、この研究の背景を明示するとともに、本論文で取り扱う課題について記述している。

第 2 章では腐植酸の同位体比組成に腐植化度および給源となった植物が与える影響を調べるために、日本各地で採取した 26 種類の未耕地土壌(黒ボク土 14 点、褐色森林土 12 点)から抽出・精製された腐植酸および日本各地より収集した植物体の $\delta^{13}C$ および $\delta^{15}N$ を測定した。黒ボク土の腐植酸は高い芳香族性、高い黒色度、低 H/C 比、低いアルキルおよび O アルキル炭素含量を示し、黒ボク土の腐植酸は腐植化過程が進行していることが示された。黒ボク土の腐植酸の $\delta^{13}C$ は非黒ボク土の腐植酸の $\delta^{13}C$ よりも有意に高く、C3 植物と C4 植物の $\delta^{13}C$ の間に分布していた。このことは、黒ボク土の腐植物質の給源として C4 植物が関与することを示している。腐植酸の全炭素に占める C4 植物の寄与率(CR_{C4})の算出する際、従来までの手法では $\delta^{13}C$ の同位体分別効果を考慮されていなかった。しかし、本研究から腐植化過程を通じて ^{13}C も濃縮されることが明らかとなり、従来の方法では過大評価していることが示唆された。そこで、微生物分解による炭素の同位体分別を考慮した新たな補正方法を提案したところ、本章で使用した腐植酸の CR_{C4} は-5～58%であり、従来の手法は平均で 22%過大評価していた。

第 3 章では日本の黒ボク土 7 点、褐色森林土 3 点、灰色低地土 3 点から抽出した腐植酸の積層ナノ構造モデルの構築に XRD を使用した。腐植酸の XRD パターンにおいて脂肪族化合物に由来するγバンドと 002 バンドをカーブフィッティングによって分離した。分離された 002 バンドのピーク位置と半値幅から炭素網面の面間隔（d_{002}）および積層ナノ構造の c 軸方向の大きさ（L_c）をシェラー式とブラッグ式から算出し、積層数（N_c）は d_{002} および L_c から推定した。L_c および N_c はそれぞれ 1.04 − 1.84 nm および 3.01 − 5.40 であった。それらの値は灰色低地土および褐色森林土から抽出された腐植酸より黒ボク土から抽出された腐植酸の方が高い値を示した。腐植酸の d_{002} はおよそ 0.34 nm であり、グラファイトの d_{002}（0.335 nm）より僅かに大きかった。L_c は芳香族炭素割合および黒色度との間に高い正の相関関係（$r = 0.938, P < 0.01$、$r = 0.961, P < 0.01$）、アルキル炭素割合および O-アルキル炭素割合の合計との間に高い負の相関関係（$r = -0.958, P < 0.01$）が認められた。これらの結果は、縮合芳香環がナノレベルで積層した

構造の集積によって腐植酸の黒色化が制御されていること意味する。さらに、積層構造の生成には非生物的な酸化反応が重要な役割を演じていることが示唆された。

第 4 章では土壌有機物の給源となった植生が大きく異なる 2 種類の土壌を用いて、加熱条件の違いによる土壌腐植酸の質的量的変化を調べた。供試土壌を 200～300℃で 0～12 時間加熱し、加熱前後の土壌における腐植酸、フルボ酸およびヒューミン含量を測定した。さらに、それらの土壌から腐植酸を抽出・精製し、黒色度、元素組成、炭素・窒素安定同位体比、^{13}C NMR および XRD を測定した。腐植酸含量は 300℃で減少したのに対し、250℃以下では増加した。黒色度は加熱時間と温度の増加によって増大した。腐植酸の黒色化の進行に伴い、芳香族炭素割合および炭素・窒素安定同位体比の増大が確認され、アルキル・O アルキル炭素割合および H/C 原子数比が低下した。XRD によって積層数を算出したところ、加熱温度の増大によってそれらの数は増加した。草本由来の土壌腐植酸の ^{13}C NMR スペクトルは加熱によって芳香族炭素とカルボキシル炭素のみとなったが、木本由来の土壌腐植酸ではそれらに加え、シャープなメチル炭素のピークが残存した。これらの結果は火による土壌有機物の化学構造特性の変化は給源となった植物種の違いに依存する事を示唆し、草本由来の土壌を加熱する事によって黒ボク土の腐植酸に極めて類似した腐植酸が生成することが明らかとなった。

第 5 章では、これまで得られた結果をもとに黒ボク土における黒色度の高い腐植酸の生成プロセスについて考察した。2 章と 3 章から、黒ボク土は他の土壌と比べて、(1) 草本由来の炭素の寄与が認められること、(2) 黒ボク土の腐植酸には生合成可能な大きさをはるかに超えた大きさの縮合環が積層したグラファイト様構造をもつことが明らかとなった。これらの結果は、(1) 黒ボク土では定期的に火入れが行われることによって、極相が森林である日本においても草本植生が維持され、(2) その時の熱によって腐植物質が熱変性されてきたことを意味する。これらの仮説は、第 4 章において黒ボク土以外の草本由来の有機物を含む土壌を加熱する事によって、黒ボク土に含まれる黒色度の高い腐植酸と化学構造が極めて類似した腐植酸が生成されることからも実証された。

以上のことから、黒ボク土における黒色度の高い腐植酸の生成には、草本植生を維持するために行われてきた火入れが重要な役割をしていると結論付けた。

Publications

本論文を構成する主要な論文

[1] **Naoya Katsumi**, Koyo Yonebayashi, Masanori Okazaki, 2015. Evaluation of stacking nanostructure in soil humic acids by analysis of the 002 band of their X-ray diffraction profiles. Soil Science and Plant Nutrition. DOI: 10.1080/00380768.2015.1034638

[2] **Naoya Katsumi**, Koyo Yonebayashi, Nobuhide Fujitake, Masanori Okazaki, 2015. Relationship between stable carbon and nitrogen isotope ratios of humic acids extracted from Andisols and non-Andisols. Catena, 127, 214-221.

[3] **Naoya Katsumi**, Koyo Yonebayashi, Masanori Okazaki, 2015. Effects of heating on composition, degree of darkness, and stacking nanostructure of soil humic acids. Science of the total Environment. Submitting.

その他の論文

[1] **Naoya Katsumi**, Koyo Yonebayashi, Masanori Okazaki, 2015. Aluminum complexation by soil humic acids, with special reference to chelating ability. Pedologist, 59, 2-11.

[2] 米林甲陽・安部真由美・神木麻里・**勝見尚也**・岡崎正規　2015. 土壌腐植酸の添加濃度が稲幼植物の養分吸収に及ぼす影響. 日本土壌肥料学雑誌, 86, 167-174.

[3] 駒井幸雄・米林甲陽・**勝見尚也**・入月俊明・辻本彰・岡崎正規 2015. 炭素・窒素安定同位体比とメイオベントス相から見た瀬戸内海の底質環境の変遷. 水環境学会誌. 38, 39-47.

[4] Masanori Okazaki, **Naoya Katsumi**, Shun Nishiyama, Ladie Anne Palermo, Masato Igura, 2014 Thermal Denaturation Properties of Non-Spiny and Spiny Sago Palm Starches under Low Moisture Content. SAGO PALM. 22, 31-37.

[5] **Naoya Katsumi**, Masanori Okazaki, Koyo Yonebayashi, Fumi Kawashima, Shun Nishiyama and Tomoe Nishi, 2014. New proposal for “crystalline index” of starch. SAGO PALM. 22, 25-30

[6] Koyo yonebayashi, **Naoya Katsumi**, Tomoe Nishi, Masanori Okazaki, 2014. Activation of nitrogen-fixing endophytes is associated with the tuber growth of sweet potato. Mass Spectrom (Tokyo). 3, A3002. DOI: 10.5702/massspectrometry.A0032

[7] Masanori Okazaki, Marcelo A Quevedo, Szette B lina, Tai-ichiro Ookawa, **Naoya Katsumi**, 2013. Breaking resistance of sago palm leaflets. SAGO PALM 21, 8-13

[8] Masanori Okazaki, Koyo Yonebayashi, **Naoya Katsumi**, Fumi Kawashima and Tomoe Nishi. 2013. Does sago palm have high $\delta^{13}C$ value? SAGO PALM 21, 1-7

References

Abe, T., Watanabe, A., 2004. X-ray photoelectron spectroscopy of nitrogen functional groups in soil humic acids. *Soil Sci*. 169, 35−43.

Akamatsu, F., Toda, H., Okino, T., 2004. Food source of riparian spiders analyzed by using stable isotope ratios. *Ecol. Res*. 19, 655−662.

Alfredsson, H., Condron, L.M., Clarholm, M., Davis, M.R., 1998. Changes in soil acidity and organic matter following the establishment of conifers on former grassland in New Zealand. *For*. *Ecol*. *Manage*. 112, 245–252.

Almendros, G., González-Vila, FJ., Martin. F., 1990. Fire-induced transformation of soil organic matter from an oak forest: An experimental approach to the effects of fire on humic substances. *Soil*. *Sci*. 149, 158−168.

Almendros,G., Dorado, J., Gonza´ lez-Vila,F.J., Martin,F., 1997. Pyrolysis of carbohydrate-derived macromolecules: its potential in monitoring the carbohydrate signature of geopolymers. *Journal of Analytical and Applied Pyrolysis* 40-41, 599–610

Almendros, G., Knicker, H., González-Vila FJ., 2003. Rearrangement of carbon and nitrogen form in peat after progressive thermal oxidation as determined by solid-state ^{13}C- and ^{15}N-NMR spectroscopy. *Org*. *Geochem*. 34, 1559−1568.

Almendros, G., González-Vila, F.J., 2012. Wildfires, soil carbon balance and resilient organic matter in Mediterranean ecosystems. A review. *Spanish J*. *Soil Sci*. 2, 8−33.

Araujo, J.R., Archanjo, B.S., de Souza, K.R., Kwapinski, W., Falcao, N.P.S., Novotny, E.H., Achete, C.A., 2014. Selective extraction of humic acids from an anthropogenic Amazon dark earth and from a chemically oxidized charcoal. *Biol*. *Fertil*. *Soils* 50, 1223−1232.

Baldock JA, Skjemstad JO. 2000. Role of the soil matrix and minerals in protecting natural or ganic materials against biological attack. *Org*. *Geochem*. 31, 697–710.

Balieiro, F.C., Benites, V.M., Caiafa, A.N., Alves, B.J.R., Fontana, A., Canellas, L.P., 2012. Vegetation influence on organic matter source of black soils from high altitude rocky complexes traced by ^{13}C and ^{15}N isotopic techniques. *Catena* 99, 97−101.

Bento-Gonçalves A, Vieira A, Úbeda X, Martin D 2012. Fire and soils: Key concepts and recent advances. *Geoderma* 191, 3-13

Bird, M.I., Ascough, P.L., 2012. Isotopes in pyrogenic carbon: A review. *Org*. *Geochem*. 42, 1529−1539.

Boutton, T.W., Archer, S.R., Midwood, A.J., Zitzer, S.F., Bol, R., 1998. δ^{13}C values of soil organic carbon and their use in documenting vegetation change in a subtropical savanna ecosystem. *Geoderma* 82, 5−41.

Bowman, D. M. J. S., et al. 2009. Fire in the Earth system. *Science* 324, 481–484.

Certini, G., 2005. Effects of fire on properties of forest soils: A review. *Oecologia* 143, 1−10.

Chen H., Abdulla H. A. N., Sanders R. L., Myneni S. C. B., Mopper K. and Hatcher P. G. 2014. Production of black carbon-like and aliphatic molecules from terrestrial dissolved organic matter in the presence of sunlight and iron. *Environ*. *Sci*. *Technol*. *Lett*. 1, 399–404.

Chuvieco, E., Giglio, L., Justice, C., 2008.Global characterization of fire activity: toward defining fire regimes from Earth observation data. *Global Change Biology* 14, 1488–1502.

Connin, S.L., Feng, X., Virginia, R.A., 2001. Isotopic discrimination during long-term decomposition in an arid land ecosystem. *Soil Biol. Biochem*. 33, 41−51.

Czimczik, C.I., Preston, C.M., Schmidt, M.W.I., Werner, R.A., Schlze, E.D., 2002. Effects of charring on mass, organic carbon, and stable carbon isotope composition of wood. *Org*. *Geochem*. 33, 1207−1223.

DeBano, L.F., 2000. The role of fire and soil heating on water repellency in wildland environments: A review. *J*. *Hydrol* 231−232, 195−206.

Dorea, C.C., Clarke, B.A., 2008. Effect of aluminium on microbial respi- ration. *Water Air Soil Pollut*. 89, 353–358

Dube, F., Zagal, E., Stolpe, N., Espinosa, M., 2009. The influence of land-use change on the organic carbon distribution and microbial respiration in a volcanic soil of the Chilean Patagonia. *For*. *Ecol*. *Manage*. 257, 1695–1704.

Fernandez, I., Cabaneiro, A., Carballas, T.. 2001. Thermal resistance to high temperatures of different organic fractions from soils under pine forests. *Geoderma* 104, 281−298.

Fernandez, I., Cabaneiro, A., González-Prieto, S.J., 2004. Use of ^{13}C to monitor soil organic matter transformations caused by a simulated forest fire. *Rapid Commun*. *Mass Spectrom*. 18, 435−442.

Foereid, B., Bellamy, P.H., Holden, A., Kirk, G.J.D., 2012. On the initialization of soil carbon models and its effects on model predictions for England and Wales. *Eur*. *J*. *Soil Sci*. 63, 32–41.

Fujimoto, H., 2003. Theoretical X-ray scattering intensity of carbons with turbostratic stacking and AB stacking structures. *Carbon* 41, 1585−1592.

Fujitake, N., Kawahigashi, M., 1999. ^{13}C NMR spectra and elemental composition of fractions with different particle sizes from an Andisol humic acid. *Soil Sci*. *Plant Nutr*. 45, 359−366.

Fujitake, N., Kusumoto, A., Tsukamoto, M., Noda, Y., Suzuki, T., Otsuka, H., 1999. Properties of soil humic substances in fractions obtained by sequential extraction with pyrophosphate solutions at different pHs. II. Elemental composition and UV-VIS spectra of humic acids. *Soil Sci. Plant Nutr*. 45, 349−358.

Fujitake, N., Asakawa, D., Yanagi, Y., 2012. Characterization of soil humic acids by ^{13}C NMR

spectroscopy and high performance size exclusion chromatography. *Bunseki Kagaku* 61, 287−298 (in Japanese with English summary).

George, E., Marschner, H., 1996. Nutrient and water uptake by roots of forest trees. Z. Pflanz. Bodenk. 159, 11–21.

Gimeno-Garcia, E., Andreu, E., Rubio, J.L., 2004. Spatial patterns of soil temperatures during experimental fires. *Geoderma* 118, 17−38.

Golchin, A., Clark, P., Baldock, J.A., Higashi, T., Skjemstad, J.O., Oades, J.M., 1997. The effect of vegetation and burning on the chemical composition of soil organic matter in a volcanic ash soil as shown by ^{13}C NMR spectroscopy. I. Whole soil and humic acid fraction. *Geoderma* 76, 155–174.

González-Pérez, J.A., González-Vila, F.J., Almendros, G., Knicker, H., 2004. The effect of fire on soil organic matter – A review. *Environ*. *Int*. 30, 855−870.

González-Vila, F. J., Tinoco, P., Almendros, G., Martin, F., 2001. Pyrolysis-GC-MS analysis of the formation and degradation stages of charred residues from lignocellulosic biomass. *Journal of Agricultural and Food Chemistry*, 49, 1128–1131.

González-Villa, F.J., Almendros, G., 2003. Thermal transformation of soil organic matter by natural fires and laboratory-controlled heatings. In: Ikan R editors. Natural and laboratory-simulated thermal geochemical processes. Netherlands: Springer; p. 153−200.

Gregorich, E.G., Kachanoski, R.G., Voroney, R.P., 1989. Carbon mineralization in soil size fractions after various amounts of aggregate disruption. *J. Soil Sci*., 40, 649–659

Hart, S.C., Newman, G.S., DeLuca, T.H., MacKenzie, M.D., Boyle, S.I., 2005. Post-fire vegetative dynamics as drivers of microbial community structure and function in forest soils. *For*. *Ecol*. *Manage*. 220, 166−184.

Hillel D. Soil in the environment, Crucible of terrestrial life. Oxford: Elsevier; 2007.

Hiradate, S., Nakadai, T., Shindo, H., Yoneyama, T., 2004. Carbon source of humic substances in some Japanese volcanic ash soils determined by carbon stable isotopic ratio, $\delta^{13}C$. *Geoderma* 119, 133−141.

Hosono, M., Sase, T., Aoki, K., 1995. Vegetational history and humus properties of buried soil rich in charcoal fragments immediately beneath the Hachinohe pumice bed. *Pedologist* 39, 42-49.

Iimura, Y., Fujimoto, M., Hirota, M., Tamura, K., Higashi, T., Yonebayashi, K., Fujitake, N., 2010. Effects of ecological succession on surface mineral horizons in Japanese volcanic ash soil. *Geoderma* 159, 122−130.

Iimura, Y., Fujimoto, M., Tamura, K., Higashi, T., Kondo, M., Uchida, M., Yonebayashi, K., Fujitake, N., 2013. Black humic acid dynamics during natural reforestation of Japanese pampas grass (Miscanthus sinensis). *Soil Biol. Biochem*. 57, 60−67.

Ikeya, K., Watanabe, A., 2003. Direct expression of an index for degree of humification of humic acids using organic carbon concentration. *Soil Sci*. *Plant Nutr*., 49, 47–53.

Ikeya, K., Yamamoto, S., Watanabe, A., 2004. Semiquantitative GC/MS analysis of thermochemolysis products of soil humic acids with various degrees of humification. *Org. Geochem*. 35, 583−594.

Ikeya, K., Ishida, Y., Ohtani, H., Yamamoto, S., Watanabe, A., 2007. Analysis of polynuclear aromatic and aliphatic components in soil humic acids using ruthenium tetroxide oxidation. *Eur*. *J*. *Soil Sci*., 58, 1050–1061.

Ikeya, K., Hikage, T., Arai, S., Watanabe, A., 2011. Size distribution of condensed aromatic rings in various soil humic acids. *Org*. *Geochem*. 42, 55–61.

Ikeya, K., Sleighter, R.L., Hacher. P.G., Watanabe. A., 2015. Characterization of the chemical composition of soil humic acids using Fourier transform ion cyclotron resonance mass spectrometry. *Geochem*. *Cosmochim*. *Acta*. 153, 169–182.

Inagaki, Y., Miura, S., Kohzu, A., 2004. Effects of forest type and stand age on litterfall quality and soil N dynamics in Shikoku district, southern Japan. *Forest Ecol. Manage*. 202, 107−117.

Iwashita, N., Park, C.R., Fujimoto, H., Shiraishi, M., Inagaki, M., 2004, Specification for a standard procedure of X-ray diffraction measurements on carbon materials. *Carbon* 42, 701–714.

Katsumi, N., Yonebayashi, K., Okazaki, M., 2014, Effect of heating on humic substances: Changes in composition, structure and degree of darkness with several heating conditions. 2014 Joint Seminar of NPUST and IPU for Environmental and Ecological Restoration, 30–34.

Katsumi, N., Yonebayashi, K., Fujitake, N., Okazaki, M., 2015, Relationship between stable carbon and nitrogen isotope ratios of humic acids extracted from Andisols and non-Andisols. *Catema* 127, 214–221.

Katsumi, N., Yonebayashi, K., Okazaki, M., 2015b. Evaluation of stacking nanostructure in soil humic acids by analysis of the 002 band of their X-ray diffraction profiles. *Soil Sci*. *Plant Nutr*.,

Katsumi N, Okazaki M, Yonebayashi K, Nishi T, Nishiyama S, Ikeda A, Nakamura T. 2015. Characteristics and genesis of nonallophanic Andisols distributed on Saigawa River terrace, Ishikawa Prefecture, central Japan. Summaries of Researches using AMS at Nagoya Nuiversity (XXVI), 163–167.

Khan, N.A., Fujitake, N., Noda, Y., Suzuki, T., Otsuka, H., 2006. Comparison of humic acid fractions derived from thermally created plant residues and natural soils: Spectroscopic and elemental analyses. *Soil Sci. Plant Nutr.* 52, 349−360.

Knicker, H., González-Vila, F.J., Polvillo, O., González, J.A., Almendros, G., 2005. Fire induced transformation of C- and N-forms in different organic soil fractions from a Dystric Cambisol under a Mediterranean pine forest (*Pinus pinaster*). *Soil Biol*. *Biochem*. 37, 701–718.

Knicker, H., 2007. How does fire affect the nature and stability of soil organic nitrogen and carbon? A review. *Biogeochemistry* 85, 91−118.

Knicker, H., Hilscher, A., González-Vila, F.J., Almendros, G., 2008. A new conceptual model for the structural properties of char produced during vegetation fires. *Org*. *Geochem*. 39: 935−939.

Knicker, H., Nikolova, R., Dick, D. P., & Dalmolin, R. S. D. 2012. Alteration of quality and stability of organic matter in grassland soils of Southern Brazil highlands after ceasing biannual burning. *Geoderma* 181-182, 11–21.

Kobo, K., Tatsukawa, R., 1959. On the colored material of fulvic acid. *Zeitschrift für Pflanzenernährung, Düngung, Bodenkunde* 84, 137–147.

Kögel-Knabner, I., Hatcher. P.G., Zech, W., 1991. Chemical structural studies of forest soil humic acids: aromatic carbon fraction. *Soil Sci. Soc. Am. J*. 55, 241−247.

Kögel-Knabner, I., 1997. ^{13}C and ^{15}N NMR spectroscopy as a tool in soil organic matter studies. *Geoderma* 80, 243−270.

Kögel-Knabner. I., Leeuw, J.W., Hacher, P.G.,1992. Nature and distribution of alkyl carbon in forest soil profiles: Implications for the origin and humification of aliphatic biomacromolecules. *Sci*. *Total Environ*. 117−118: 175−185.

Kraal, P., Nierop, K.G.J., Kaal, J., Tietema, A., 2009. Carbon respiration and nitrogen dynamics in Corsican pine litter amended with alumin- ium and tannins. *Soil Biol*. *Biochem*. 41, 2318–2327.

Kramer, R.W., Kujawinski, E.B., Hacher, P.G., 2004. Identification of black carbon derived structures in a volcanic ash soil humic acid by Fourier Transform Ion Cyclotron Resonance Mass Spectrometry. *Environ*. *Sci*. *Technol*., 38, 3387–3395.

Kumada, K., 1987. Chemistry of Soil Organic Matter. Japan Scientific Societies Press, Tokyo; Elsevier Science Publishers, Amsterdam.

Kumada, K., Hurst, M., 1967. Green humic acid and its possible origin as a fungal metabolite. *Nature* 214, 631–633.

Kumada, K., Sato, O., 1980. Characteristics of the green fraction of P type humic acid. *Soil Sci*. *Plant Nutr*. 26, 309−316.

Kuwatsuka, S., Tsutsuki, K., Kumada, K., 1978. Chemical studies on soil humic acids. I. Elementary composition of humic acids. *Soil Sci. Plant Nutr*. 24, 337−347.

Lal R. 2001. Fate of the eroded soil carbon: emission or sequestration. in: Lal R (Ed.), Soil

carbon sequestration and the greenhouse effect, Soil Science Society if America special publication pp. 173–181.

Lal, R., 2004. Soil carbon sequestration to mitigate climate change. *Geoderma* 123, 1−22.

Lehmann, J., Skjemstad, J., Sohi, S., Carter, J., Barson, M., Falloon, P., Krull, E. 2008. Australian climate–carbon cycle feedback reduced by soil black carbon. *Nature Geoscience* 1, 832–835.

Lu, L., Sahajwalla, V., Harris, D., 2000. Characteristics of chars prepared from various pulverized coals at different temperatures using drop-tube furnace. *Energy & Fuels* 14, 869–876.

Marin-Spiotta, E., Silver, W., Swanston, C.W., Ostertag, R., 2009. Soil organic matter dynamics during 80 years of reforestation of tropical pastures. Global Change Biol. 15, 1584−1597.

Marschner, H., Dell, B., 1994. Nutrient uptake inmycorrhizal symbiosis. Plant Soil 159, 89–102.

Matsui Y, Kumada K, Shiraishi M 1984: An X-ray diffraction study of humic acids. *Soil Sci*. *Plant Nutr*., 30, 13–24.

Mataix-Solera, J., Cerdà, a., Arcenegui, V., Jordán, a., Zavala, L. M. 2011. Fire effects on soil aggregation: A review. *Earth-Science Reviews* 109, 44–60.

Miltner, A., Zech, W., 1997. Effects of minerals on the transformation of organic matter during simulated fire-induced pyrolysis. *Org. Geochem*.

Miyamoto, T., Kawahara, M., Minamisawa, K., 2004. Novel endophytic nitrogen-fixing Clostridia from the grass Miscanthus sinensis as revealed by terminal restriction fragment length polymorphism analysis. *Appl. Environ. Microbiol.* 70, 6580−6586.

Nadelhoffer, K.J., Fry, B., 1988. Controls of natural nitrogen-15 and carbon-13 abundances in forest soil organic matter. *Soil Sci. Soc. Am. J*. 52, 1633−1640.

Nishimura S, Hirota T, Hirahara O, Shindo H, 2006: Contribution of charred and buried plant fragments to humic and fulvic acids in Japanese volcanic ash soils. *Soil Sci*. *Plant Nutr*. 52, 686–690.

O'Leary, M.H., 1988. Carbon isotopes in photosynthesis. *BioScience* 38, 328−336.

Otsuka, H., Kimiwada, K., Uehara, Y., 1994. Genesis of humic acid derived from each plant residue of susuki (*Miscanthus sinensis*), sasa (*Sasa nipponia*), or Kashiwa (*Quercus dentata*) in fresh volcanic ash. *Japanese Journal of Soil Science and Plant Nutrition* 65, 629−636. (in Japanese with English summary)

Pardo, L.H., Hemond, H.F., Montoya, J.P., Pett-Ridge, J., 2007. Natural abundance 15N in soil and litter across a nitrate-output gradient in New Hampshire. *Forest Ecol. Manage*. 251, 217−230.

Peri, P.L., Ladd, B., Pepper, D.A., Bonser, S.P., Laffan, S.W., Amelung, W., 2012. Carbon ($\delta^{13}C$) and nitrogen ($\delta^{15}N$) stable isotope composition in plant and soil in Southern Patagonia's

native forests. *Global Change Biology* 18, 311−321.

Ponomarenko, E.V., Anderson, D.W., 2001. Importance of charred organic matter in Black Chernozem soils of Saskatchewan. *Can*. *J*. *Soil Sci*. 81, 285-297.

Poole, I., Braadbaart, F., Boon, J.J., van Bergen, P.F., 2002. Stable carbon isotope changes during artificial charring of propagules. *Org*. *Geochem*. 33, 1675−1681.

Reshetenko, T.V., Avdeeva, L.B., Ismagilov, Z.R., Pushkarev, V.V., Cherepanova, S.V., Chuvilin, A.L., Likholobov, V.A., 2003. Catalytic filamentous carbon structural and textural properties. *Carbon* 41, 1605–1615.

Rivas, Y., Matus, F., Rumpel, C., Knicker, H., Garrido, E., 2012. Black carbon contribution in volcanic soils affected by wildfire or stubble burning. *Org*. Geochem. 47, 41−50.

Rivas, Y., Huygens, D., Knicker, H., Godoy, R., Matus, F., Boeckx, P., 2012. Soil nitrogen dynamics three years after a severe Araucaria−Nothofagus forest fire. *Austral Ecol*. 37, 153−163.

Rodeghiero, M., Heinemeyer, A., Schrumpf, M., Bellamy, P., 2009. Determination of soil carbon stocks and changes. in Kutsch WL, Bahn M, Heinemeyer A (Eds.), soil carbon dynamics an integrate methodology. Cambridge University Press, New York, pp. 49–75.

Rodríguez-Alleres, M., Varela, M. E., Benito, E., 2012. Natural severity of water repellency in pine forest soils from NW Spain and influence of wildfire severity on its persistence. *Geoderma* 191, 125–131.

Saito, L., Miller, W.W., Johnson, D.W., Qualls, R.G., Provencher, L., Carroll, E.M., Szameitat, P., 2007. Fire effects on stable isotopes in a Sierran forested watershed. *J*. *Environ*. *Qual*. 36, 91−100.

Sato, T., 1984. Organo-mineral complex status in soils 1. Thermal analytical characteristics of humus in the soils. *Soil Sci*. *Plant Nutr*., 30, 1−12.

Sase, T., Hosono, M., 1996. Vegetation histories of Holocene volcanic ash soils in Japan and New Zealand: Relationship between genesis of melanic volcanic ash soils and human impact. *Earth Science* 50, 466−482.

Schnitzer, M., Preston, C.M., 1986. Analysis of humic acids by solution and solid-state carbon-13 nuclear magnetic resonance. *Soil Sci*. *Soc*. *Am*. *J*. 50, 326–331.

Schnitzer, M., Kodama, H., Ripmeester, J.A., 1991. Determination of the aromaticity of humic substances by X-ray diffraction analysis. *Soil Sci*. *Soc*. *Am*. *J*. 55, 745–750.

Schimel, D.S., 1995. Terrestrial ecosystems and the carbon cycle. *Global change biology*, 1, 77–91.

Schwartz, D., Mariotti, A., Lanfranchi, R., Guillet, B., 1986. $^{13}C/^{12}C$ ratios of soil organic matter as indicators of vegetation changes in the Congo. *Geoderma* 39, 97−103.

Sase, T., 1986. Plant opal analysis of Andisols in North Island, New Zealand. *Pedologist* 35,

21-33 (in Japanese with English summary).

Shindo, H., Y. Matsui, and T. Higashi, 1986, A possible source of humic acids in volcanic ash soils in Japan -Charred residue of Miscanthus sinensis, *Soil Sci*., 141, 84 – 87

Shindo, H., Urabe, M., 1993. Changes in the humus composition of volcanic ash soils by heating at various temperatures. *Soil Sci*. *Plant Nutr*. 39, 189–192.

Shindo, H., Honma, H., 1998. Comparison of humus composition of charred susuki (Eulalia, *Miscanthus sinensis*) plants before and after HNO_3 treatment. *Soil Sci*. *Plant Nutr*. 44, 675–678.

Shindo, H., Honna, T., Yamamoto, S., Honma H., 2004. Contribution of charred plant fragments to soil organic carbon in Japanese volcanic ash soils containing black humic acids. *Org*. *Geochem*. 35, 235−241.

Shindo, H., Yoshida, M., Yamamoto, A., Honma, H., Hiradate, S., 2005. $\delta^{13}C$ values of organic constituents and possible source of humic substances in Japanese volcanic ash soils. *Soil Sci.* 170, 175−182.

Shoji, S., Ito, T., Nakamura, S., Saigusa, M., 1987. Properties of humus of Andosols from New Zealand, Chili, and Ecuador. *Jp. J. Soil Sci. Plant Nutr*., 58, 473-479 (in Japanese).

Shoji, S., Nanzyo, M., Dahlgren, R.A., 1993. Volcanic Ash Soils -Genesis, Properties and Utilization. Developments in Soil Sciences 21. Elsevier, Amsterdam.

Sollins, P., Homann, P., Caldwell, B.A., 1996. Stabilization and destabilization of soil organic matter: mechanisms and controls. *Geoderma* 74, 65–105.

Sonibare, O.O., Haeger, T., Foley, S.F., 2012. Structural characterization of Nigerian coals by X-ray diffraction, Raman and FTIR spectroscopy. *Energy* 35, 5347–5353.

Stevenson, F.J., 1994. Humus Chemistry: Genesis, Composition, Reactions. 2nd ed. John Wiley and Sons, New York.

Sultana, N., Ikeya, K., Shindo, H., Nishimura, S., Watanabe, A., 2010. Structural properties of plant charred materials in Andosols as revealed by X-ray diffraction profile analysis. *Soil Sci*. *Plant Nutr*. 56, 793–799.

Sultana, N., Ikeya, K., Watanabe, A., 2011. Partial oxidation of char to enhance potential interaction with soil. *Soil Sci*.176, 495−501.

Takagi, H., Maruyama, K., Yoshizawa, N., Yamada, Y., Sato, Y., 2004. XRD analysis of carbon stacking structure in coal during heat treatment. *Fuel* 83, 2427–2433.

Takahashi, T., Dahlgren, R.A., Sase, T., 1994. Formation of Melanic Epipedons under forest vegetation in the Xeric moisture regime of Northern California. *Soil Sci*. *Plant Nutr*. 40, 617-628.

Tate, K.R., Yamamoto, K., Churchman, G.J., Meinhold, R., Newman, R.H., 1990. Relationships between the type and carbon chemistry of humic acids from some New Zealand and

Japanese soils. *Soil Sci. Plant Nutri.* 36, 611−621.

Tinoco, P., Almendros, G., Sanz, J., González-Vázquez, R., González-Vila, FJ., 2006. Molecular description of the effect of fire on soils under pine forest in two continental Mediterranean soils. *Org. Geochem*. 37, 1995−2018.

Tiunov, A.V., 2007. Stable isotopes of carbon and nitrogen in soil ecological studies. *Biology Bulletin* 34, 395−407.

Tonneijck, F.H., Jansen, B., Nierop, K.G.J., Verstraten, J.M., Sevink, J., De Lange, L., 2010. Towards understanding of carbon stocks and stabilization in volcanic ash soils in natural Andean ecosystems of northern Ecuador. *Eur J Soil Sci* 61, 392–405

Trompowsky, P.M., Benites, V.M., Madari, B.E., Pimenta, A.S., Hockaday, W.C., Hatcher, P.G., 2005. Characterization of humic like substances obtained by chemical oxidation of eucalyptus charcoal. *Org. Geochem*. 36, 1480–1489.

Tsutsuki, K., 2005: Soil organic matter. *In*: Introductory soil science. Saigusa, M., and Kimura, M. (ed.). Buneido Publishing Co., Tokyo, pp. 138–148. (in Japanese)

Turney, C.S.M., Wheeler, D., Chivas, A.R., 2006. Carbon isotopic fractionation in wood during carbonization. *Geochim. Cosmochim. Acta* 70, 960–964.

van der Werf, G. R., Randerson, J. T., Giglio, L., Collatz, G. J., Mu, M., Kasibhatla, P. S., Morton, D. C., DeFries, R. S., Jin, Y., and van Leeuwen, T. T. 2010. Global fire emissions and the contribution of deforestation, savanna, forest, agricultural, and peat fires (1997–2009), Atmos. Chem. Phys., 10, 11707-11735.

van Krevelen, D.W., 1950. Graphical-statistical method for the study of structure and reaction process of coal. *Fuel* 29, 269−284.

Vergnoux, A., Guiliano, M., Di Rocco, R., Domeizel, M., Theraulaz, F., Doumenq, P., 2011. Quantitative and mid-infrared changes of humic substances from burned soils. *Environ. Res.* 111, 205−214.

von Fischer, J.C., Tieszen, L.L., 1995. Carbon isotope characterization of vegetation and soil organic matter in subtropical forests in Luquillo, Puerto Rico. *Biotropica* 27, 138−148.

Wada, K., Higashi, T., 1976. The categories of aluminium- and iron-humus complexes in Ando soils determined by selective dissolution. *J. Soil Sci*., 27, 357–368.

Wadle, D.A., Hornberg. G., Zackrisson, O., Kalela, Bundin, M., Coomes, D.A., 2003. Long-term effects of wildfire on ecosystem properties across an island area gradient. *Science* 300, 972−975.

Wagai, R., Mayer, L. M., Kitayama, K., Shirato, Y. 2013. Association of organic matter with iron and aluminum across a range of soils determined via selective dissolution techniques coupled with dissolved nitrogen analysis. *Biogeochemistry* 112, 95–109.

Wagai. R., Kishimoto-Mo, A.W., Yonemura, S., Shirato, Y., Hiradate, S., Yagasaki, Y., 2013.

Linking temoreature sensitivity of soil organic matter decomposition to its molecular structure, accessibility, and microbial physiology. *Global Change Biology* 19, 1114–1125.

Wang, G., Feng, X., Han, J., Zhou, L., Tan, W., Su, F., 2008. Paleovegetation reconstruction using $\delta^{13}C$ of soil organic matter. *Biogeosciences* 5, 1325−1337.

Watanabe, A., Kuwatsuka, S., 1991. Triangular diagram for humus composition in various types of soils. *Soil Sci. Plant Nutr*. 37, 167−170.

Watanabe, A., Fujimori, H., Nagai, Y., Miyajima, T., Kuwatsuka, S., 1996. Analysis of the green fraction of humic acids. *Eur. J. Soil Sci*. 47, 197–204.

Watanabe, A., Takada. H., 2006. Structural stability and natural ^{13}C abundance of humic acids in buried volcanic ash soils. *Soil Sci. Plant Nutr*. 52, 145−152.

Watanabe, A., Fujitake, N., 2008. Comparability of composition of carbon functional groups in humic acids between inverse-gated decoupling and cross polarization/magic angle spinning ^{13}C nuclear magnetic resonance techniques. *Analytica Chimica Acta* 618, 110−115.

Xing, B., Chen, Z., 1999. Spectroscopic evidence for condensed domains in soil organic matter. *Soil Science*, 164, 40–47.

Yamada, Y., 1986. The characterization of humus accumulation in Andosols by ^{14}C dating. *Bulletin of National Institute for Agro-Environmental Sciences* 3, 23−86 (in Japanese with English summary).

Yamane, I., Matsui, T., Irisawa, S., Okazaki, M., Hosono, M., 1978. Illustrated Soils of Japan. Asakura Publishing Co., Tokyo, Japan. (in Japanese)

Yamane, I., The meaning of *Miscanthus sinensis* in the formation of kuroboku soil. *Pedologist* 17, 84–94. (Japanese English summary)

Yanagi, Y., Hamaguchi, S., Tamaki, H., Suzuki, T., Otsuka, H., Fujitake, N., 2003. Relation of chemical properties of soil humic acids to decolorization by white rot fungus-Coriolus consors. *Soil Sci. Plant Nutr*. 49, 201−206.

Yen, T.F., Erdman, J.G., Pollack, S.S., 1961. Investigation of the structure of petroleum asphaltene by X-ray diffraction. *Anal. Chem.*, 33, 1587−1594.

Yonebayashi, K., Kyuma, K., Kawaguchi, K., 1974. Thermogravimetric analysis for organo-clay complex in soil. *Japanese J. Soil Sci Plant Nutr.* 45, 421−425. (in Japanese)

Yonebayashi, K., Hattori, T., 1988. Chemical and biological studies on environmental humic acids. I. Composition of elemental and functional groups of humic acids. Soil Sci. Plant Nutr. 34, 571−584.

Yonebayashi, K., 1989. Research methods for humic substances: II. *Pedologist* 33, 37−48 (in Japanese).

Yonebayashi, K., 1994. Humic component distribution of humic acids as shown by adsorption chromatography using XAD-8 resin, in: Senesi, N., Miano, T.M. (Eds.), Humic Substances

in the Global Environment and Implications on Human Health. Elsevier, Amsterdam, pp.181−186.

Yonebayashi, K., 1997. Soil organic matter. in: Kyuma, K. (Ed.) Current Soil Science. Asakura Shoten, Tokyo, Japan, pp. 43−53 (in Japanese).

Yoneyama, T., Nakanishi, Y., Morita, A., Liyanage, B.C., 2001. $\delta^{13}C$ values of organic carbon in cropland and forest soils in Japan. *Soil Sci. Plant Nutr.* 47, 17−26.

Zancada, M. C., Almendros, G., Jime´nez-Ballesta, R., 2003. Humus quality after eucalypt reforestations in Asturias (Northern Spain). Sci. Total Environ. 313, 245–258.